DEVELOPMENT OF A FAST AND COST-EFFECTIVE ASPHALT MIXTURE FATIGUE TEST SYSTEM

By

Aksel Seitllari

A DISSERTATION

Submitted to
Michigan State University
In partial fulfilment of the requirements
for the degree of

Civil Engineering—Doctor of Philosophy

2020

ABSTRACT

DEVELOPMENT OF A FAST AND COST-EFFECTIVE ASPHALT MIXTURE FATIGUE TEST SYSTEM

By

Aksel Seitllari

Fatigue cracking is one of the critical distress modes in asphalt pavements. Accurate prediction and evaluation of fatigue performance are crucial to extending the service life of asphalt mixtures. Naturally, laboratory testing methods for fatigue characterization are time-consuming and require sophisticated procedures. Any effort to improve the speed and quality of the information gained from laboratory fatigue tests is valuable. This research work presents the results of a study investigating the possibility of implementing a new approach to characterize asphalt mixture fatigue behavior. This new approach includes cyclic tests run on cylindrical asphalt specimens in three-point beam mode (herein referred to as three-point bending cylinder (3PBC) geometry). Timoshenko beam theory along with the viscoelastic continuum damage (VECD) theory was implemented to model the mechanical response of the specimens. An excellent correlation between the results of 3PBC tests and uniaxial push-pull fatigue tests were observed. The 3PBC setup possesses the most advantages of uniaxial push-pull tests and includes more advantages such as not requiring a saw to cut the ends of the sample, not requiring gluing operation (and the gluing jig) and the possibility of estimating Poisson's ratio from the data. The proposed 3PBC approach was evaluated through laboratory tests conducted on various asphalt mixtures with varying binder types, mix components and volumetric properties. The approach proposed herein was validated through finite element analysis. In addition, ruggedness evaluation of the 3PBC testing approach through varying factors and their levels were investigated and presented.

To My Beloved Selma
Të Shtrenjtës Sime Selma

ACKNOWLEDGMENTS

All praise due to God, the Most Merciful, and the All-Knowing. It is God's grace solely that devices the will and materializes it. Little did I know that at one point in time I will be writing this paragraph, concluding the end of my doctorate studies. Praised be the Almighty for all the blessings.

This research work was performed under the guidance and supervision of Dr. M. Emin Kutay. I would like to thank Dr. Kutay for his continuous support, guidance, patience, and dedication through my graduate school. I am lucky to have had him as an example and mentor. I am also grateful to my dissertation advisory committee members; Dr. Karim Chatti, Dr. Neeraj Buch, and Dr. Sara Roccabianca for the feedback they have provided to improve this work. This experience has been a lot smoother with the support and care of technical staff and department secretaries.

This research work was funded by the National Cooperative Highway Research Program Innovations Deserving Exploratory Analysis (NCHRP IDEA). The program is sponsored by the member states of the American Association of State Highway and Transportation Officials. Their support is greatly appreciated.

Family is the place of rest and tranquility, knowledge and love. It is the safest bay to anchor before the sail. The support and spiritual lectures from my mother (Manushaqe), teaching notes from my father (Kujtim), peace (Selma) and trust (Inar) from my siblings instilled in me the desire to pursue this road. It has been much easier with my soul companion (Jonida) and her never-ending support when far and near to complete this dissertation. It is the warmth of my Seitllari's that I could make it so far.

My doctorate journey couldn't have been more joyful if it wasn't for the great time and broad conversations with my dear friend Dr. Yogesh Kumbargeri. Bits of advice from Dr. Michele Lanotte and Dr. Ilker Boz. The vividness and fellowship of the pavement research group (soon to be Drs.) Mahdi Ghazavi, M. Munum Masud, Angela Farina, Hao Ye, Mumtahin Hasnat, and many others who I had the pleasure of knowing.

I am thankful as this journey introduced me to great people, with brilliant minds and high spirits. One journey's end is the dawn of a new one. Perhaps more challenging, exciting, or both, perhaps none. Eager, curious, persistent and thankful for every moment the Almighty blesses me with, until the twinkle that the wayfarer resumes the sail, I will pursue my dream and send good ahead.

TABLE OF CONTENTS

LIST OF TABLES

LIST OF FIGURES

1. INTRODUCTION

Increasing service life, reducing cost, and improving sustainability of asphalt pavements have always been the goals of engineers and researchers over the years. Emerging new construction technologies and materials provide solutions satisfying the long-term performance goals of asphalt pavement. Typically, the long-term performance of asphalt pavements is evaluated based on different means. The recent FHWA Distress Identification Manual lists fifteen different distresses in asphalt pavements among which, cracking shares the major part (Miller & Bellinger, 2014). Since 1948, cracking, caused by the repeated bending distresses in pavements, has been a primary concern for the engineers involved in pavement management (Carl L Monismith, 1994). In 1955, Hveem (Hveem, 1955) acknowledged the need for assessing the fatigue characteristics of asphalt concrete while Monismith et al. (C L Monismith, Secor, & Blackmer, 1961) emphasized the importance of material characterization on fatigue performance of asphalt pavements.

Fatigue phenomenon in asphaltic layers is caused by repeated traffic loading applications and predominantly happens at intermediate temperatures. Excessive tensile strains at the bottom and top of the asphalt layers lead to microcracks, which eventually grow, coalesce and lead to serious structural deterioration. Generally, two types of fatigue cracking can occur, depending on the place the cracks initiate. While bottom-up fatigue cracking is mostly observed in relatively thin asphalt layers because of the flexural bending, top-down fatigue cracks can be seen in both thick and thin asphalt layers on the wheel path evolving between the tire edge and the asphalt layer. To better understand and assess the resistance of asphalt mixtures to fatigue cracking, numerous laboratory tests have been developed to simulate the traffic load applications in the field. Traditionally, the four-point bending fatigue test mode has been the most common test method to characterize the fatigue resistance of asphalt mixtures (Huurman & Pronk, 2012). United States

practice for four-point bending beam fatigue (4PBB) test follows AASHTO T321 and ASTM D7460 testing protocols (AASHTO T321, 2017; ASTM D7460 − 10, 2013). However, in general, these tests are lengthy, cumbersome and expensive. As an alternative, uniaxial fatigue tests (Kutay, Gibson, Youtcheff, & Dongré, 2009; Aksel Seitllari, Lanotte, & Kutay, 2019b; Zeiada, Kaloush, Underwood, & Mamlouk, 2016) have been gaining wide acceptance for fatigue evaluation of asphalt pavements because of their advantages. Ease of application of constitutive models (i.e., Viscoelastic Continuum Damage Theory) to uniaxial testing geometry has been a great advantage. However, the most challenging issues with the uniaxial testing are (i) two ends of the sample need to be cut parallel and (ii) the gluing end platens using a gluing jig can be cumbersome. As a result, many end-failures are experienced when sample ends are not cut parallel or gluing is not done properly leading to excessive sample preparation time and consumption of material. While the uniaxial testing is still superior to 4PBB testing, it is currently not suitable for as a routine testing alternative for balanced and performance-based mix design approaches. Hence, there is a need for a test which addresses not only the above challenges but is also simple, sensitive to asphalt mix design, repeatable and practical.

This research study introduces a more practical fatigue testing alternative to the uniaxial fatigue tests and corresponding analyses based on the Viscoelastic Continuum Damage (VECD) theory. Each aspect of test development is presented individually in separate chapters. Chapter 2 presents a comprehensive literature review on various methods of fatigue evaluation of asphalt mixtures. Chapter 3 presents the objectives of this research study followed by a research plan. The experimental program and materials used in this study are presented in chapter 4. The new test setup that was introduced in this study has been explained in chapter 5. Chapters 6 focuses on the application of Timoshenko Beam Theory while chapter 7 deals with verification and validation of

this theory. In chapter 8 the implementation of Viscoelastic Continuum Damage Theory is presented. Chapter 9 discusses the ruggedness results for the test that has been developed in this study. In chapter 10 are presented the summary and conclusions of this study.

2. LITERATURE REVIEW

This section includes a literature review on cracking characterization methods of asphalt mixtures. Also, a tabulated summary (see Table 2.1) is provided with the details of each testing approach.

Federal Aid Highway Act of 1956 lead to the construction of the United States Interstate network, which consequently increased the truck traffic volume and truck loading, threatening the in-service life of the pavement structures. WASHO program and AASHTO Road Test shifted the primary focus on the influence of pavement layers and their effects on the general performance of the pavement (AASHTO, 1962; WASHO, 1955). Among the outcomes of these projects, cracking was observed to be strongly related to surface deflection and the concept of 'thicker pavement structure performs better' was acclaimed. Hveem (Hveem, 1955) investigated the relationship between surface deflection and pavement cracking, acknowledging the necessity for assessing the fatigue characteristic of asphalt concrete. The pavement community struggled with the cracking phenomena for decades and acknowledged the cracking failure to be the primary concern in asphalt pavements (Carl L Monismith, 1994).

Fatigue cracking is one of the main failure modes of pavement structures, which results in degradation of the pavement materials and eventually pavement structure. Repeated traffic loading applications in asphaltic layers cause fatigue phenomenon which primarily happens in intermediate temperatures. Typically, the fatigue phenomenon manifests itself in two types of cracking. Bottom-up cracking (a.k.a. alligator cracking) initiates from underside the asphalt layer and propagates upward. This type of cracking adheres to two phases; crack formation and crack propagation. The first phase consists of the formation of hairline microcracks leading to stiffness reduction and the second phase is the coupling of the formed microcracks leading to macro-cracks. The formation

and propagation of cracks are caused by the presence of tensile and shear stresses generated by traffic loads and environmental effects (Prowell et al., 2010). The second type of fatigue cracking is top-down which is mainly observed on the wheel path evolving between the tire edge and the asphalt layer. This failure generally initiates at the surface of the asphalt pavement and propagates through it. This failure type is commonly addressed as a combination of shear strains and surface tension at the tire edge aided by aging and thermal stresses (Lytton, Zhang, Gu, & Luo, 2018). Proper mix design, structural design, and enhanced material selection can significantly slow down the fatigue cracking and lengthen the life cycle of asphalt pavements.

In recent years, however, the growing use of Reclaimed Asphalt Pavement (RAP), warm mix asphalt (WMA) technologies, use of alternative aggregates, binder additives (Ground Tire Rubber (GTR) materials) and other technological advances are changing asphalt concrete beyond the traditional Superpave mix design method and characterization. For these developments to be beneficial, the incorporation of new materials should be well characterized to enhance pavement field performance. Performance-based testing of various mixture properties as part of mix design procedures can provide more details reflecting the pavement field performance (S. D. Diefenderfer & Bowers, 2019). Yet, not all of the performance characteristics can be accurately characterized using performance-based tests and not many of performance-based tests are ready for implementation as part of mix design methods. According to a recent survey done as part of the NCHRP 20-07 project, 36 DOTs (out of 43 responded) consider fatigue cracking as the most common failure mode that the agency wants to address (West, Rodezno, Leiva, & Yin, 2018). However, in the same survey, 34 of the DOTs also indicated that fatigue cracking test is not required in their mix design specifications. This is primarily because a simple, practical, and robust fatigue test is not available. State DOTs and road agencies are interested in ways to specify asphalt

mix designs better in an effort to improve their pavements fatigue life, make the roadway network more sustainable, longer-lasting, and more economical. By developing fatigue performance criteria through a practical fatigue test, this goal can be achieved.

In the design process of the asphalt mixtures, addressing fatigue performance is crucial. To this end, numerous laboratory tests have been developed to simulate the traffic load applications in the field and provide general information. Usually, the tests are subjected to two types of loading modes; stress-controlled mode and strain-controlled mode. It is anticipated that thick pavements with high modulus materials behave more like stress controlled mode while relatively thin pavements with softer modulus materials behave more like the strain-controlled mode (C.L Monismith, 1966). The number of cycles to failure (N_f) has traditionally been used to quantify the fatigue resistance of the tested material regardless of the loading mode. Considerable effort has been done to describe the point of failure (a.k.a. failure criteria) for characterizing the fatigue performance in laboratory tests. Several failure criteria have investigated by different researchers (Aksel Seitllari, Boz, Habbouche, & Diefenderfer, 2020; Aksel Seitllari et al., 2019b; Soltani & Anderson, 2005; Underwood, B. Shane, 2006; Y. D. Wang, Keshavarzi, & Kim, 2018; Zeiada et al., 2016; Zhang, Sabouri, Guddati, & Kim, 2013). Sabouri and Kim proposed new energy-based failure criteria denoted as G^R which represents the relationship between the number of cycles to failure and the average rate of the pseudo-strain energy that is released until failure (Sabouri & Kim, 2014). Kutay et al. (Kutay, Gibson, & Youtcheff, 2008) used numerous commonly used failure criteria to define the point of failure in laboratory tests using both stress-controlled and strain-controlled modes. While for strain-controlled tests 50 % reduction in stiffness was recommended, it was noted that the stress-controlled tests experienced an inverse relationship with the field data and was not recommended for fatigue characterization.

The selection of a laboratory fatigue testing method is crucial in addressing the fatigue distress encountered in constructed asphalt pavements. The following section provides a detailed discussion of the current state of practice for most recognized test methods to characterize load-related cracking (fatigue cracking). The discussion provides characteristics associated with each test method with a detailed summary provided in Table 2.1.

2.1 Non-homogenous test methods

These types of fatigue testing are commonly referred to as non-homogeneous tests due to the varying internal stress-strain distribution throughout specimen geometry (Ning Li, Molenaar, Van De Ven, & Wu, 2013).

2.1.1 Four-point bending beam fatigue (4PBB)

Traditionally, the four-point bending beam (4PBB) fatigue test mode has been the most common test method to characterize the fatigue resistance of asphalt mixtures (Huurman & Pronk, 2012; Mateos, Wu, Denneman, & Harvey, 2018). Upon the completion of the SHRP program, the test was standardized hence improving the reliability of the test results. United States practice for the 4PBB test follows both testing protocols AASHTO T321[1] and ASTM D7460 – 10[2]. Later, the AASHTO T321 was refined after the original work proposed by Professor Monismith at the University of California Berkley (Tayebali, Deacon, Coplantz, Harvey, & Monismith, 1994). While the loading mode of the ASTM standard is haversine, the recent version is due and revisions are required to match the loading mode with AASHTO protocol (Braham & Underwood, 2016).

[1] Standard Method of Test for Determining the Fatigue Life of Compacted Asphalt Mixtures Subjected to Repeated Flexural Bending

[2] Standard Test Method for Determining Fatigue Failure of Compacted Asphalt Concrete Subjected to Repeated Flexural Bending

According to AASHTO T321, the 4PBB test specimen dimensions are 380 ± 6 mm in length, 50 ± 6 in height and 63 ± 6 mm in width. The test is performed in strain-controlled or stress-controlled mode at a certain frequency (i.e., 10Hz). After mounted in the apparatus, the beam is clamped in four locations and loaded in the two inner clamps. As a result, the center portion of the beam is subjected to pure bending deformation. For each loading cycle, the change in local stiffness varies for every unit volume from a maximum compression to maximum tension, which is believed to be similar behavior of an asphalt layer in the field. However, in general, flexure tests are lengthy, cumbersome and expensive. The extensive material requirement for sample preparation, difficulty in meeting air void target, a large number of samples needed for testing, and excessive equipment cost are some of the challenges encountered when running these tests (Chiangmai, 2010; Zhou et al., 2016).

The 4PBB test has proven to be sensitive to mix design properties and testing conditions. Further, it serves as a key test in mechanistic-empirical fatigue pavement design approaches, which are used to estimate the pavement performance for various distress mechanisms through its design life (ARA Inc. ERES Consultants Division, 2004; Ullidtz, Harvey, Tsai, & Monismith, 2006).

2.1.2 Trapezoidal beam fatigue (a.k.a. two-point bending beam test)

The flexural bending fatigue test on trapezoidal beam specimens has been commonly used as a fatigue testing approach in Europe. Several research groups have conducted extensive research on trapezoidal beam fatigue tests under both stress and strain-controlled modes (Van Dijk 1975; Verstraeten 1972; Rowe 1993). This practice is detailed by the European standard EN 12697[3]. The size of tested trapezoidal beam specimens depends upon the nominal maximum aggregate size of the gradation mixture. Generally, the dimensions at major base cross-section are 55 mm by 20 mm,

[3] Bituminous mixtures – Test methods for hot mix asphalt. Part 24: Resistance to fatigue

the minor base cross-section is 25 mm by 25 mm and height of 250 mm. The specimens are sawed from compacted asphalt mixture slabs. However, the fabrication of required quality test specimens with the correct dimensions is a challenging task in this test.

Prior to testing, the major base is attached to a metal plate in an upright position while a thin metallic plate is glued to a minor base and connected to a load cell. The specimen is then subjected to sinusoidal loading in strain-controlled mode. Similar to the 4PBB test, the number of cycles to failure is usually recorded when stiffness value reduces by half of its initial value. Typically, the test requires a minimum of 18 samples to be tested. In addition to difficulties in meeting the volumetric criteria, premature failure due to improper gluing operations and geometry imperfections demand a higher number of replicates. The test was proven sensitive to the viscoelastic properties of the asphalt mixtures and binder content and is of widespread use in the French pavement design method (Verstraeten, 1972).

2.1.3 Supported flexure fatigue test

The flexure fatigue tests are supported in multiple ways intending to simulate similar behavior of an asphalt layer in the field. Researchers have applied different geometries and supports to investigate any potential relationship between the stresses/strains and fatigue life of the asphalt mixtures. Researchers at Ohio State University developed a circular slab specimen setup supported on a rubber mat (Majidzadeh & Kauffmann, E. M Ramsamooj, 1971). The specimens were subjected to repeated load at the center of the specimen. Similarly, in another study rectangular asphalt beams were supported on a rubber mat (Barksdale & Miller, 1977). Before testing, the setup was conditioned using the environmental chamber and subjected to a haversine load pulse. These test methods were better representing the field conditions but at the same time challenging for routine use. The complexity of the test, setup high cost, testing time and

complicated test machine were some of the serious concerns constraining further development of these methods.

2.1.4 Diametral test

The diametral test (a.k.a. indirect tensile test) is an alternative fatigue testing method to evaluate the fatigue performance of asphalt mixtures using cylindrical specimens. The dimensions of the test specimen are 100 mm diameter and 64 mm thick which makes it easy to prepare and/or extract from road cores. Typically, the cylindrical samples are subjected to sine/haversine diametral load pulse at a frequency of 20 - 120 cycles per minute. The test can be run using any hydraulic or pneumatic system and is relatively fast. The Center for Highway Research at the University of Texas at Austin conducted extensive research on the implementation of this test method in evaluating fundamental properties of asphalt mixtures (Cowher & Kennedy, 1975; Kennedy, 1977; Moore & Kennedy, 1971). The geometry of this test provides a biaxial stress system which might be a better representative of the field conditions. Nonetheless, several concerns were raised including the potential permanent deformation of the test specimen and underestimation of fatigue life of asphalt pavements if principal tensile stress is used as a fatigue evaluation criterion.

2.1.5 Loaded wheel tester

The loaded wheel tester (LWT) includes laboratory and in situ wheel test tracks. This test is usually used to evaluate the rutting performance, moisture susceptibility and fatigue resistance of asphalt mixtures. The concept was implemented in Hamburg, Germany. The so-called Hamburg Wheel Tracking Device (HWTD) device was manufactured by Helmut-Wind, Inc. and used to evaluate the rutting and stripping potential of asphalt mixtures (Aschenbrenter, 1995). Similarly, the same concept was explored by different agencies over the years including the French Rutting

Tester (FRT), Third-Scale Model Mobile Load Simulator (MMLS3) and Asphalt Pavement Analyzer (APA). The latter was a joint effort of the Georgia Department of Transportation (GDOT) and the Georgia Institute of Technology (GIT) to evaluate rutting susceptibility of asphalt mixture. The differences among these approaches are mainly on the dimensions of tested specimens, tire type, and pressure, and testing conditions, however, the concept is similar. Generally, a loaded wheel rolls back and forth over an asphalt specimen (i.e., beam or cylindrical) and the rut depth is measured after a certain number of loading cycles.

Limited studies on evaluating the fatigue performance of asphalt mixtures using the LWT concept exist in the literature. Van Dijk used a small wheel tracking device to measure the fatigue performance of asphalt mixtures in laboratory conditions (Van Dijk, 1975). The important outcome of this study was the understanding of fatigue characterization of asphalt mixtures in terms of crack initiation and real crack development. A similar study was performed by (G. M. Rowe & Brown, 1997). Researchers at Worcester Polytechnic Institute explored MMLS3 in characterizing the fatigue performance of the asphalt mixtures. The experimental result agreed well with the numerical analysis (Bhattacharjee, Gould, Mallick, & Hugo, 2004). Other studies modified APA to test the fatigue performance of the asphalt mixtures (Wu, Huang, & Shu, 2014). The fatigue performance of the mixtures measured through LWT would rank similar to other fatigue tests (i.e., 4PBB). Nonetheless, the concept had numerous issues including testing time, wheel speed, special equipment requirement and associated cost, failure to measure fundamental properties and rutting deformation in low stiffness asphalt mixtures prompted its development. Alternatively, accelerated loading test (ALT) facilities were introduced. These facilities can simulate field conditions with actual pavement structure. However, in addition to challenges

encountered in LWT, ALT has extremely initial, operational and maintenance costs hampering its advancement.

2.2 Homogenous test methods

Homogenous test methods refer to uniaxial fatigue tests on cylindrical specimens. Unlike the non-homogenous tests where the stress-strain application is not uniform thorough the tested specimen, this approach assumes constant stress state across the specimen section which can be related to fundamental properties of the tested materials.

The uniaxial fatigue test system was developed in the Transport Research Laboratory (TRL) in tension only and the University of Nottingham in tension-compression loading (Pell & Cooper, 1975; Raithby & Sterling, 1972). The uniaxial fatigue loading was further explored by different research groups over the years (N Li, Molenaar, Van De Ven, & Wu, 2013; Nguyen, Pouget, Di Benedetto, & Sauzéat, 2009). In the United States, this approach was utilized by several institutions as an alternative to the standardized 4PBB test (Christensen & Bonaquist, 2009; B. K. Diefenderfer, Bowers, & Diefenderfer, 2015; Kim, Hyon-Jong, & Little, 1997; Kutay et al., 2008; Prowell et al., 2010; Soltani & Anderson, 2005). Research programs were developed to characterize the fatigue performance by simply relating the stress/strain to fatigue life (number of cycles to failure) or investigate fundamental theories (i.e., fracture and damage mechanics) which could be used for pavement design and field performance predictions.

Uniaxial push-pull (Arambula & Kutay, 2009; Kutay et al., 2009) and pull-pull tests (Kim et al., 2018; Zeiada et al., 2016) have been gaining wide acceptance for fatigue evaluation of asphalt pavements because of their advantages. These advantages include homogenous stress-strain distribution throughout the sample geometry, ability to produce samples using the Gyratory compactor and straightforward application of the constitutive models to predict fatigue

performance of asphalt pavements, such as the Viscoelastic Continuum Damage (Chehab, Kim, Schapery, Witczak, & Bonaquist, 2002; Lee & Kim, 1998; Luo, Luo, & Lytton, 2013; Soltani & Anderson, 2005; N. Tapsoba, Sauzéat, Di Benedetto, Baaj, & Ech, 2015; Walubita, Martin, Cleveland, & Lytton, 2006). However, one of the most challenging issues with the uniaxial testing is that two ends of the sample need to be cut parallel and the gluing end platens using a gluing jig can be cumbersome (Zeiada et al., 2016). As a result, many of the end-failures are experienced when sample ends are not cut parallel or gluing is not done properly. Since the samples are expected to fail in the center, many of the samples and their results are discarded, leading to excessive sample preparation time and consumption of material. While the uniaxial testing is still superior to FPBB testing, it is currently not suitable for as a routine testing alternative for balanced and performance-based mix design approaches.

2.3 Screening tests

There exist several tests commonly used to provide a hierarchical classification of cracking susceptibility of asphalt mixtures. The features of these tests differ and they are usually employed for screening purposes to reduce the crack related risks for particular asphalt mix design (Aksel Seitllari et al., 2020). While these tests are useful in ranking mixtures, they are monotonic fracture tests (or low frequency cyclic in the case of overlay tester) and they cannot be (or haven't yet been) used to calibrate the field-scale fatigue models (i.e., the one in the AASHTOWare Pavement ME Design software). Hence, there is a need for a test which addresses not only the above challenges but is also simple, sensitive to asphalt mix design, repeatable and practical.

2.3.1 Texas overlay tester

The Texas overlay test (OT) was initially designed by Germann and Lytton at Texas A&M Transportation Institute (TTI) (Germann & Lytton, 1979). The primary objective of this test was

to evaluate the types of anti-reflection cracking measures. The test setup and procedure were later updated and besides reflective cracking, OT serves as a test in a balanced mix design system and pavement design for TxDOT (Zhou, Hu, Hu, & Scullion, 2009). The test specimen size is 76 mm wide, 38 mm thick and 150 mm long, and can be prepared from SGC compactor or extracted from field cores. Before testing, the test specimen is glued on two steel plates; one fixed and the second one movable in horizontal direction simulating the movements of cracks beneath the overlay. A cyclic triangular waveform to a maximum displacement of 0.006 mm is applied on the horizontally moving steel plate at a frequency of 10 seconds per cycle. The tests are usually conducted at a temperature of 25 ºC. Generally, the crack initiates at the bottom of the specimen and propagates upward. The test stops when a 93 % reduction of initial load occurs or within 1200 cycles whichever develops first. Several studies have indicated a good correlation between the OT and FHWA-ALF fatigue cracking and the structural test sections at NCAT 2006 test track (Hu, Zhou, Scullion, & Leidy, 2012; Ozer et al., 2018; Zhou, Hu, Chen, & Scullion, 2007). Nonetheless, issues were aroused regarding the high variability of the test attributed mainly to the fabrication quality and precise test specimens, and improper gluing operation; necessitating to repeat some of the tests to acquire reliable data.

2.3.2 Indirect tension test

The indirect tension test (IDT) has was originally developed and applied to evaluate the thermal cracking performance of asphalt mixtures under the SHRP-A-407 program (Roque & Buttlar, 1992). Creep compliance and tensile strength were two parameters derived to distinguish between the mixtures. Subsequently, the test was standardized (AASHTO T322[4]) and currently is

[4] Determining the Creep Compliance and Strength of Hot Mix Asphalt (HMA) Using the Indirect Tensile Test Device

a key input in mechanistic-empirical fatigue pavement design approaches to estimate the pavement thermal cracking performance through its design life. According to AASHTO T322, the IDT specimens are subjected to a constant deformation rate until failure. Given its simplicity and the relatively inexpensive testing equipment, the IDT test was further investigated to evaluate the asphalt concrete performance at intermediate temperatures. The testing rates and conditioning temperatures vary depending on the local practice of the test. Various analysis methods were developed to interpret the fatigue cracking performance of asphalt mixtures at intermediate temperatures (Witzcak, Kaloush, Pellinen, El-Basyouny, & Von Quintus, 2002). Several studies performed monotonic IDT tests on laboratory and field cores. Fracture energy (area under the normalized stress-strain curve in the loading portion) was shown to correlate well with field fatigue performance of the asphalt pavements (Kim & Wen, 2002; Roque, Birgisson, Drakos, & Dietrich, 2004; Roque & Buttlar, 1992; C. Wang, Castorena, Zhang, & Richard Kim, 2015).

Recently, a new analysis approach for the IDT test, named the indirect tensile asphalt cracking test (IDEAL-CT), was introduced to investigate the cracking resistance of asphalt mixtures at intermediate temperatures (Zhou, Im, Sun, & Scullion, 2017). In this test, a monotonic load at a constant displacement rate (50 mm/min) is applied to a cylindrical specimen (usually with a 150-mm diameter), and the resulting load-displacement curve is analyzed to determine the crack performance index of asphalt mixtures: the CT_{index}. This cracking index has shown good correlations with the cracking performance of asphalt mixtures in the field. Several state agencies are currently evaluating this test as a potential tool to screen their mixtures for cracking susceptibility as part of their mix design process and/or quality control process (Bennert, Haas, &

Wass, 2018; S. D. Diefenderfer & Bowers, 2019). It should be noted that ASTM D8225-19[5] is available for this test.

2.3.3 Semi-circular beam test

The semi-circular beam (SCB) test method was originally suggested only for asphalt mixture fracture property characterization. The SCB test for low temperature is run as per the AASHTO TP105 protocol; *Determining the Fracture Energy of Asphalt Mixtures Using the Semicircular Bend Geometry (SCB)*. Since its introduction, the SCB test has emerged as a simple, quick, and reliable test to evaluate the cracking susceptibility of asphalt mixtures. This test uses a monotonic loading mode at a constant displacement rate, and the resulting load-displacement curve is further considered to evaluate the susceptibility of an asphalt mixture to load-related cracking. Although there are several different versions of this test (i.e., tests using different loading rates and notch depths), LTRC method and IFIT method are the commonly implemented practices (Al-Qadi, Ozer, Lambros, Khatib, & Singhvi, 2015; Mohammad, Kim, & Challa, 2016). The LTRC method is typically run in accordance with ASTM D8044[6] and the critical strain energy release rate is measured. High values of critical strain energy release rate suggest tougher materials which are desirable for fracture resistant mixtures. The test was proven to be sensitive to mix design properties (Nsengiyumva, Kim, & You, 2015). For the IFIT method, there exists a provisional AASHTO TP124[7] testing protocol. This protocol was

[5] Determination of Cracking Tolerance Index of Asphalt Mixture Using the Indirect Tensile Cracking Test at Intermediate Temperature

[6] Evaluation of Asphalt Mixture Cracking Resistance using the Semi-Circular Bend Test (SCB) at Intermediate Temperatures

[7] Determining the Fracture Potential of Asphalt Mixtures Using Semicircular Bend Geometry (SCB) at Intermediate Temperature

introduced in 2016 as the Illinois flexibility index (FI) test. While the FI test has shown the capability to distinguish the fatigue cracking performance of asphalt mixtures, numerous studies have highlighted the high variability of this approach as well as its lack of sensitivity with regard to some mix design variables (Kaseer et al., 2018; Nemati, Haslett, Dave, & Sias, 2019; Zhou et al., 2017). Further, it has been reported that the post-peak response of brittle materials cannot be captured, hence hindering the calculation of the FI parameter (Zhu, Dave, Rahbar-Rastegar, Sias Daniel, & Zofka, 2017).

2.3.4 Disc-shaped compact tension test

The disc-shaped compact tension (DCT) test is used to determine the fracture energy of the asphalt mixtures at low temperatures by using a disc-shaped specimen. This test has become an ASTM standardized test method (ASTM D7313[8]). Even though there is no current application of DCT fracture energy on predicting the fatigue cracking performance of asphalt pavements, researchers have shown a positive but weak correlation with the ALF performance results (Ozer et al., 2018). DCT sample preparation requires boring holes and notching which, compared to IDT and SCB tests involves a longer time for sample preparation, but its greatest advantage is that the crack path is longer and provides more robust information on the fracture behavior of the mixtures. A testing time for running the test is relatively short and a minimum of technical training is required to perform the test.

[8] Determining Fracture Energy of Asphalt-Aggregate Mixtures Using the Disk-Shaped Compact Tension Geometry

Table 2.1 Summary of laboratory fatigue test methods

Test class	Test ID	Testing protocol and specimen dimensions	Test effort: Advantages	Test effort: Limitations	Equipment price	Test control mode	Performance measure criteria	Sample preparation and test duration (days)	Test validation
Non-Homogeneous	Four-point bending beam fatigue (4PBB)	AASHTO TP 107 L = 380 mm, W = 63 mm, T = 50 mm	- Established test method, - Similar to field behavior of asphalt pavement, - Medium training required, - Implemented in pavement design, - Easy data analysis and interpretation	- Lengthy, - Costly - Extensive material required, - Troublesome specimen fabrication and precision - High variability	~ $45,000	- Stress controlled - Strain controlled - Fracture mechanics - Fundamental	- Breaking stress - Breaking strain - Reduction in stiffness	> 20	Field
	Trapezoidal beam fatigue	EN 12697 B = 55 mm x 20 mm, b = 25 mm x 25 mm, L or H = 250 mm	- Common testing method in Europe, - Medium training required, - Implemented in pavement design, - Easy data analysis and interpretation	- Lengthy, - Costly - Extensive material required, - Troublesome specimen fabrication and precision - High variability - Gluing operation required	~ $45,000	- Stress controlled - Strain controlled - Fundamental	- Breaking stress - Breaking strain - Reduction in stiffness	> 20	4PBB

Table 2.1 (cont'd)

Supported flexure fatigue test	Barksdale, 1977	- Good simulation of field conditions	- The test is more time consuming than many other fatigue tests - Lengthy, - Costly - Relatively expensive		- Intermediate loading - Fundamental	- Breaking stress - Breaking strain - Reduction in stiffness	> 20	4PBB
Diametral test	Kennedy, 1977 T = 64 mm, D = 100 mm	- Simple test method, - Similar to field behavior of asphalt pavement, - Low training required, - Same equipment for other purposes - Easy data analysis and interpretation - Easy run on lab & field samples - Repeatable	- Underestimate fatigue life - Accumulation of permanent deformation	~ $50,000	- Stress controlled - Fundamental	- Breaking stress - Reduction in stiffness	> 20	4PBB
Loaded wheel tester	Van Dijk, 1975	- Good simulation of field conditions - Fatigue behavior under wheel loads - Crack evolution can be monitored	- Lengthy, - Costly - Special equipment required - Accumulation of permanent deformation	> $50,000	- Stress controlled - Strain controlled	- Breaking stress - Breaking strain	> 10	

Table 2.1 (cont'd)

Homogenous	Uniaxial fatigue test	AASHTO TP 107 L = 130 mm, D = 100 mm Texas A&M L = 150 mm, D = 100 mm MSU* L = 130, 150 mm, D = 100, 75, 68 mm	- Established test method, - Implemented in pavement design, - Simpler, faster, cheaper if compared to 4PBB - *in Tension-Compression, similar to field behavior of asphalt pavement,	- Lengthy, - Costly - Special equipment required - Long training required, - Troublesome specimen fabrication and precision - High variability - Gluing operation required - Complex data analysis and interpretation	> $50,000	- Stress controlled - Strain controlled - Fracture mechanics - Fundamental	- Breaking stress - Breaking strain - Reduction in stiffness	> 10	Field 4PBB Diametral test
Screening	Texas overlay tester	TxDOT Standard Tex-248-F L = 150 mm, W = 76 mm, T = 38 mm	- Good field correlation - Medium training required - Implemented in pavement design - Easy data analysis and interpretation	- Lengthy, - High variability - Gluing operation required	~ $45,000	- Displacement controlled - Fracture mechanics	- Reduction in load	> 3	Field

Table 2.1 (cont'd)

Indirect tension test	AASHTO T 322 T = 50 mm, D = 150 mm ASTM D 8225 T = 62 mm, D = 150 mm	- Simple test method, - Low training required, - Same equipment for other purposes - Easy data analysis and interpretation - Easy run on lab & field samples - Repeatable	- Numerous fatigue performance evaluation criteria - Under development for fatigue evaluation - Not able to implement in pavement design	> 10,000	- Fracture mechanics	- CT_{index} - TI - N_{flex} Factor	> 1	Field
Semi-circular beam test	AASHTO TP124 T = 50 mm, D = 150 mm, Notch = 15 mm LTRC T = 57 mm, D = 150 mm, Notch = 25.4, 31.8, 38.0	- Relatively simple test method, - Medium training required, - Same equipment for other purposes - Easy data analysis and interpretation - Can be run on lab & field samples - Well correlated with field data	- High variability - Not sensitive to some of mix design properties - Not able to implement in pavement design	> 10,000	- Fracture mechanics	- FI - Jc	> 3	Field

Table 2.1 (cont'd)

Disc-shaped compact tension test	ASTM D 7313 T = 50 mm, D = 150 mm, Notch = 35 mm	- Relatively simple test method, - Medium training required, - Same equipment for other purposes - Easy data analysis and interpretation - Can be run on lab & field samples - Well correlated with field data at low temperature	- High variability - Not sensitive to some of mix design properties - Not able to implement in pavement design	> 10,000	- Fracture mechanics	- Fracture energy	> 3	Field

3. OBJECTIVES AND RESEARCH PLAN

The overall goal of this study is to develop a practical fatigue testing alternative to characterize the fatigue performance of asphalt mixtures, sensitive to various aspects of asphalt mix design, repeatable and simple. In order to achieve this goal, the following specific objectives were established:

- Development of practical laboratory equipment and protocol to characterize the fatigue performance of the asphalt mixtures.
- Implementation of Timoshenko Beam Theory to analyze the 3PBC test results.
- Investigate the applicability of Viscoelastic Continuum Damage theory formulations to new test protocol and estimate fatigue lives (N_f) of asphalt mixtures at various strain levels, temperatures, and frequencies from a single test run at one strain level/temperature/frequency combination.
- Investigate the potential of estimating the Poisson's ratio using the test data.
- Perform ruggedness evaluation of the test.

A research plan was devised to materialize these objectives. The tasks for the preliminary research plan are summarized in the sub-section below:

Stage I. Development of the Three-Point Bending Cylinder (3PBC) fatigue test system

As part of this stage, the development of the 3PBC fatigue testing system was discussed. Data analysis methodologies were detailed and validated for different testing conditions. The specific tasks are summarized below:

3.1 Task 1: Development of the Three-Point Bending Cylinder (3PBC) Test Setup

The objective of Task 1 is the design of a robust 3PBC test setup for testing cylindrical asphalt specimens. The test setup was designed for its seamless integration into the Material

Testing System (MTS) and Asphalt Mixture Performance Tester (AMPT) units. Of particular interest was the speed of mounting of asphalt sample into the fixture, which is important to reduce temperature equilibration time. The test setup was made of high-strength steel to avoid any undesirable bending while testing the specimen.

3.2 Task 2: Application of Timoshenko Beam Theory to analyze the 3PBC test results

Mathematical formulations were developed based on the Timoshenko Beam Theory to calculate the dynamic modulus (damaged) for each loading cycle. The developed formulations were validated through a series of 3D finite element (3D FE) analyses. Furthermore, numerous 3PBC laboratory tests were performed to validate the theoretical results obtained from the application of the Timoshenko Beam Theory. Also, the developed formulations were used to perform indirect estimation of Poisson's ratio from the 3PBC test data.

3.3 Task 3: Application of Viscoelastic Continuum Damage (VECD) theory to 3PBC test

One of the main objectives of this work was to develop a test method to reduce the testing burden. The adaptation of VECD theory in fatigue characterization of asphalt mixtures significantly reduces the experimental burden required to calibrate phenomenological fatigue life formulation. Implementation of VECD theory to model the mechanical response of the cylindrical specimens tested using the 3PBC test results as part of this task. Various mixtures were tested at different strain levels, temperatures and frequencies and their N_f were measured. The VECD constitutive model was implemented to construct the damage characteristic curve (C-S), which is a unique curve that can be used to predict the fatigue life of asphalt mixtures at different frequencies and temperatures at a required strain level.

Stage II. Ruggedness evaluation

This stage focuses on performing the ruggedness test of the 3PBC test. To achieve this goal, the task for the execution of ruggedness testing is presented below:

3.4 Task 4: Ruggedness evaluation of the developed 3PBC test system

The important results and inferences obtain from the previous tasks were utilized to investigate the ruggedness of the developed 3PBC test system. This task was performed in general accordance with ASTM E 1169[9]. The ruggedness testing plan executed in this project involves (i) identifying the major test factors that may influence the 3PBC test and (ii) developing a statistically sound yet efficient laboratory experimental design.

[9] Standard Practice for Conducting Ruggedness Tests

4. EXPERIMENTAL PROGRAM AND MATERIALS

A laboratory experimental program was developed including 3PBC fatigue, linear viscoelastic dynamic modulus ($|E^*|_{LVE}$) and push-pull (tension-compression) fatigue tests. The work plan was divided into two stages: Stage I involves the examination of the design and robustness of the 3PBC test system, and data analysis methodology. Stage II focuses on ruggedness evaluation of the developed 3PBC test system to identify the effects of certain parameters that influence the test results and determine acceptable limits.

4.1 Experiments for Stage I. Development of the Three-Point Bending Cylinder (3PBC) fatigue test system (Tasks 1 through 3)

As part of this stage, three different mixtures with two different binder types, aggregate gradations, and mix designs were tested. The nominal maximum aggregate size (NMAS) of the considered mixtures is 12.5 mm (see Table 4.1). Crumb rubber and polymer modified binders with different asphalt contents were used for each mixture. A summary of the mix design characteristics and volumetric properties are provided in Table 4.1. The Superpave Gyratory Compactor (SGC) was used to produce all the performance testing samples (i.e., 3PBC, |E*| and PP). All samples had 7 ± 0.5 % air void content after coring and/or cutting. Figure 4.1 illustrates the overall experimental flowchart. In Stage I, the linear viscoelastic dynamic modulus ($|E^*|_{LVE}$) tests were conducted using the AMPT, and the |E*| master curves were developed in general accordance with the AASHTO T378 and R84 protocols. All test specimens were compacted to a height of 180 mm using the SGC with a minimum of two replicates per mixture. The $|E^*|_{LVE}$ tests in AMPT were conducted at temperatures of 4, 20, 40 and 54 ºC, and at loading frequencies of 10, 1 and 0.1 Hz.

The diameters of specimens for both 3PBC and PP tests were 68 mm. The heights of the PP samples were 150 mm. The heights of the 3PBC samples were the same as the gyratory

compactor, which was 180 mm. It should be noted that this height may be reduced to save material in the future for 3PBC samples but for consistency between PP and 3PBC test samples, the SGC height was kept the same. The PP and 3PBC tests were conducted at varying levels of frequency, temperature and strain level combinations (see Figure 8.2 - Figure 8.4). This was done to investigate and validate the applicability of the Viscoelastic Continuum Damage (VECD) theory on the 3PBC samples. The axial deformations of PP samples were measured by means of three LVDTs mounted on the samples at 120 ^{o} intervals over the middle 70 mm of the sample, whereas the central deflections needed in 3PBC formulations were measured using 2 LVDTs placed in the middle clamp (see Figure 5.1).

Table 4.1 Mixture volumetric properties and gradations for asphalt mixtures

	Stage I			Stage II	
Mixture ID	4E3DVR[(1)]	4E3SBS[(2)]	4E30SBS[(2)]	5E3Neat	3E3Neat
Aggregate type	A	A	B	C	D
Mix Design ESALs (Millions)	3	3	30	3	3
NMAS (mm)	12.5	12.5	12.5	9.5	19.0
Asphalt PG	PG70-28	PG70-28	PG70-28	PG64-28	PG58-28
Asphalt cement (%)	5.7	5.5	5.8	6.3	5.2
N_{design}	86	86	109	86	86
Design air voids (%)	3.0	3.0	3.0	3.5	3.0
VMA[(3)] (%)	18.5	19.6	18.8	16.4	13.8
VFA[(4)] (%)	64.8	63.5	65.2	78.7	78.3
RAP[(5)] (%)	20	20	15	22	28
Sieve size		Percent passing, %			
inch	mm				
3/4"	19	100.0	100.0	100.0	100.0	100.0
1/2"	12.5	91.2	91.2	99.3	99.9	89.2
3/8"	9.5	88.3	88.3	89.4	99.3	82.1
#4	4.75	78.2	78.2	65.9	78.4	61.7
#8	2.36	53.8	53.8	53.3	63.5	51.5
#16	1.18	36.9	36.9	40.9	46.3	37.9
#30	0.6	25.8	25.8	28.4	31.2	25.3
#50	0.3	15.8	15.8	12.9	16.2	13.1
#100	0.15	7.8	7.8	6.2	7.9	7.2
#200	0.075	5.1	5.1	4.5	5.0	4.7

Note: [(1)] DVR = De-vulcanized Rubber modified asphalt binder, [(2)] SBS = Styrene-Butadiene-Styrene modified asphalt binder, [(3)] VMA = Voids in Mineral Aggregate, [(4)] Voids Filled With Asphalt, [(5)] RAP = Recycled Asphalt Pavement

4.2 Stage II. Ruggedness evaluation

As part of this stage, two new asphalt mixtures, particularly 3E3 and 5E3, were selected and tested. The 3E3 is a base mixture with 19.0 mm NMAS and PG58-28 binder grade, whereas, 5E3 is a surface mixture with 9.5 mm NMAS and PG64-28 binder grade. Mix design details and volumetric properties are shown in Table 4.1. Sample preparation and |E*| test procedure were performed in accordance with the same procedures followed in Stage I.

The purpose of the ruggedness testing is to identify the factors that significantly influence the results of the 3PBC test (i.e., that influence number of cycles to failure and damage characteristics (C - S) curve). Based on previous experiences in fatigue testing of asphalt mixtures

and the literature review conducted at the time of preparing this document, several general factors have been identified as factors that may potentially influence the 3PBC test results. These tentative factors and their levels for consideration in the ruggedness experimental design are summarized and discussed. To fulfill this goal, the analysis of the data was performed in general accordance with ASTM E 1169 standard. Factor effects are calculated as the difference between average responses obtained after conducting 3PBC testing using high and low levels of the factor in question.

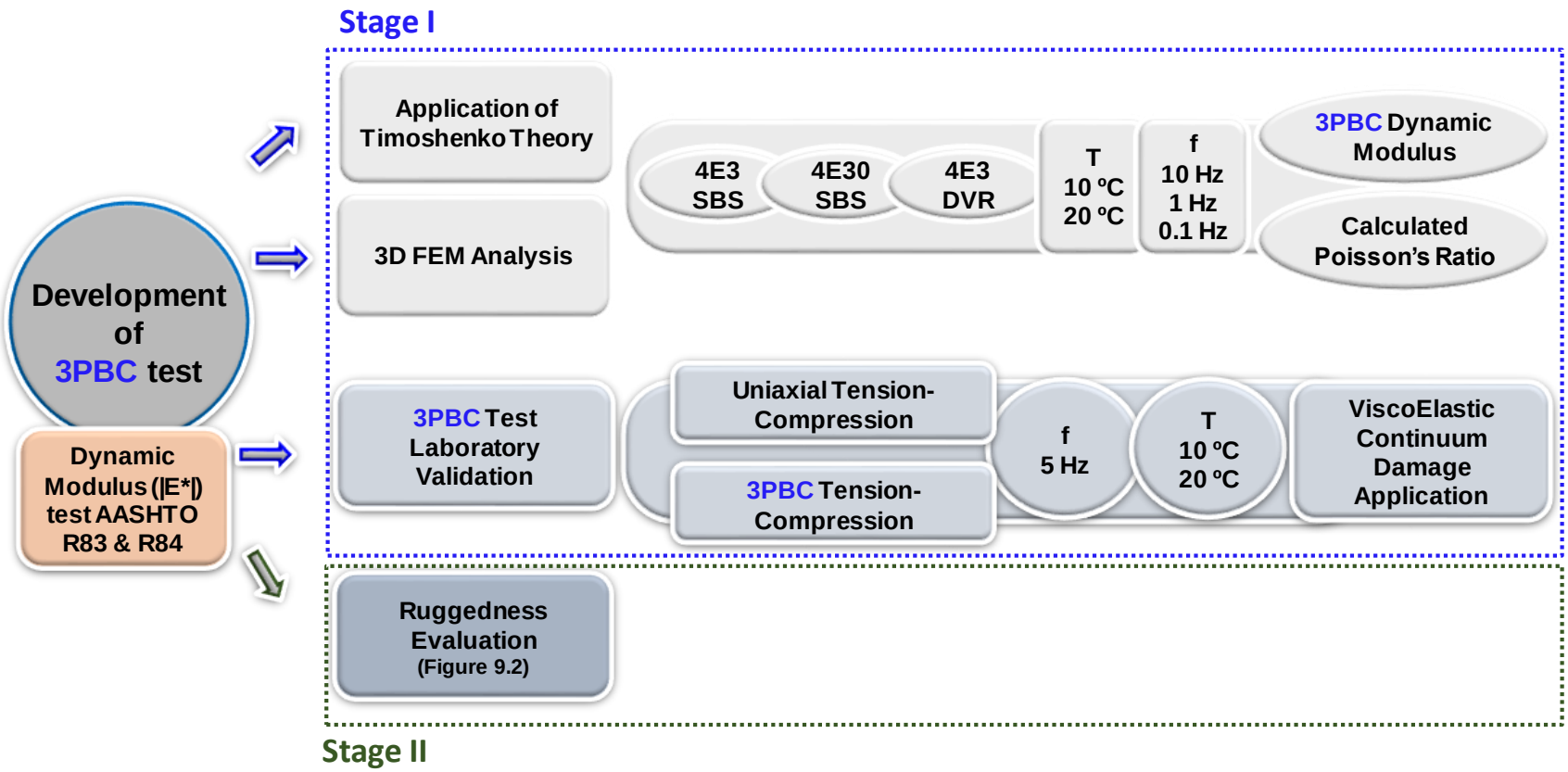

Figure 4.1. Experimental flow chart.

5. DEVELOPMENT OF THE THREE-POINT BEAM CYLINDER (3PBC) TEST SETUP (*Task 1*)

The objective of this part of the study was the design of the 3PBC fatigue testing system. Factors including production cost, easy to use and compatibility with different testing units were considered during the design process. Figure 5.1 illustrates the latest Three-Point Bending Cylinder (3PBC). Test setup, which is composed of a solid base, two fixed end supports used to clamp the sample and a central clamp for application of cyclic (zero-mean) vertical load. Supports and loading clamps are composed of two C-shaped pieces, which are screwed together to hold the asphalt sample in-place. The lower C-shaped pieces are connected (screwed or welded) to the base plate. The distance between two supports is 125 mm (4.9") and the inner diameters of clamps are 68 mm (2.7") each. All the parts (except the LVDT holders) are made of high-strength steel to prevent any undesirable deformation during the test.

The base plate includes four orienting knobs to provide proper placement of the central clamp to ensure that the load is applied at the center of the specimen.

The tests in this study were conducted using a servo-hydraulic Material Testing System (MTS) unit as presented in Figure 5.2a. Nevertheless, the 3PBC test setup is very well suited to be placed within the chambers of the Asphalt Mixture Performance Tester (AMPT) unit (Figure 5.2b). It should be noted that, for verification purposes, multiple 3PBC tests were run in AMPT using the uniaxial fatigue protocol in AMPT and very promising results were obtained. A testing protocol well suited with 3PBC test requirements is still under development, therefore no results are presented herein.

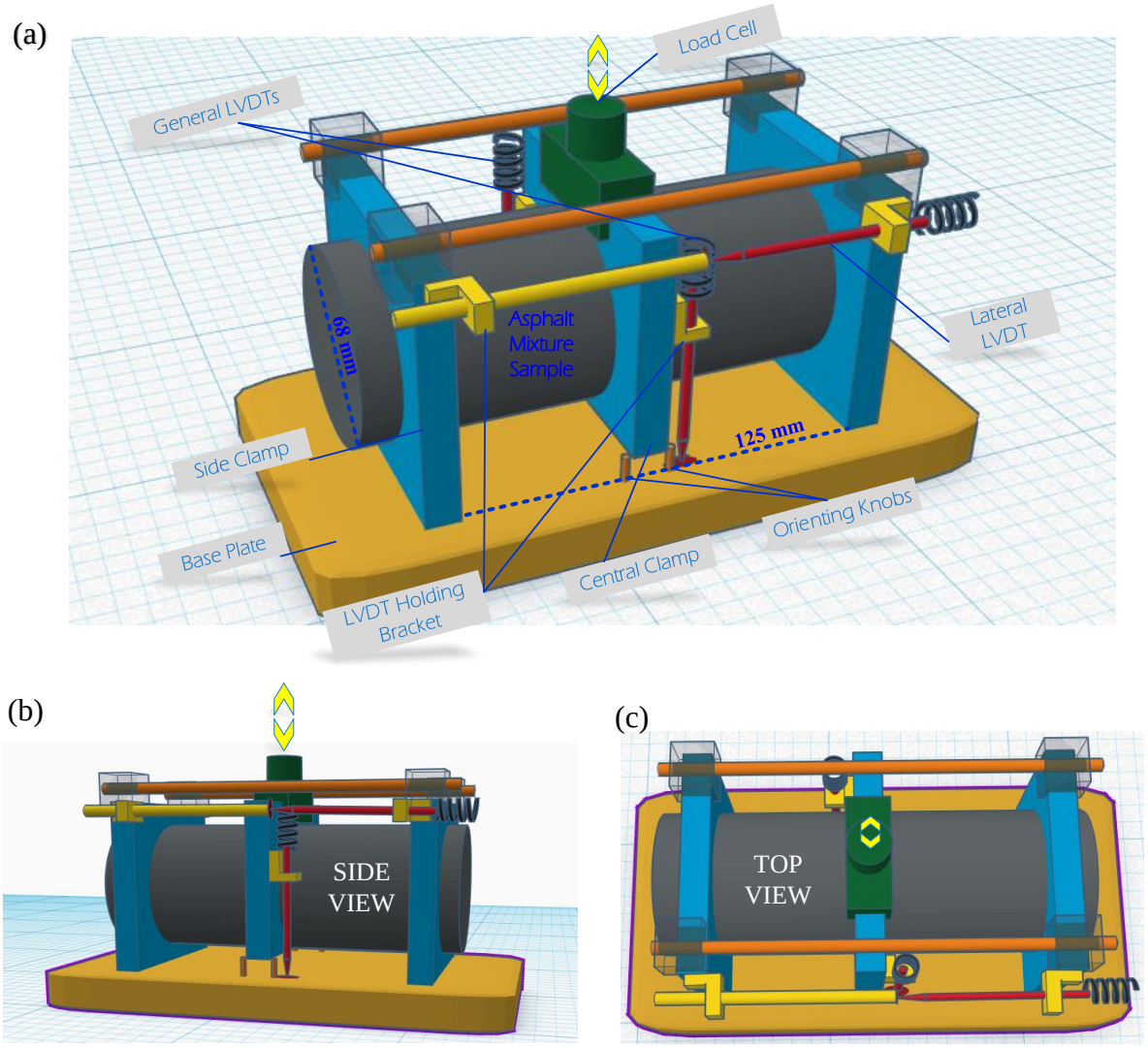

Figure 5.1. (a) General schematic of the 3PBC fixture, (b) side view and (c) top view with a loaded specimen.

The testing temperature in MTS was controlled through a forced-air draft conditioning chamber. A sinusoidal strain-controlled vertical load (with zero mean) is applied at the center of the specimen through the vertically free-moving clamp as illustrated in Figure 5.1 and Figure 5.2.

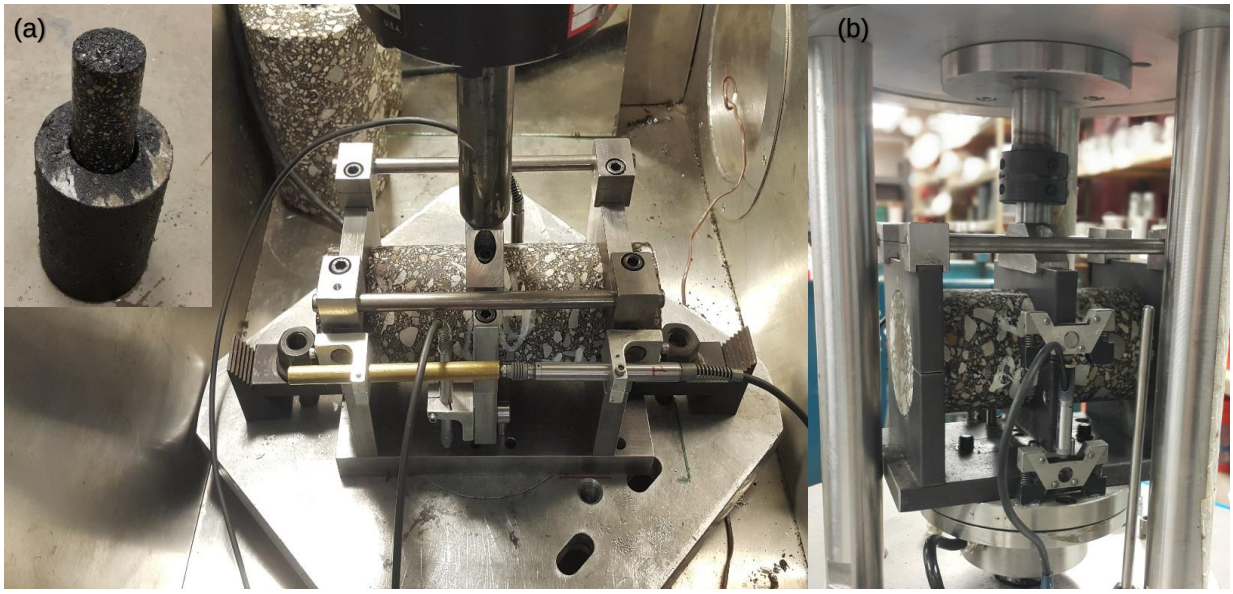

Figure 5.2. 3PBC test setup with a loaded specimen in the (a) Material Testing System (MTS) and (b) Asphalt Mixture Performance Tester (AMPT).

The displacement measurements required for calculating the maximum strain at the bottom-center (or top-center) of the specimen were obtained using two linear variable displacement transducers (LVDTs) attached on both sides of the central clamp. The difference between the two LVDTs was observed to be very low. However, during the test, the strain level was controlled through the actuator strain gauge and not LVDTs. This was done to avoid equipment damage due to the potential instabilities of actuator caused by the slow feedback of LVDT measurements. This problem is less pronounced in most AMPTs, therefore, on-specimen LVDT controlled testing is quite possible with the AMPTs. Besides, a third LVDT was attached to the top of the fixed supports to measure any potential lateral displacement due to steel bending, which is not desirable. As mentioned earlier, the 3PBC is a zero-mean cyclic strain-controlled test and the test ends when the microcracks propagate through the entire sample diameter (which can be observed visually). The stresses and strains for each cycle were computed using the Timoshenko Beam Theory.

The current design of the 3PBC test setup possesses the most advantages of the current state of practice tests and includes more improvements. The new test system proposed in this research study is a cyclic three-point beam test setup, where the sample is a cylindrical asphalt specimen prepared using a gyratory compactor. Samples do not need to be cut, i.e., a diamond saw is not necessary. Also, there is no need for end-platens and gluing jig. These characteristics reduce the cost of the equipment, amount of material needed to run the test, and overall test duration (from sample preparation to the end of testing) is much shorter than the traditional fatigue testing alternatives.

6. APPLICATION OF TIMOSHENKO BEAM THEORY TO 3PBC SETUP (*Task 2)*

The Euler beam theory commonly used for the analysis of slender isotropic beams considers the beam kinematics in terms of flexural stiffness. The low aspect ratio of 3PBC requires considerations of shear-induced deformations in the so-called "thick-beam", i.e., Timoshenko Beam Theory (Cowper, 1966; Timoshenko & Gere, 1972).

The analytical formulations presented herein for the stiffness of thick 3PBC are based on the following assumptions:

- The 3PBC is considered as a short beam with both ends clamped
- The central clamp restrains the sample from bending and moves parallel to end-clamps
- Poisson's ratio of 3PBC is assumed to be constant at a given cycle, during a particular test at a certain frequency/temperature combination (see the end of this section for a discussion on Poisson's ratio).

6.1 Timoshenko Beam Model and Poisson's Ratio Prediction

Initially, the Timoshenko beam theory has been presented herein by considering 3PBC as a linear elastic material. The formulations are then extended to viscoelastic behavior (for a given frequency/temperature combination) using the elastic-viscoelastic correspondence principle (Schapery, 1984). For a linear elastic, isotropic homogenous slender beam with both ends fixed and loaded at the center by a force P_z, the Euler theory states that the maximum vertical deflection (δ_z) can be calculated as follows (Timoshenko, 1940):

$$\delta_z = \frac{P_z L^3}{192 E I_{xx}} \qquad [6.1]$$

where, δ_z is the maximum vertical deflection, L is the span length, E is Young's modulus and I_{xx} is the moment of inertia along axis xx. The schematic view of a fixed beam with a central load is illustrated in Figure 6.1.

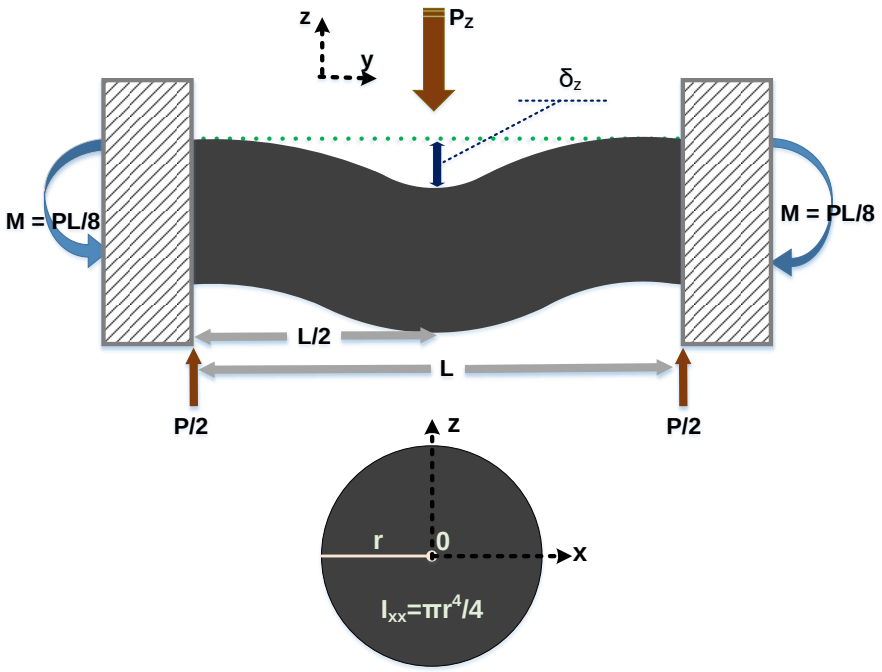

Figure 6.1. Exaggerated deflection of a fixed beam with a central load.

When the aspect ratio (length to diameter ratio) of a cylindrical beam is less than 6, the shear-induced deflection becomes significant and Euler theory does not apply (Du, Lin, Lu, & Zhang, 2010). For such beams, Timoshenko beam theory needs to be used to calculate the deflection as follows (Timoshenko & Gere, 1972);

$$\delta_z = \frac{P_z L^3}{192 E I_{xx}} + \frac{2\beta P_z L(1+\nu)}{EA} \qquad [6.2]$$

where, β is the shear coefficient, A is the cross-sectional area.

Hutchinson (Hutchinson, 2001) derived the following expression for the shear coefficient (β) for beams with low aspect ratio:

$$\beta = \frac{6(1+\nu)^2}{7+12\nu+4\nu^2} \quad [6.3]$$

where, ν is the Poisson's ratio.

Equation [6.2] can be rearranged to yield elastic modulus as a function of the vertical load (P_z) and measured deflection at the center (δ_z):

$$E = \frac{P_z L[AL^2 + 384\beta I_{xx}(1+\nu)]}{192\delta_z I_{xx} A} \quad [6.4]$$

For viscoelastic materials that are exposed to cyclic load at a constant frequency, Equation [6.4] can be used to calculate the magnitude of the dynamic modulus at each cycle N (i.e., $|E^*|_N$) as follows:

$$|E^*|_N = K\frac{P_z(N)}{\delta_z(N)} \quad [6.5]$$

$$\mathrm{K} = \frac{\mathrm{L}[\mathrm{AL}^2 + 384\beta\mathrm{I_{xx}}(1+\nu)]}{192\mathrm{I_{xx}A}} \quad [6.6]$$

where, $|E^*|_N$ is the (damaged or undamaged) dynamic modulus at each cycle N, $P_z(N)$ and $\delta_z(N)$ are the peak-to-peak load and deflection, respectively.

Selection of the appropriate Poisson's ratio is important for the accuracy of the $|E^*|_N$ in Equation [6.5]. It has been shown that the Poisson's ratio of an asphalt mixture is well correlated to the dynamic modulus (|E*|) (Maher & Bennert, 2008; N. Tapsoba et al., 2015). Maher and Bennert (Maher & Bennert, 2008) showed that the following relationship can be used to compute the Poisson's ratio from the |E*|:

$$\nu = a * ln|E^*| + b \quad [6.7]$$

where, a and b are the slope and intercept of the $\nu - |E^*|$ relationship.

One of the important advantages of the 3PBC test is that one can determine the a and b constants of $\nu - |E^*|$ relationship, i.e., the Poisson's ratio of an asphalt mixture. This can be

achieved by running the 3PBC test at a relatively low load level (so that the sample is within linear viscoelastic range) at a few temperatures/frequencies. Then the error between the $|E^*|$ computed using the Equations [6.5] through [6.7] (herein referred to as $|E^*|_{3PBC}$) and corresponding $|E^*|$ obtained from the traditional uniaxial dynamic modulus test using the Asphalt Mixture Performance Tester (herein referred to as $|E^*|_{AMPT}$) is minimized by varying the a and b constants (Equation [6.7]) as follows:

$$|E^*|_{3PBC} - |E^*|_{AMPT} = 0 \quad [6.8]$$

Steps of estimating Poisson's ratio-|E*| relationship from 3PBC tests can be summarized as follows:

1) Run Dynamic Modulus (|E*|) tests following AASHTO T378 and generate the |E*| master curve in accordance with AASHTO R84.
2) Calculate the |E*| corresponding to the frequency and temperature combination for the planned 3PBC test. This |E*| is herein called $|E^*|_{AMPT}$.
3) Run the 3PBC test at the planned frequency and temperature combination.
4) Assume initial a and b values for the Poisson's ratio formulation (Equation [6.7]).
5) Compute the Poisson's ratio using Equation [6.7], by using |E*| computed from the dynamic modulus master curve obtained in step 1 (i.e., $\nu = a * ln|E^*|_{AMPT} + b$)
6) Plugin the Poisson's ratio computed in step 5 to Equation [6.6] to compute K. Then plug in the computed K (as well as P_z and δ_z) to Equation [6.5] to compute the |E*|. This |E*| is herein called $|E^*|_{3PBC}$.
7) Compute the difference between $|E^*|_{3PBC}$ and $|E^*|_{AMPT}$.

8) Vary the a and b values, repeat the steps 5, 6 and 7 until the error between $|E^*|_{3PBC}$ and $|E^*|_{AMPT}$ is minimized (Equation [6.8]).

In order to verify this procedure to estimate a and b constants, a 3D finite element analysis (3D FE) was performed to simulate a perfect 3PBC test, using the exact geometry of the 3PBC sample and the fixtures. The results of the 3D FE analyses are shown in the next section. In addition, actual 3PBC tests at a low strain (load) level were also conducted and the a and b constants computed and compared against the measured a and b constants reported in (Maher & Bennert, 2008). Results are presented in the later sections.

Once a and b constants (for the Poisson's ratio-|E*| relationship) are estimated for the linear viscoelastic (undamaged) state, they can be used in 3PBC fatigue tests in the damaged state because Poisson's ratio is known not to change significantly during the fatigue tests (N. Tapsoba et al., 2015). Since both left- and right-hand side of the Equation [6.6] includes the |E*|, another iterative procedure is needed. However, the fact that Poisson's ratio does not change significantly from one cycle to another can be used to simplify the computational steps. A summary of the steps of computing |E*| at each cycle (i.e., $|E^*|_N$) as damage grows are summarized below:

1) Using the known values of a and b constants, compute the Poisson's ratio using Equation [6.7] for cycle N = 1 (initial condition), by using |E*| computed from the dynamic modulus master curve (i.e. ($\nu_{N=1} = a * ln|E^*|_{AMPT} + b$)). This condition is the undamaged state.
2) Since the Poisson's ratio does not change from one cycle to another significantly (N. Tapsoba et al., 2015), it is assumed that $\nu_{N+\Delta N} \cong \nu_N$.
3) Calculate $\beta_{N+\Delta N}$ using in Equation [6.3] and $K_{N+\Delta N}$ using Equation [6.6].

4) For the next cycle N+ΔN, compute the damaged modulus,$|E^*|_{N+\Delta N}$, using Equation [6.5].
5) For the next cycle N+ΔN, compute the Poisson's ratio using Equation [6.7], by using |E*| computed from the previous cycle (i.e. ($\nu_{N+\Delta N} = a * ln|E^*|_N + b$))
6) Repeat steps 2 through 5 for all subsequent cycles.

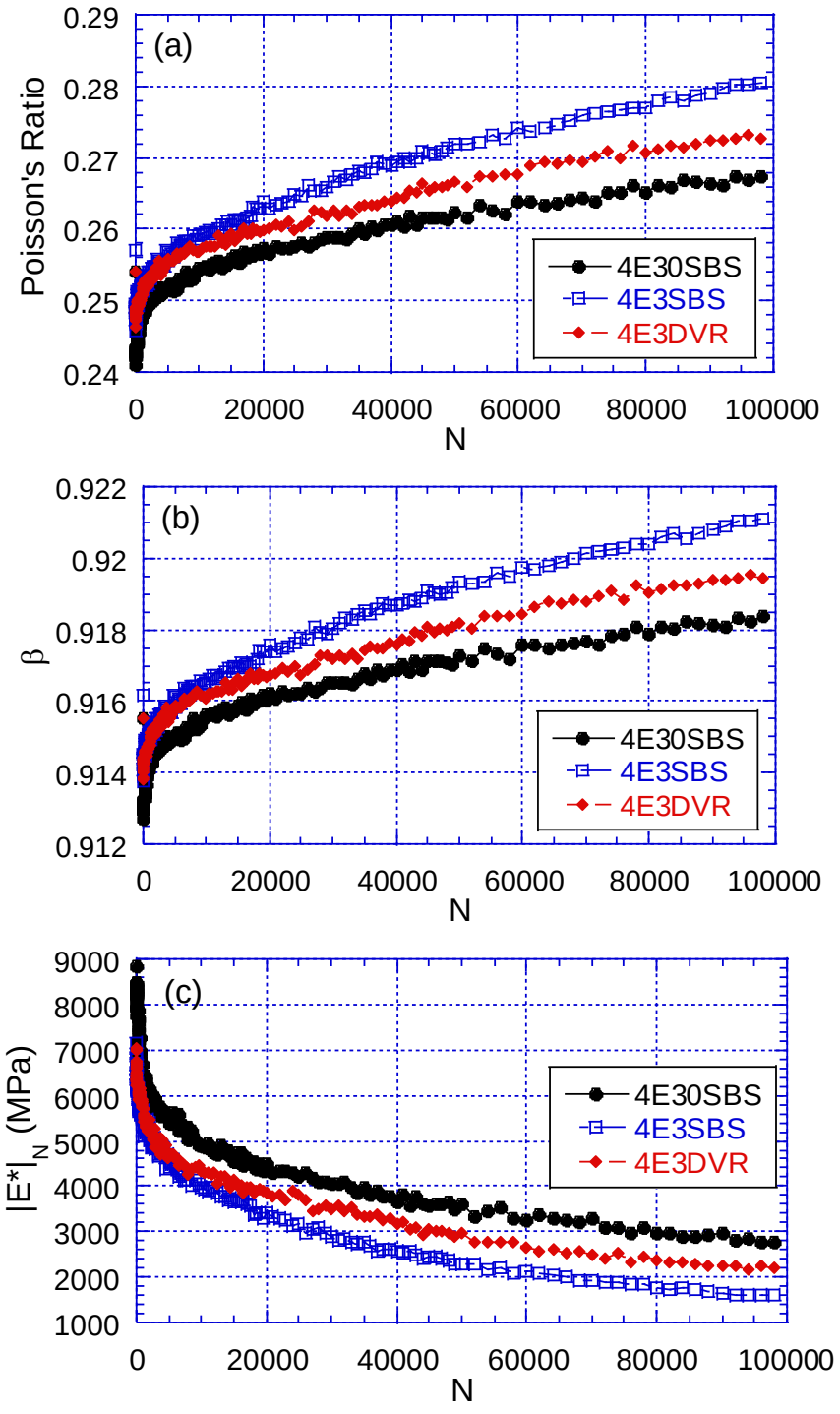

Figure 6.2. Evolution of (a) Poisson's ratio, (b) β and (c) |E*| values with cycles during 3PBC tests.

Figure 6.2 shows three examples of the evolution of (a) Poisson's ratio (ν_N), (b) β and (c) $|E^*|_N$ values with cycles during 3PBC tests. As shown in Figure 6.2a, the Poisson's ratio increases with cycles (as expected), however, the total increase in ν_N (at the end of 100,000 cycles) is about 10% of the initial value, which is relatively low. The increase in β is much lower than that of ν_N, where the total increase at the end of 100,000 cycles is less than 1%. Therefore, these values may be assumed as constant to further simplify the formulations of 3PBC. However, this simplification was not done in this particular study for the purpose of keeping the level of accuracy as high as possible.

Lastly, it should be noted that the maximum tensile and compressive stresses in the 3PBC sample occur on the farthest point from the neutral axis. For a circular cross-section the maximum tensile and compressive stresses are equal and can be obtained from the following expression:

$$(\sigma_y)_{max} = -(\sigma_y)_{min} = \frac{M}{S} \quad [6.9]$$

where, σ_x is the normal stress, M is the maximum bending moment at the center of the beam ($M = P_z L/8$ for the 3PBC setup), S is the section modulus, which (for a solid circular cross-section) is calculated as $S = \pi d^3/32$ (where d=diameter).

Even though Equation [6.9] was developed for pure bending with no shear presence, studies have shown that the effect of shear on normal stresses is negligible (American Wood Council, 2005; Timoshenko & Gere, 1972).

7. VERIFICATION AND VALIDATION OF 3PBC TEST (*Task 2)*

In order to be able to verify the applicability of Timoshenko Beam Theory on different asphalt mix samples, three-dimensional finite element (3D FE) analyses were performed to simulate the 3PBC test, using the exact geometry of the 3PBC sample and the fixture. In addition, the Timoshenko formulations were validated using the 3PBC laboratory tests and calculate the laboratory-measured |E*|values. The corresponding dynamic moduli at the respective temperature/frequency combinations were compared with the |E*| master curve of the asphalt samples measured using the AMPT.

7.1 Verification of Applicability of Timoshenko Beam Formulations to 3PBC setup using 3D Finite Element Analysis

Three-dimensional finite element (3D FE) analyses were performed to validate the theoretical results obtained from the application of the Timoshenko beam theory. For this purpose, the 3PBC test setup and loading were modeled in ABAQUS. Figure 7.1 shows a view of the 3D FE mesh used.

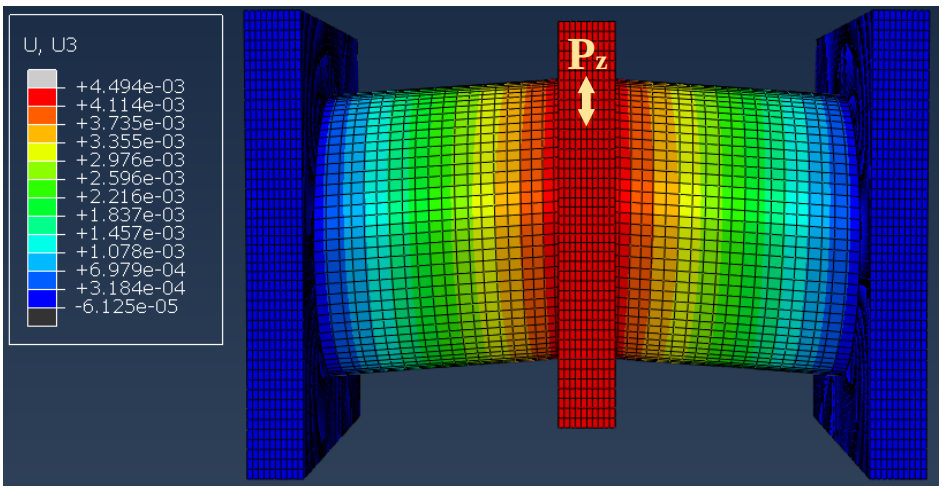

Figure 7.1. Deformation of the 3PBC test sample simulated in 3D FE (ABAQUS) (Deformation scale factor = 1000).

The simulations were run for two intermediate temperatures: 10 ºC and 20 ºC at the following frequencies; 10 Hz, 1 Hz, and 0.1 Hz. The asphalt samples in the 3D FE simulations were modeled in two modes using (i) elastic and (ii) viscoelastic properties. The first mode (elastic) was selected for its simplicity and computational efficiency. It is worth noting that the viscoelastic materials (i.e., asphalt) can be treated as elastic materials when subjected to a cyclic zero-mean test with a constant frequency. This practice is theoretically valid when the peak-to-peak results (i.e., force, displacement) are used. The respective moduli for each temperature/frequency combination were computed from the laboratory-measured dynamic modulus ($|E^*|_{AMPT}$) master curve of the asphalt mixtures utilized in this study, and used as input elastic modulus to 3D FE analysis.

As mentioned earlier, it has been shown that the Poisson's ratio is a function of frequency and temperature and related to the mixture |E*| (Maher & Bennert, 2008; Nouffou Tapsoba et al., 2014). In this part of the study, Equation [6.7] was used to estimate Poisson's ratio value as an input to each ABAQUS simulation and also in the application of the Timoshenko beam theory (i.e., Equation [6.6]).

For the ABAQUS simulations, *a* and *b* values of -0.024 and 0.45 were used, respectively. These values were obtained from the reference (Maher & Bennert, 2008) for mixtures with PG76-22, which is the closest PG to the mixtures used in this study. Simulations were in displacement control and corresponding forces in the center clamp were retrieved, then used in Equation [6.5] to calculate the |E*|. Since Equation [6.5] requires Poisson's ratio, an iterative procedure was performed using the Equations [6.7] and [6.8] to back-calculate the *a* and *b* values and these values were compared against the input a and b. The error (ξ) for each iteration was minimized using Equation [7.1]:

$$Error\ (\%) = \xi = \frac{|E^*|_{AMPT} - |E^*|_{3PBC}}{|E^*|_{AMPT}} * 100 \quad [7.1]$$

In addition, the viscoelastic 3D FE analyses were performed as an attempt to better simulate the real mechanical behavior of an asphalt mixture under cyclic loading. Therefore, the viscoelastic properties of the asphalt mixtures were assigned using Prony series coefficients. The relaxation modulus Prony series coefficients for each asphalt mixture at a certain testing temperature were obtained through interconversion from $|E^*|_{AMPT}$ master curve. Table 7.1 shows the relaxation times (τ_i) and dimensionless elastic coefficients (g_i) of the generalized Maxwell model (Prony series) at temperatures of 10 °C and 20 °C.

Figure 7.2a illustrates the input |E*|, which were obtained from the measured master curve (i.e., $|E^*|_{AMPT}$) and the corresponding |E*| (i.e., $|E^*|_{3PBC}$) calculated after ABAQUS simulations using Timoshenko beam theory. As shown in the figure, both the computed elastic $|E^*|_{3PBC}$ as well as the viscoelastic $|E^*|_{3PBC}$ values match very well with the values obtained from $|E^*|_{AMPT}$ master curve. While the ξ in computed elastic $|E^*|_{3PBC}$ ranges from 0.2 % to 16 %, the ξ computed for viscoelastic $|E^*|_{3PBC}$ is less than 12 %. The change in error range between the two simulation modes is primarily related to the assigned material properties and their effects on the mechanical response of the asphalt mixture when subjected to loading. The results also indicate that typically, the error increases with the decrease in loading frequency. However, at high frequency (i.e., 10 Hz), the error for both elastic and viscoelastic simulations is smaller than 5 % which is very low considering all the errors that can emanate from sample preparation. As a result, the 3PBC tests are recommended to be performed at a frequency of 5 Hz and above, where the maximum error is smaller compared to lower frequencies.

Figure 7.2b shows the comparison between the input Poisson's ratio versus the back-calculated elastic Poisson's ratio and viscoelastic Poisson's ratio for different simulations run at

different frequencies and temperatures. As shown, both the back-calculated Poisson's ratio values match very well with the input Poisson's ratio.

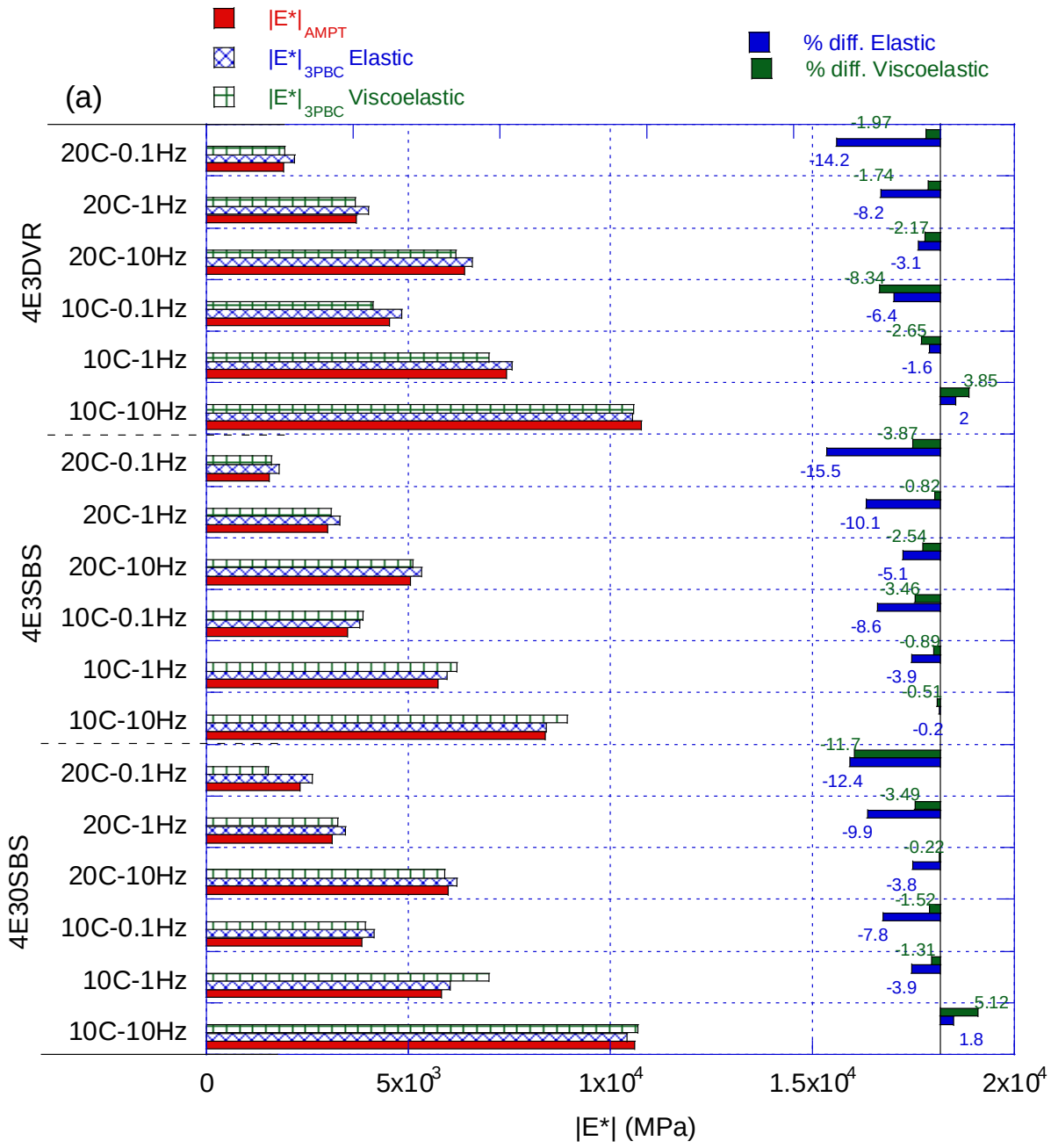

Figure 7.2. Comparison of (a) |E*| values input to 3D FE and those computed by the Timoshenko beam theory and (b) input Poisson's ratio and the back-calculated Poisson's ratio in elastic and viscoelastic modes.

Figure 7.2 (cont'd)

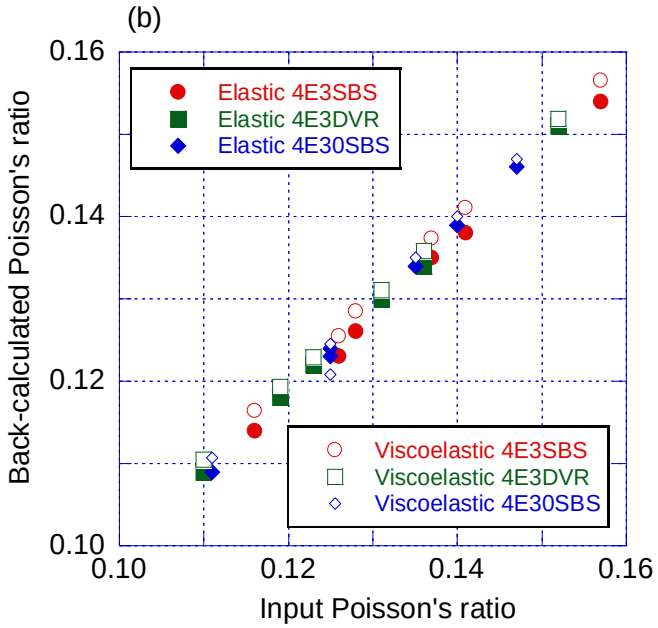

7.2 Timoshenko Beam Model Validation Using Laboratory Tests

The Timoshenko formulations were further evaluated using the 3PBC laboratory tests. After the 3PBC tests, the Equations [6.5] through [6.7] were used to calculate the laboratory-measured $|E^*|_{3PBC}$. The tests were run under cyclic loading with zero-mean at three intermediate temperatures: 10, 15, and 20 $^{\circ}$C at the following frequencies; 5 Hz and 1 Hz. The corresponding dynamic moduli at these temperature/frequency combinations were extracted from the |E*| master curve of the asphalt samples measured using the AMPT. The Poisson's ratio values were back-calculated using the same principle as described in the previous section.

Figure 7.3a shows the |E*| values that were obtained from the measured master curve (i.e., $|E^*|_{AMPT}$) and the corresponding |E*| (i.e., $|E^*|_{3PBC}$) calculated using Timoshenko beam theory. As shown, the |E*| values match reasonably well. The error ξ ranges from 0.4 % to 16 %, which are low considering the errors that can be caused by the sample-to-sample variability. Generally, it was observed that the ξ increases with the decreasing frequency and increasing temperature.

Figure 7.3b illustrates the back-calculated Poisson's ratio for different |E*| values, where a and b coefficients retrieved from (Maher & Bennert, 2008) match well with the back-calculated values from 3PBC setup.

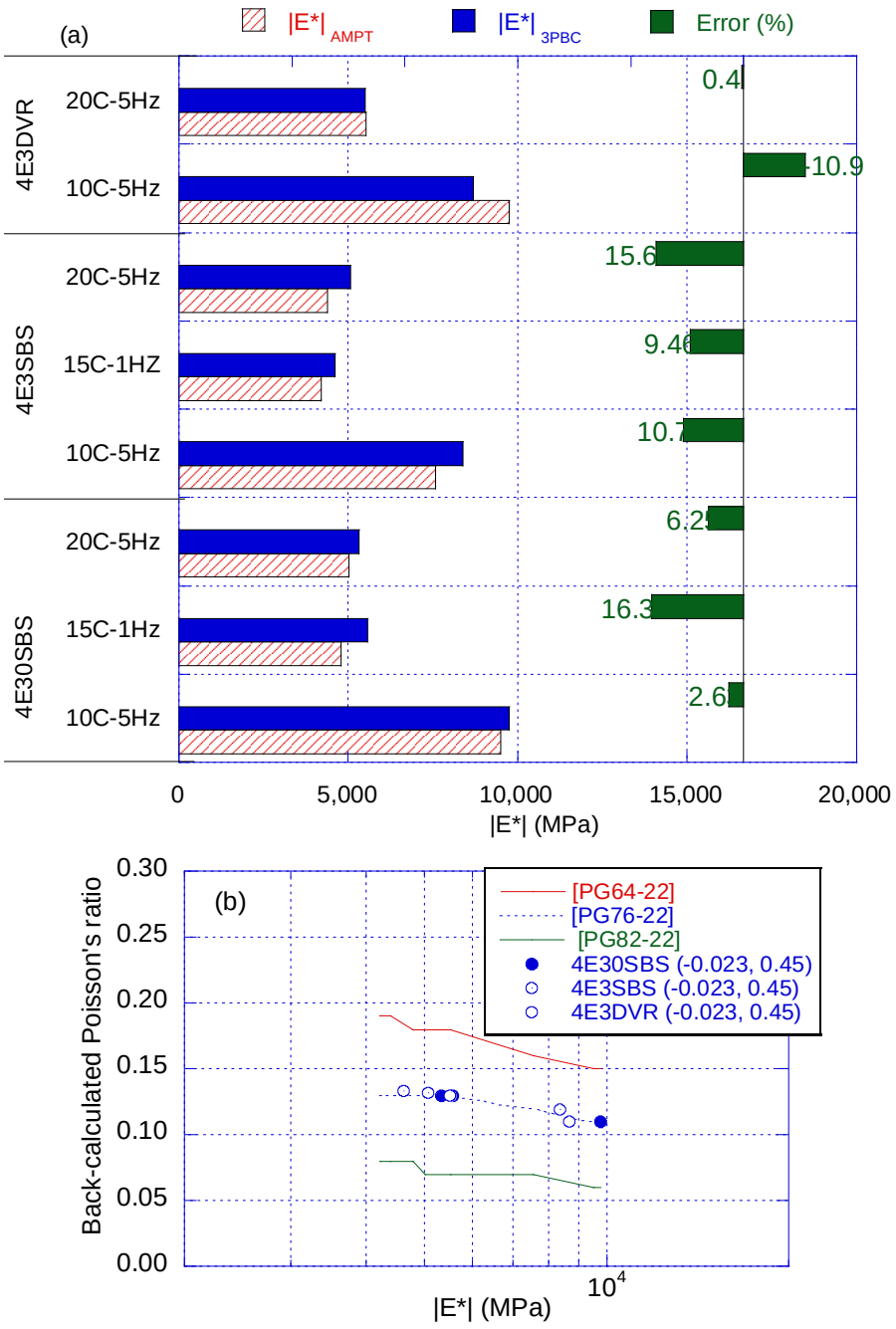

Figure 7.3. Comparison of (a) |E*| values obtained from |E*| master curve ($|E^*|_{AMPT}$) and those computed by the Timoshenko beam theory ($|E^*|_{3PBC}$) and (b) the back-calculated Poisson's ratio compared to the |E*| - Poisson's ratio relationships retrieved from (Maher & Bennert, 2008).

7.3 Summary of chapter findings

The objective of this part of the study was to evaluate the applicability of the Timoshenko theory on 3PBC test results via 3D finite element (3D FE) analysis. Also, several laboratory tests

were performed to validate the Timoshenko beam model results. The research findings from this study have been summarized as follows:

- Based on 3D FE analyses, it was shown that the error in elastic $|E^*|_{3PBC}$ ranges from 0.2 % to 16 %, whereas for viscoelastic $|E^*|_{3PBC}$ is less than 12 %. The results also indicate that typically, the error increases with the decrease in loading frequency. The 3PBC tests are recommended to be performed at 5 Hz and above, where the maximum error is less than 5 %. Additionally, the back-calculated Poisson's ratio values match very well.
- The laboratory results indicated that the |E*| values obtained from the measured master curve (i.e., $|E^*|_{AMPT}$) and the corresponding |E*| (i.e., $|E^*|_{3PBC}$) calculated using Timoshenko beam theory match reasonably well. The calculated error ranges from 0.4 % to 16 %. Generally, it was observed that the error increases with the decreasing frequency and increasing temperature.
- Also, the back-calculated Poisson's ratio for different |E*| values, where a and b coefficients retrieved from (Maher & Bennert, 2008) match well with the back-calculated values from 3PBC setup.

Overall, this part of the study showed the applicability of the Timoshenko beam theory to analyze data obtained from the 3PBC tests. Also, an indirect estimation of Poisson's ratio from the 3PBC test data was confirmed (Aksel Seitllari & Kutay, 2019).

Table 7.1 Prony series coefficients for (a) 4E30SBS, (b) 4E3SBS and (c) 4E3DVR at 10 °C and 20 °C

(a)

T (ºC), f (Hz), Poisson's ratio	10, 10, 0.11	10, 1, 0.13	10, 0.1, 0.14	20, 10, 0.12	20, 1, 0.14	20, 0.1, 0.15
G_o (Pa)	9.05E+09	8.89E+09	8.74E+09	9.57E+09	9.40E+09	9.32E+09
g_i	0.0361	0.0361	0.0361	0.1013	0.1013	0.1013
	0.0443	0.0443	0.0443	0.1058	0.1058	0.1058
	0.0887	0.0887	0.0887	0.1709	0.1709	0.1709
	0.1532	0.1532	0.1532	0.2137	0.2137	0.2137
	0.2212	0.2212	0.2212	0.2013	0.2013	0.2013
	0.2282	0.2282	0.2282	0.1275	0.1275	0.1275
	0.1463	0.1463	0.1463	0.0535	0.0535	0.0535
	0.0569	0.0569	0.0569	0.0171	0.0171	0.0171
	0.015	0.015	0.015	0.0047	0.0047	0.0047
	0.0094	0.0094	0.0094	0.0036	0.0036	0.0035
τ_i (s)	1.0E-07	1.7E-06	2.8E-05	4.6E-04	7.7E-03	1.3E-01	2.2E+00	3.6E+01	6.0E+02	1.0E+04

(b)

T (ºC), f (Hz), Poisson's ratio	10, 10, 0.12	10, 1, 0.13	10, 0.1, 0.14	20, 10, 0.13	20, 1, 0.14	20, 0.1, 0.16
G_o (Pa)	8.52E+09	8.45E+09	8.37E+09	8.97E+09	8.89E+09	8.73E+09
g_i	0.0732	0.0732	0.0732	0.1624	0.1624	0.1624
	0.0716	0.0716	0.0716	0.1333	0.1333	0.1333
	0.1132	0.1132	0.1132	0.1706	0.1706	0.1706
	0.1528	0.1528	0.1528	0.177	0.177	0.177
	0.1823	0.1823	0.1823	0.157	0.157	0.157
	0.1752	0.1752	0.1752	0.1086	0.1086	0.1086
	0.1263	0.1263	0.1263	0.0566	0.0566	0.0566
	0.0663	0.0663	0.0663	0.0229	0.0229	0.0229
	0.0246	0.0246	0.0246	0.0077	0.0077	0.0077
	0.0139	0.0139	0.0139	0.0032	0.0032	0.0032
τ_i (s)	1.0E-07	1.7E-06	2.8E-05	4.6E-04	7.7E-03	1.3E-01	2.2E+00	3.6E+01	6.0E+02	1.0E+04

Table 7.1 (cont'd)

(c)										
T (°C), f (Hz), Poisson's ratio	10, 10, 0.11		10, 1, 0.12		10, 0.1, 0.13		20, 10, 0.12		20, 1, 0.14	20, 0.1, 0.15
G_o (Pa)	1.20E+10		1.19E+10		1.18E+10		9.14E+09		8.98E+09	8.90E+09
g_i	0.0931		0.0931		0.0931		0.1169		0.1169	0.1169
	0.0881		0.0881		0.0881		0.1095		0.1095	0.1095
	0.1324		0.1324		0.1324		0.1608		0.1608	0.1608
	0.1666		0.1666		0.1666		0.1902		0.1902	0.1902
	0.1836		0.1836		0.1836		0.1839		0.1839	0.1839
	0.1605		0.1605		0.1605		0.1311		0.1311	0.1311
	0.1022		0.1022		0.1022		0.0669		0.0669	0.0669
	0.0467		0.0467		4.67E-02		0.0262		0.0262	0.0262
	0.0156		0.0156		1.56E-02		0.0084		0.0084	0.0084
	0.0107		0.0107		1.0700E-02		0.0055		0.0055	0.0055
τ_i (s)	1.0E-07	1.7E-06	2.8E-05	4.6E-04	7.7E-03	1.3E-01	2.2E+00	3.6E+01	6.0E+02	1.0E+04

8. APPLICATION OF VISCOELASTIC CONTINUUM DAMAGE (VECD) THEORY TO 3PBC TEST (*Task 3)*

Adaptation of VECD theory in fatigue characterization of asphalt mixtures significantly reduced the experimental burden required to calibrate phenomenological fatigue life formulation (i.e., $N_f = a\varepsilon^{-b}E^{-c}$). Extensive literature exists on the VECD and its practical applications in characterizing uniaxial fatigue behavior of asphalt mixtures (Christensen Jr & Bonaquist, 2005; Kim, Lee, & Little, 1997; Kutay et al., 2008; Kutay & Lanotte, 2017; Park, Kim, & Schapery, 1996; Underwood, B. Shane, 2006). Several recent studies have presented the application of the VECD theory on the analysis of fatigue behavior on flexural tests (Mello, Farias, & Kaloush, 2018; Tarefder, Bateman, & Swamy, 2013).

The VECD constitutive model is based on Schapery's proposed elastic-viscoelastic correspondence (E-VC) principle, which can be applied to both linear and non-linear viscoelastic materials, and work potential theory (Schapery, 1990). The E-VC principle states that the constitutive equations for a particular viscoelastic media are equivalent to equations of elastic media when the concept of pseudostrain is used instead of actual physical strain. The pseudostrain in the time domain can be computed using the following convolution integral:

$$\varepsilon^R = \frac{1}{E^R}\int_0^t E(t-\tau)\frac{d\varepsilon}{d\tau}d\tau \qquad [8.1]$$

where, ϵ^R is the pseudostrain, E_R is a reference modulus often set as unity. Once E_R is assumed as unity, ε^R corresponds to linear viscoelastic stress, *E(t)* is the linear viscoelastic relaxation modulus, t is the time and τ is the time variable of integration.

The amount of work required for initiation and coalescing of microcracks is conveniently determined by the use of damage parameters (internal state variables). The mathematical approach

to describe these phenomena includes the simplest form of pseudostrain energy density function and a single internal state variable S described as follows (Park et al., 1996):

$$\sigma = \frac{\partial W^R}{\partial \varepsilon^R} = C(S)\varepsilon^R \quad [8.2]$$

$$W^R = \frac{I}{2} C(S)\varepsilon^{R^2} \quad [8.3]$$

$$\frac{dS}{dt} = \left(-\frac{\partial W^R}{\partial S}\right)^{\alpha} \quad [8.4]$$

where, σ is the stress, $W^R$is the pseudostrain energy density function, C(S) is pseudostiffness as a function of a single damage parameter, $dS\ /\ dt$ represents the damage evolution rate, I is an initial stiffness parameter used to eliminate the sample to sample variability, t is time and α is a constant related to the rate of damage growth in viscoelastic media ($\alpha = 1/m$, where m is the maximum slope of the relaxation modulus master curve in log-log scale).

In the case of cyclic loading at a constant frequency with no rest periods which is also applied in this study, the pseudostrain (ε^R) and the pseudostiffness (C) values at each cycle can be calculated as follows:

$$C_N = \frac{|E^*|_N}{|E^*|_{LVE}} \quad [8.5]$$

$$\varepsilon_N^R = \frac{\sigma_N}{C_N} \quad [8.6]$$

where, $|E^*|_{LVE}$ is the linear viscoelastic dynamic modulus (i.e., $|E^*|_{LVE} = |E^*|_{N=1}$), $|E^*|_N$ is the dynamic modulus and ε_0^N is the peak strain measured at the N^{th} cycle.

The damage parameter (S) at the peak of each cycle was calculated using a practical procedure proposed by Kutay et al. (Kutay et al., 2008) :

$$S_{N+\Delta N} = S_N + \left(\frac{\Delta N}{f_R}\right)^{\frac{1}{1+\alpha}} \left[-0.5 I \varepsilon_N^{R^2} (C_{N+\Delta N} - C_N)\right]^{\frac{\alpha}{1+\alpha}} \quad [8.7]$$

where, ΔN is the cycle increment and f_R is the reduced frequency.

It is noted that the damage characteristic curve (C-S) is a unique curve that can be used to predict the fatigue life of asphalt mixtures at different frequencies and temperatures at a required strain level. The C-S curve is computed from the peak-to-peak stress-strain data retrieved for each cycle. However, the C-S curve should not be used to rank the fatigue performance of different mixtures since it is a normalized curve. Mixture classification should be done based on their fatigue life (number of cycles to failure (N_f)) at a certain temperature, frequency and strain level.

It is important to select a fatigue failure criterion, i.e., the N_f. Numerous failure criteria have investigated by different researchers (Soltani & Anderson, 2005; Underwood, B. Shane, 2006; Y. D. Wang et al., 2018; Zeiada et al., 2016; Zhang et al., 2013). Kutay et al. (Kutay et al., 2008)summarized different failure criteria existing in the literature and compared the fatigue failure results against the field cracking data retrieved from the FHWA's accelerated pavement testing facility (APT). It was concluded that the selected failure criteria had the same trends with the FHWA's APT field cracking data. Hence, a 50 % reduction in stiffness was recommended, therefore applied in this study. The fatigue life (N_f) was calculated using the following expression derived for the specific case of cyclic tests at constant frequency with no rest periods (Kutay et al., 2009):

$$N_f = \sum_{S=1}^{S_f} \left[-\frac{\varepsilon_0^2 |E^*|_{LVE}^2}{2} \left. \frac{dC}{dS} \right|_{at\ S} \right]^{-\alpha} f \Delta S_S \qquad [8.8]$$

where, S_f is the damage parameter value corresponding to C = 0.5.

8.1 Results of Uniaxial |E| Tests using the AMPT*

One of the prerequisite steps of the VECD-based characterization is the determination of the linear viscoelastic |E*| master curve. Therefore, |E*| test needs to be run for analysis of both

3PBC and PP test results. In this study, the following shift factor and sigmoidal relationships were used to construct the |E*| master curve:

$$\log(a_T(T)) = a_1\left(T^2 - T_{ref}^2\right) + a_2(T - T_{ref}) \quad [8.9]$$

$$log(|E^*|) = c_1 + \frac{c_2}{1 + e^{(-c_3 - c_4 log(f_R))}} \quad [8.10]$$

where, $T_{ref}$is the reference temperature, a_1 and a_2 are the shift factors polynomial coefficients, c_1, c_2, c_3, c_4 are the sigmoidal coefficients, f_R is the reduced frequency ($f_R = fa(T)$).

The $T_{ref}$was selected as 20 ºC. Figure 8.1a and Figure 8.1b illustrate the |E*| master curves in log scale and semi-log scale for each mixture, respectively. Also, the relationship between the shift factors and the temperature is presented in Figure 8.1c. The dynamic modulus master curve and shift factor coefficients are presented in Table 8.1. Overall, all mixtures had similar |E*| values. The 4E3DVR was slightly stiffer than the two SBS modified mixtures.

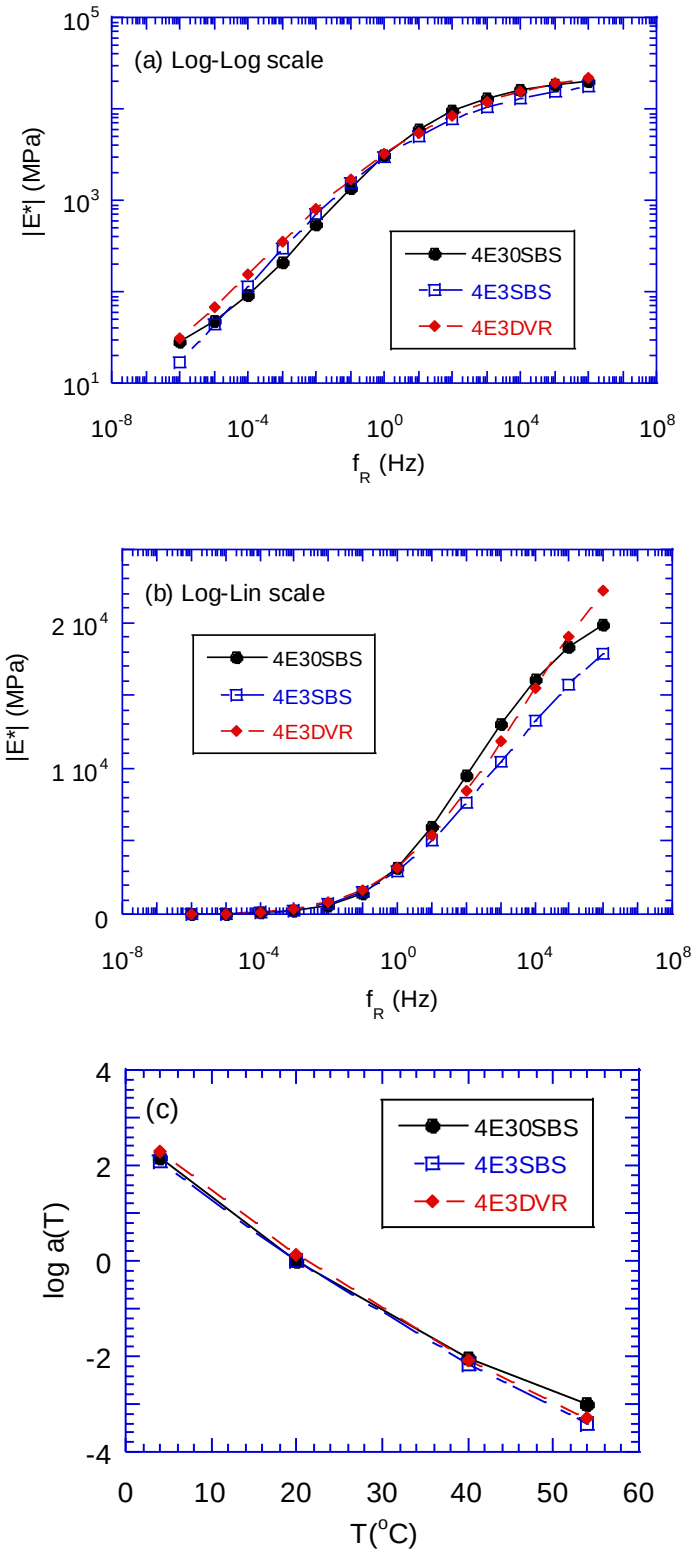

Figure 8.1. Linear viscoelastic properties of the mixtures: (a) log-log scale and (b) semi-log scale plots of dynamic modulus master curves for 4E30SBS, 4E3SBS, and 4E3DVR, and (c) shift factor coefficients as a function of temperature.

Table 8.1 Dynamic modulus master curve and shift factor coefficients

Shift Factor (a(T)) Coefficients	Mixture ID		
	4E30SBS	4E3SBS	4E3DVR
a_1	0.0009	0.0006	0.0007
a_2	-0.1568	-0.1456	-0.1508
Sigmoidal Coefficients			
c_1	1.0892	-0.5296	-0.0166
c_2	3.2607	4.9230	4.5466
c_3	-1.0345	1.4746	1.2303
c_4	-0.5102	0.3417	0.3227

8.2 Comparison of 3PBC and PP fatigue test results

The damage characteristic (C-S) curves were constructed for each replicate of PP and 3PBC tests run at various temperatures and frequency combinations. Equations [8.5] through [8.7] were used to compute C and S values at each loading cycle. According to the VECD theory, C-S curves computed from the data of each replicate should collapse to form a unique curve.

The C-S curves of 4E30SBS mixture are shown in Figure 8.2a and Figure 8.2b, for 3PBC and PP testing methodologies, respectively. It is clear that the C-S curve collapsed to form a single curve (with slight variations due to sample-to-sample variability) regardless of strain level, temperature, and frequencies. The C-S curves of 4E3SBS and 4E3DVR mixtures followed a similar trend, as shown in Figure 8.3 and Figure 8.4.

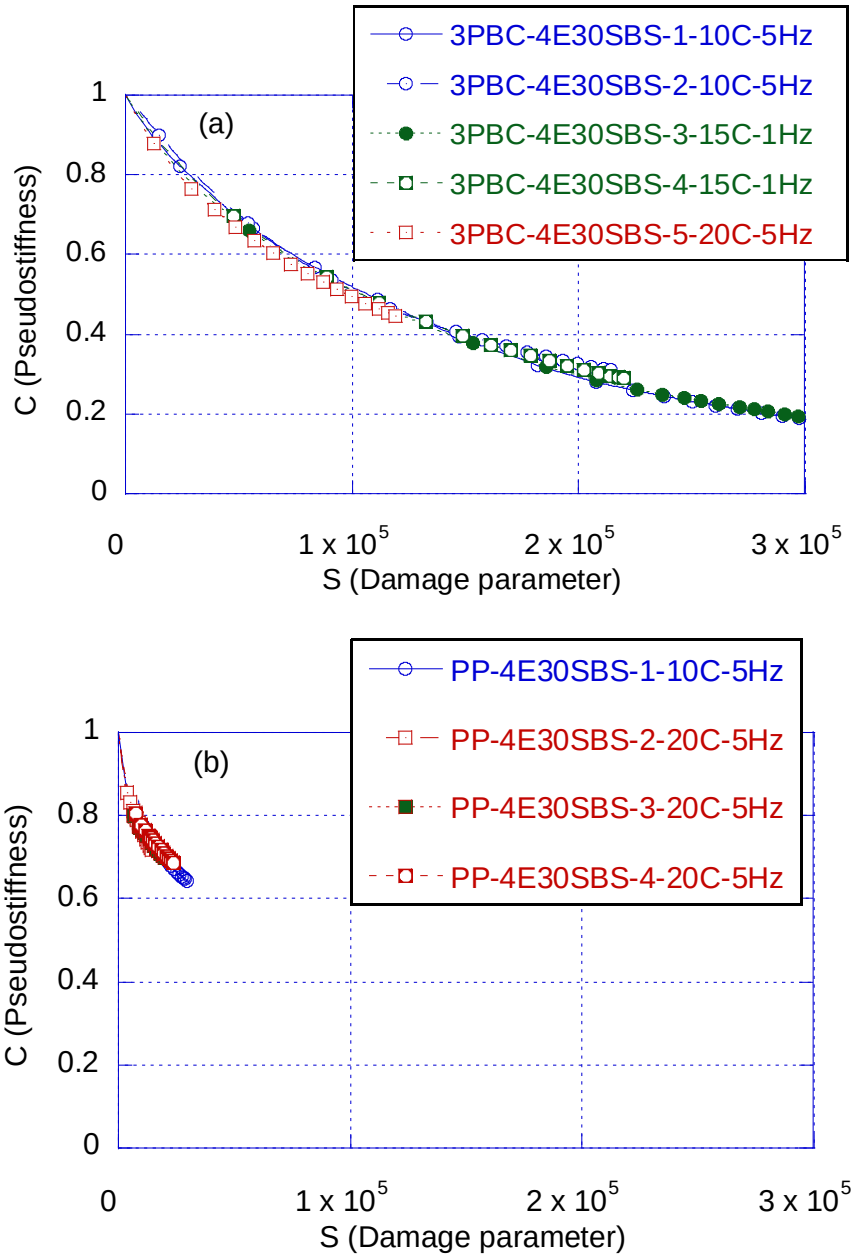

Figure 8.2. Damage characteristic curves of 4E30SBS for (a) 3PBC and (b) PP test results.

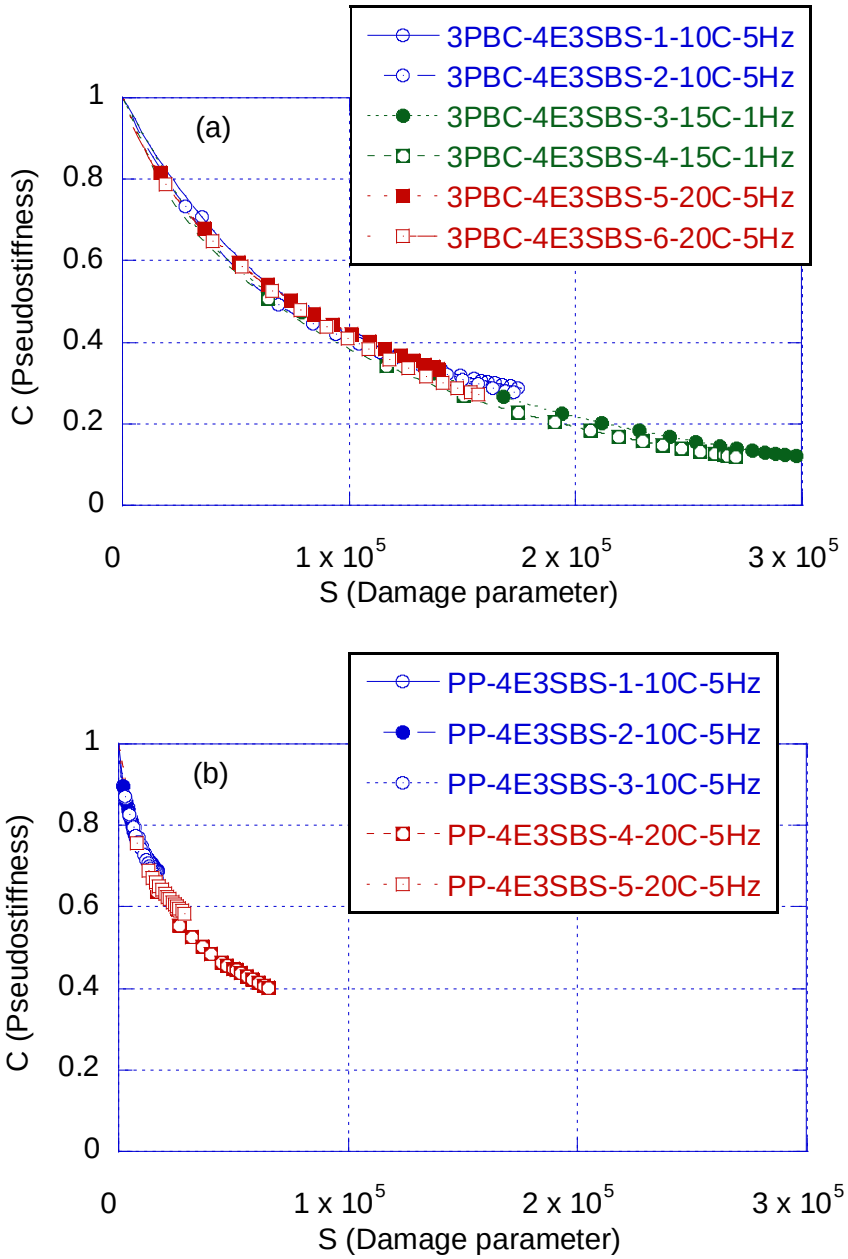

Figure 8.3. Damage characteristic curves of 4E3SBS for (a) 3PBC and (b) PP test results.

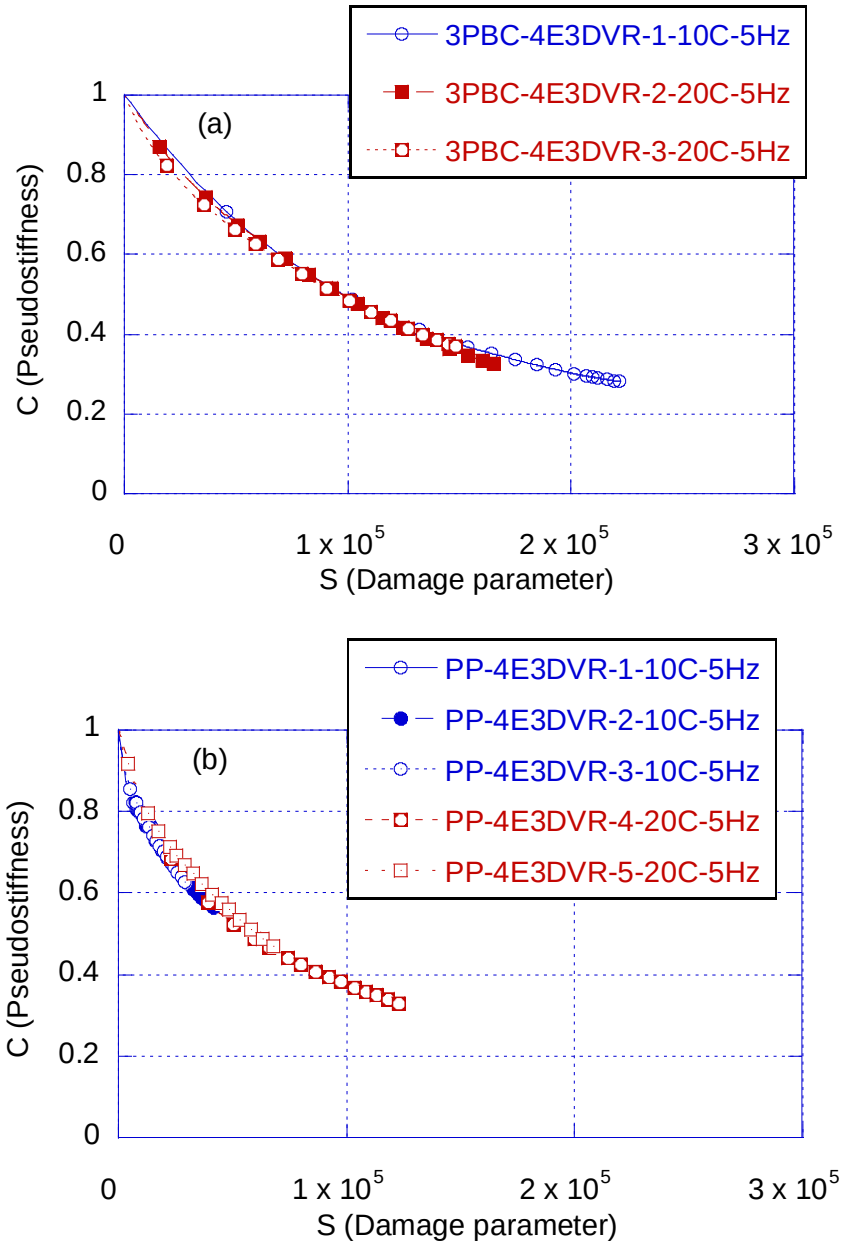

Figure 8.4. Damage characteristic curves of 4E3DVR for (a) 3PBC and (b) PP test results.

Figure 8.5 shows the best fit C-S curves for all three mixtures tested using 3PBC and PP testing methods. Overall, it can be observed that the C-S curves from 3PBC tests seem to be shifted upwards, by about the same amount for all mixtures. Since the C-S is a normalized curve, it is better to analyze the 3PBC and PP tests result in terms of the number of cycles to failure (N_f).

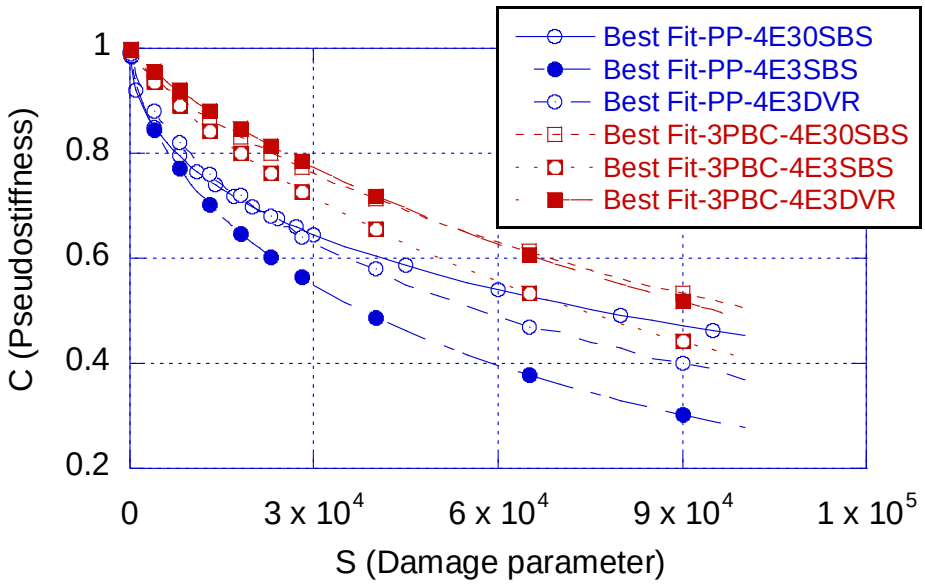

Figure 8.5. Best fit damage characterization curves for 3PBC and PP test results.

In this study, the failure criterion is selected as a 50 % reduction of pseudo-stiffness (C = 0.5). The C-S curves shown in Figure 8.2 through 11 were employed to calculate the asphalt mixture fatigue life under the following conditions: frequency = 10 Hz, temperature = 10, 15, and 20 ºC, and strain level=100, 200, 300, 400, 500 and 600 microstrain (mm/mm x 10^{-6}). The N_f values for each temperature/frequency/strain level combination were computed using Equation [8.8].

The N_f values for the 3PBC test and PP test are illustrated in Figure 8.6a, where N_f values obtained from 3PBC analyses were generally higher than those obtained the PP test results. This finding is consistent with literature comparing uniaxial and flexural fatigue tests (Ning Li et al., 2013). Figure 8.6b shows a direct comparison between the N_f values computed from 3PBC and PP tests. As shown, there is a strong correlation between the PP test results and the 3PBC results. Overall, 3PBC tests resulted in about N_f values 4.5 times those obtained from PP tests. These results demonstrate that the 3PBC is a promising alternative test method for fatigue characterization of asphalt mixtures.

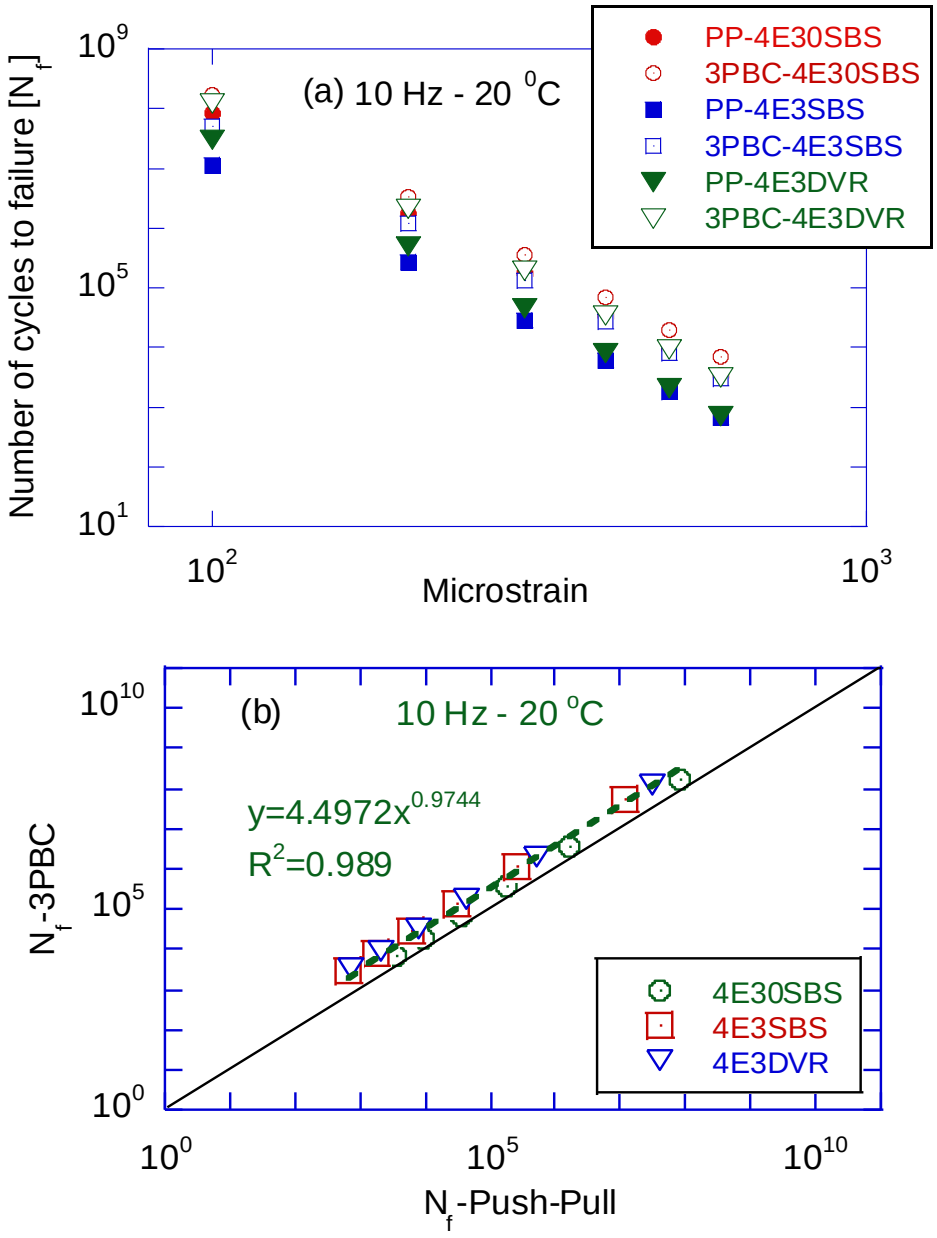

Figure 8.6. Comparisons of (a) the number of cycles to failure (N_f) versus strain relationship of 4E30SBS, 4E3SBS and 4E3DVR asphalt mixtures for 3PBC and PP test at f = 10 Hz, T = 20 ^{o}C, and (b) direct comparisons of N_f values.

8.3 Summary of chapter findings

The objective of this part of the research study was to investigate the implementation of VECD theory to model the fatigue response of the 3PBC test results at multiple frequency-temperature-strain levels. In order to achieve this objective, laboratory cylindrical samples from

three different asphalt mixtures were prepared and subjected to 3PBC tests. Also, push-pull (PP) tests were performed on the same mixtures. Based on the results presented in this part, the following conclusions can be made:

- It was shown that the viscoelastic continuum damage theory can be used to model the fatigue life of an asphalt mixture at many temperature/frequency/strain level combinations, by simply running the 3PBC tests at a few temperatures/strain levels.
- The 3PBC testing results were analyzed using the same VECD formulations developed for PP data analysis. The damage characteristic curves (C-S) were generated and compared. It was shown that the C-S curves obtained from the 3PBC test collapsed to form a unique curve, just like the C-S curves of PP tests. However, the C-S curves of 3PBC and PP tests were not the same. The C-S curves of 3PBC tests were generally shifted upwards compared to the PP-based C-S curve for a given mixture. This difference is understandable since the mode of loading is different.
- Asphalt mixture hierarchical ranking obtained from 3PBC and PP tests agreed very well with each other. Overall, the number of cycles to failure obtained from 3PBC test results were about 4.5 times those obtained from the PP tests.

The results presented in this part of the research study are quite promising, however, the 3PBC test method should still be considered to be under development. A ruggedness study should be performed to develop a proper test specification (Aksel Seitllari & Kutay, 2019).

9. RUGGEDNESS STUDY OF THREE-POINT BEAM CYLINDER (3PBC) TEST (*Task 4*)

As reported in the previous chapters, promising experimental results of the 3PBC test were obtained for characterizing the fatigue behavior of asphalt pavements. The next step was a ruggedness evaluation of the 3PBC test setup, where the effects of certain parameters that influence the test results were identified and quantified. An effort to establish acceptance limits for these parameters is presented in this chapter.

The Three-Point Bending Cylinder (3PBC) test is a promising method that can be used for routine testing practices by state DOTs and roadway agencies. However, it should be noted that this test is still considered to be under development. Hence, identifying and investigating the potential sources of variability in this test is crucially important to improve its accuracy and to develop test specifications. According to (Bonaquist, 2008), any developed test method is expected to provide accurate results that can only be achieved through decent control of the sources of variability in the test procedure. Ruggedness evaluation is the appropriate method to identify important sources of variability by intentionally varying the most influential parameters. Such examination provides evidence on the reliability of the test technique during ordinary usage and helps establish control thresholds. Hence, ruggedness testing is a crucial part of the development of a new test method and as such, was performed in this study. ASTM E1169, *Standard Practice for Conducting Ruggedness Test* provides a practical procedure for concurrently evaluating the effects of certain changes in each of the operating conditions in an independent manner. This practice recommends the ruggedness testing should involve a single laboratory on uniform material and potentially followed up by an inter-laboratory (round-robin) study. The inter-

laboratory study was not within the scope of this work, but it should be considered in a future study.

The details of a proper ruggedness study are comprehensively described in ASTM E1169. Typically, the primary considerations in the design of a ruggedness test are (i) selection of the potential factors and their levels and (ii) selection of the test conditions. The general procedure requires seven factors and two different levels (low and high) usually determined based on experience. In this study, however, three factors were selected with several corresponding levels. To meet the protocol requirement of seven factors, factors were duplicated. Table 9.1 illustrates the potential factors affecting 3PBC tests, and the ranges of the parameters selected for this study.

Table 9.1 Factors and levels of ruggedness analysis

Factor	Variable	Lower Level Value	Upper Level Value
A	Air void [%]	6	8
B	Span length [mm]	100	135
C	Specimen diameter [mm]	38	100

Based on ASTM E1169, the level setting is indicated by 1 and -1 for the expected high level and low level, respectively. An orthogonal design approach is followed to determine the effect of each factor on the final results. To achieve this task, a specific combination of factor variables and their levels is required, as detailed in Table 9.2. According to this condition, two combinations for each level will yield a total of 16 tests to complete the experimental work.

Table 9.2 Experimental design for ruggedness testing (ASTM E1169)

Determination number	*Factors*						
	Air void [%]	Span length [mm]	Span length [mm]	Span length [mm]	Specimen diameter [mm]	Specimen diameter [mm]	Specimen diameter [mm]
1	1	1	1	-1	1	-1	-1
2	-1	1	1	1	-1	1	-1
3	-1	-1	1	1	1	-1	1
4	1	-1	-1	1	1	1	-1
5	-1	1	-1	-1	1	1	1
6	1	-1	1	-1	-1	1	1
7	1	1	-1	1	-1	-1	1
8	-1	-1	-1	-1	-1	-1	-1

Note: the level cells were color-coded for better visualization

9.1 Mixture sampling and sample preparation

The asphalt mixture used for the ruggedness evaluation was obtained as a loose mix from a local asphalt plant in Lansing, MI. The mix design and volumetric properties of the loose mixture were shown in Table 4.1 (5E3 Neat mixture). The loose mix was carefully sampled in 5-gallon metallic pails to avoid segregation. Usually, from a 5-gallon metallic pail, 3 Superpave Gyratory Compactor (SGC) specimens can be prepared. Prior to loose mixture separation, the 5-gallon metallic pail is reheated at 110 ºC until the loose mix is easily spreadable. This process usually takes less than 3 hours. The loose mixture is poured in a metallic pan and mixed to provide homogeneity. Then, three smaller pans are filled with the required mass of the specimen and placed in a preheated oven at the compaction temperature. To minimize the aging of the loose mix, the temperature of the material was frequently checked using thermocouples. Then the material was poured in compaction molds and an SGC Pine compactor was used to compact the specimen at a specific height to meet required target air voids. Before any further mechanical processing, the compacted samples are stored to cool down at room temperature overnight. All the SGC samples were compacted at a height of 180 mm and a diameter of 150 mm. Depending on the performance test, cylindrical samples were cored and cut at desired diameters and heights. Subsequently, the

physical properties of the resized specimens were measured and recorded. The specimens falling out of the predefined air void range were discarded from further testing.

9.2 Uniaxial Dynamic Modulus (|E|) Test*

Samples for uniaxial dynamic modulus (|E*|) were obtained from cylindrical samples (150 mm diameter, 180 mm height) compacted with the Superpave Gyratory Compactor (SGC) in general accordance with the AASHTO R83 protocol. Cores were extracted from those samples using a diamond-coring stand, while the ends of the cores were trimmed using a masonry saw in order to obtain smooth and parallel end surfaces. The final height of the testing samples was set to 150 mm in all cases. The diameters of the cored samples were 100 mm. The mass of mixture compacted by the SGC was determined to reach the target air voids content of 7 % ± 0.5 % at the sample core. At least two replicates for each test and mix were prepared.

The |E*| measurements were carried out in accordance with the AASHTO R84 protocol using the Asphalt Mixture Performance Testing (AMPT) device. Samples were subjected to uniaxial sinusoidal compressive stress at four temperatures (4, 20, 40 and 54 °C) and three frequencies (10, 1, and 0.1 Hz) at each temperature. The dynamic modulus master curve was obtained using the time-temperature superposition (TTS) principle (Kutay & Lanotte, 2017)(Aksel Seitllari, Lanotte, & Kutay, 2019a). As described in Section 8.1, raw data were shifted horizontally at a reference temperature (T_{ref} = 21 °C) using shift factor coefficients (a (T)). A second-order polynomial function (Equation [8.9]) and a sigmoidal model (Equation [8.10]) were used to fit shift factors and the |E*| master curve, respectively.

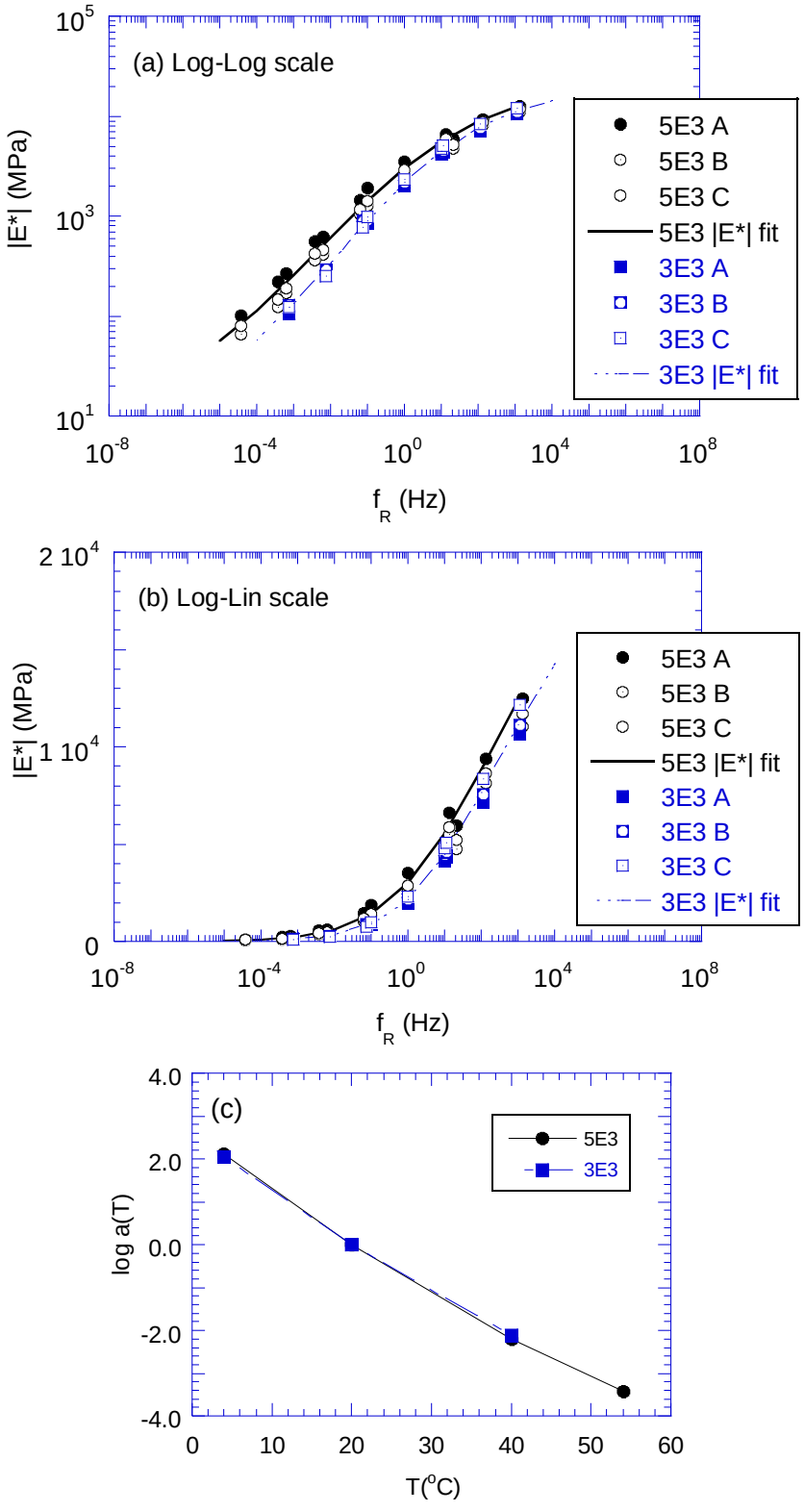

Figure 9.1. Linear viscoelastic properties in (a) log-log scale, (b) semi-log scale plots of dynamic modulus master curves and (c) shift factor coefficients as a function of temperature for 5E3 and 3E3 asphalt mixtures.

Figure 9.1a and Figure 9.1b illustrate the |E*| master curves in log scale and semi-log scale for each respective replicate. Also, the relationship between the shift factors and the temperature is shown in Figure 9.1c. More information for |E*| master curve and shift factor coefficients are detailed in Table 9.3.

Table 9.3 Dynamic modulus master curve and shift factor coefficients for 5E3 and 3E3 mixtures

Shift factor (a(T)) coefficients				
		a_1	a_2	
	5E3	0.0006	-0.1478	
	3E3	0.0006	-0.1417	
Sigmoidal Coefficients				
	c_1	c_2	c_3	c_4
5E3	0.9344	3.4658	1.0157	0.4397
3E3	0.8882	3.4522	0.8942	0.4932

9.3 Factors and levels of ruggedness analysis

It is significant to investigate the influence of certain parameters on the 3PBC test results and establish acceptance limits. A general test matrix designed to perform the ruggedness study is visualized in Figure 9.2. The presented test matrix includes the linear viscoelastic characterization of the asphalt mixture, variations in specimen geometry (diameter and span length) and the air void content for each combination along with the estimated replicate number.

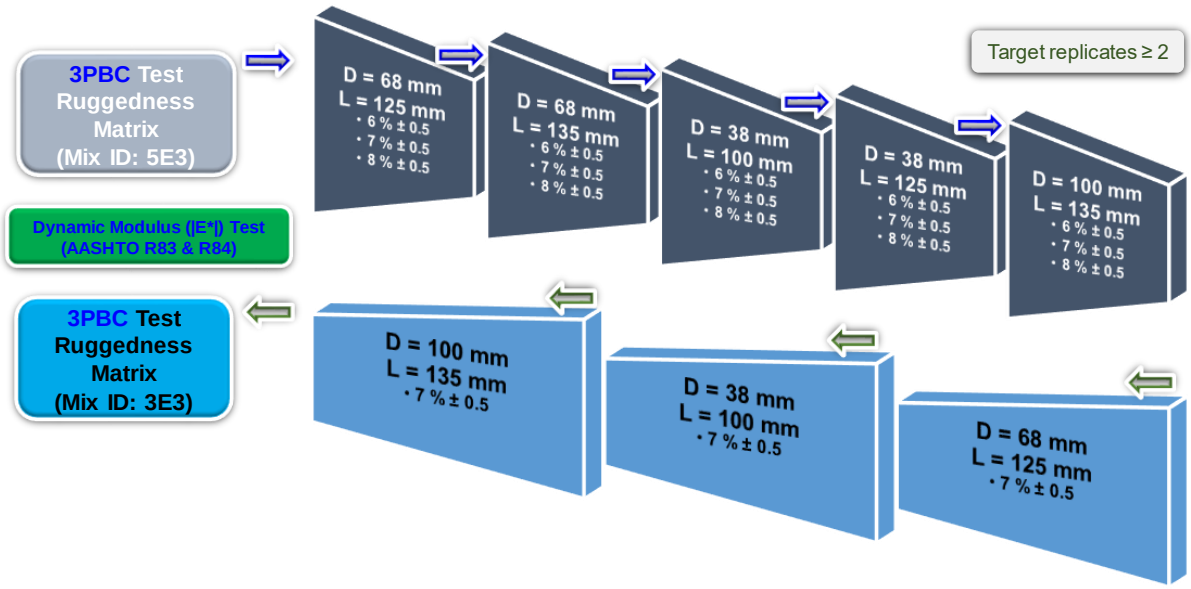

Figure 9.2. Ruggedness study flow chart.

The number of cycles to failure (N_f) was measured using a closed-loop servo-hydraulic material testing system (MTS) containing an environmental chamber. Prior to testing, the temperature of the test specimens was checked using a dummy specimen of the same size as the |E*| samples with a thermocouple inside. The displacement level at the actuator was initially selected through a trial and error process to ensure the on-specimen LVDT measurements showed the strain level on the sample was only about 200 microstrains (με). The frequency of the 3PBC tests was 5 Hz, and the tests were conducted at a temperature of 15 ºC. The testing conditions were kept the same for all the evaluated test combinations. Viscoelastic Continuum Damage (VECD) theory was then used to analyze the data from the 3PBC test results. This allowed determination of fatigue life (N_f) at target strain level (i.e. 150, 300 με), the temperature of 15 ºC and frequency of 5 Hz.

The following subsection presents the arrangements incorporated in the 3PBC test setup to accommodate the required changes for the ruggedness study. Further, the selected factors and the

two levels for the ruggedness testing as well as the sensitivity of the 3PBC test toward these factors were discussed.

9.3.1 3PBC test setup designs

Three different 3PBC test setup designs were optimized to adopt the factors and their levels considered for the ruggedness study as presented in Table 9.4. In this table, the initial geometry of the 3PBC test setup herein referred to as reference geometry, and other geometry combinations are detailed. As previously mentioned, the air void sensitivity for each combination was investigated. It is worth noting that all test samples were cored in a vertical direction.

Table 9.4 Factors and corresponding levels for the ruggedness evaluation of 3PBC test

	Reference geometry	1st	2nd	3rd	4th
Air Voids (%)	6, 7, 8	-	-	-	-
SGC specimen height (mm)	180	-	-	-	-
Test specimen height (mm)	68	68	38	38	100
Span length (mm)	125	135	100	125	135
Coring Direction	Vertical	Vertical	Vertical	Vertical	Vertical
Test temperature	15	-	-	-	-
Test frequency (Hz)	5	-	-	-	-
Strain (με)	150	-	-	-	-

Figure 9.3 illustrates the test setups and cored test specimens for additional designs. The reference design was not shown here for brevity (see Figure 5.2). As shown in Figure 9.3a, for 38 mm diameter samples, the 3PBC test setup components were kept the same as the reference setup designed for 68 mm samples. For 100 mm diameter samples, as shown in Figure 9.3b, the thickness of the base plate and side claps were increased. This was mainly done to avoid any undesired deformation of the fixed ends which could influence the test results.

(a)

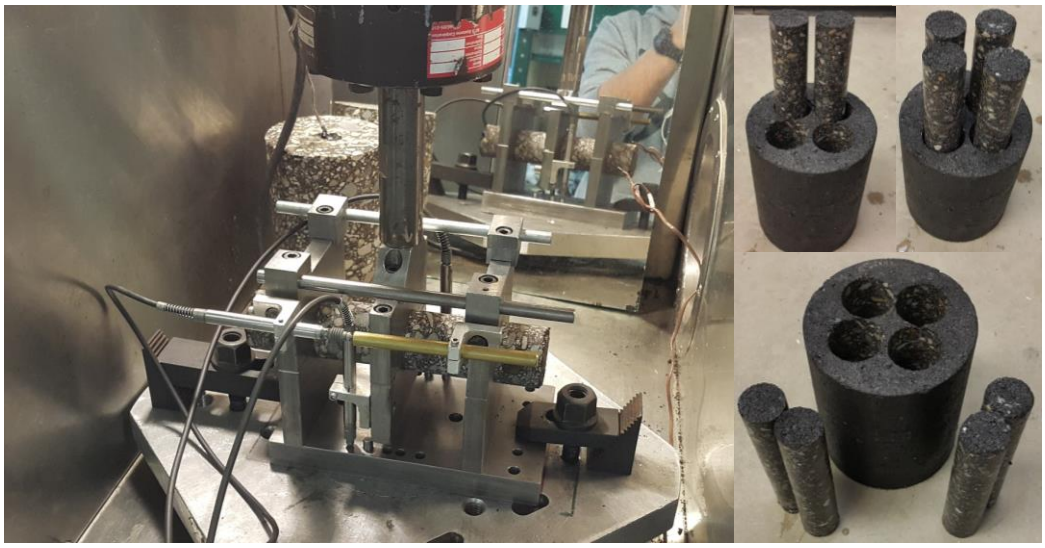

(b)

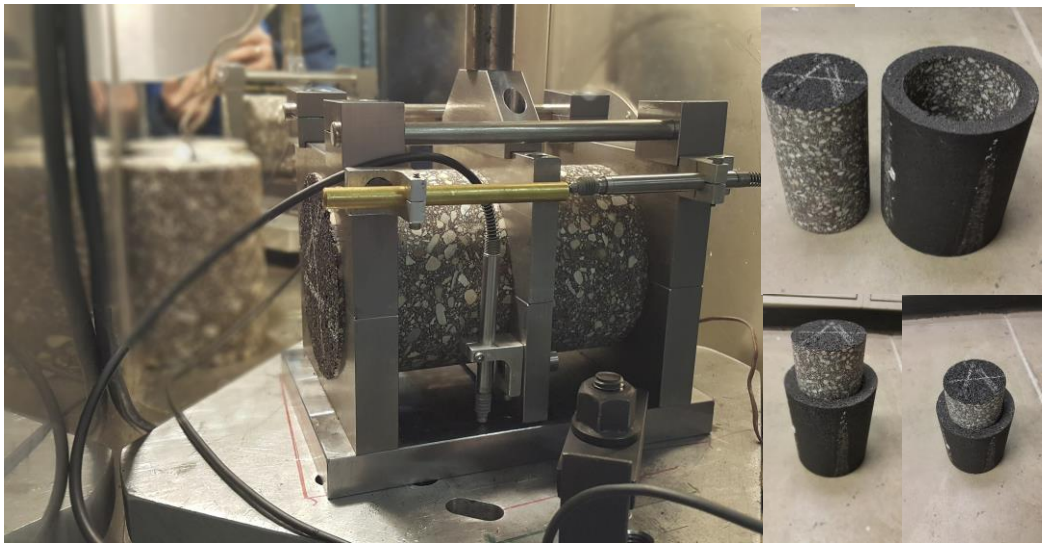

Figure 9.3. 3PBC test setup with loaded specimens Material Testing System (MTS) with a diameter of (a) 38 mm and (b) 100 mm.

9.3.2 Air void content

The effect of air void content on fatigue performance of the mixtures is important, as demonstrated in several studies (Harvey & Tsai, 1996; West, Rodezno, Leiva, & Taylor, 2018). Close control of this parameter is a crucial task. The current state of practice addresses ± 0.5 % air void tolerance. A wider tolerance range is helpful to optimize the specimen preparation time and resources. Generally, the required field air void content is 7 % and used in this study as control air void content for the tested mixtures.

To investigate test sensitivity to the air void content and establish rugged limits; 6 %, 7 % and 8 % ± 0.5 % were selected as shown in Table 9.4. Loose material was used to prepare SGC samples as described in the preceding sections. While several trial samples for each combination were used to ensure the on-specimen strain level is close to 200 microstrains, the lateral LVDT was used to measure the lateral displacement of the side clamps. The results obtained from this task are presented in Figure 9.4. As shown in this figure, in general, the lateral displacement is less than 10 % of the vertical displacement except for two cases for 6 % air void content. Since the lateral displacement at 7 % and 8 %, air void contents were below 10 % the vertical displacement, the lateral displacement limit was preliminary set at 10 % of the vertical displacement. However, for future reference, further detailed FE analysis will be performed to quantify if the lateral displacement limit threshold of 10 % affects the stress-strain results on the loaded specimen.

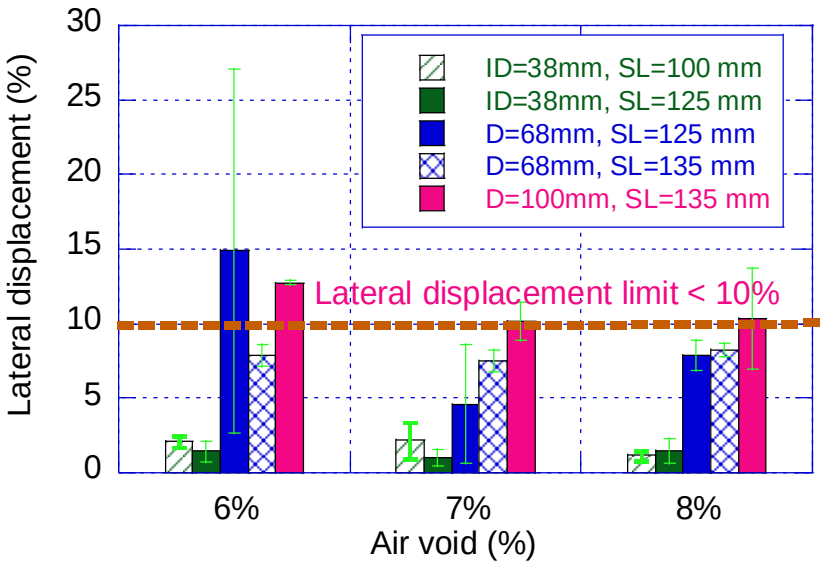

Figure 9.4. Lateral displacement limit for 3PBC test. Vertical axis shows the lateral displacement divided by the vertical displacement in the central clamp, in percentage.

Figure 9.5 - Figure 9.9 present the damage characteristic (i.e., C vs S) curves and (an example) the number of cycles to failure (at the frequency of 5 Hz, temperature of 15 °C and strain level of 150 με) obtained from specimens tested at 6 %, 7 %, and 8 % air void contents, for different

specimen geometries. As shown, in all geometries, variability between the individual tests for each air void content is low, as evidenced by the clear collapse of the C (pseudostiffness) versus S (damage parameter) curves. There were few exceptions to this (see Figure 9.8a), presumably caused by issues with the sample preparation and testing. It is interesting to note that, in most of the samples, effect of air voids on the number of cycles to failure (N_f) results was somewhat minimal, within the narrow air void range from 6 % to 8 %. Statistical analysis is presented in the later part of this section.

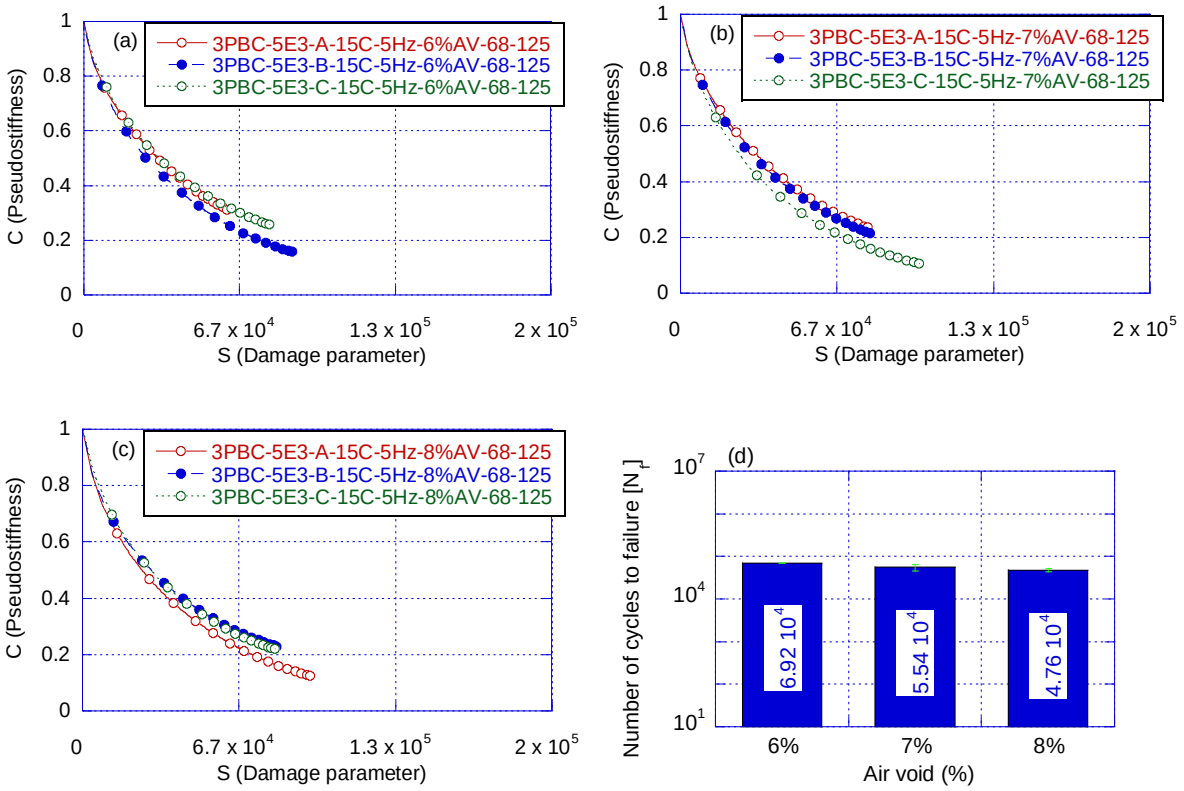

Figure 9.5. (a) – (c) Damage characteristic curves for 6 %, 7 % and 8 % air void contents, respectively and (d) number of cycles to failure (N_f) results at frequency of 5 Hz, temperature of 15 °C and strain level of 150 microstrain, for 68 mm - 125 mm (reference) geometry (5E3 mix).

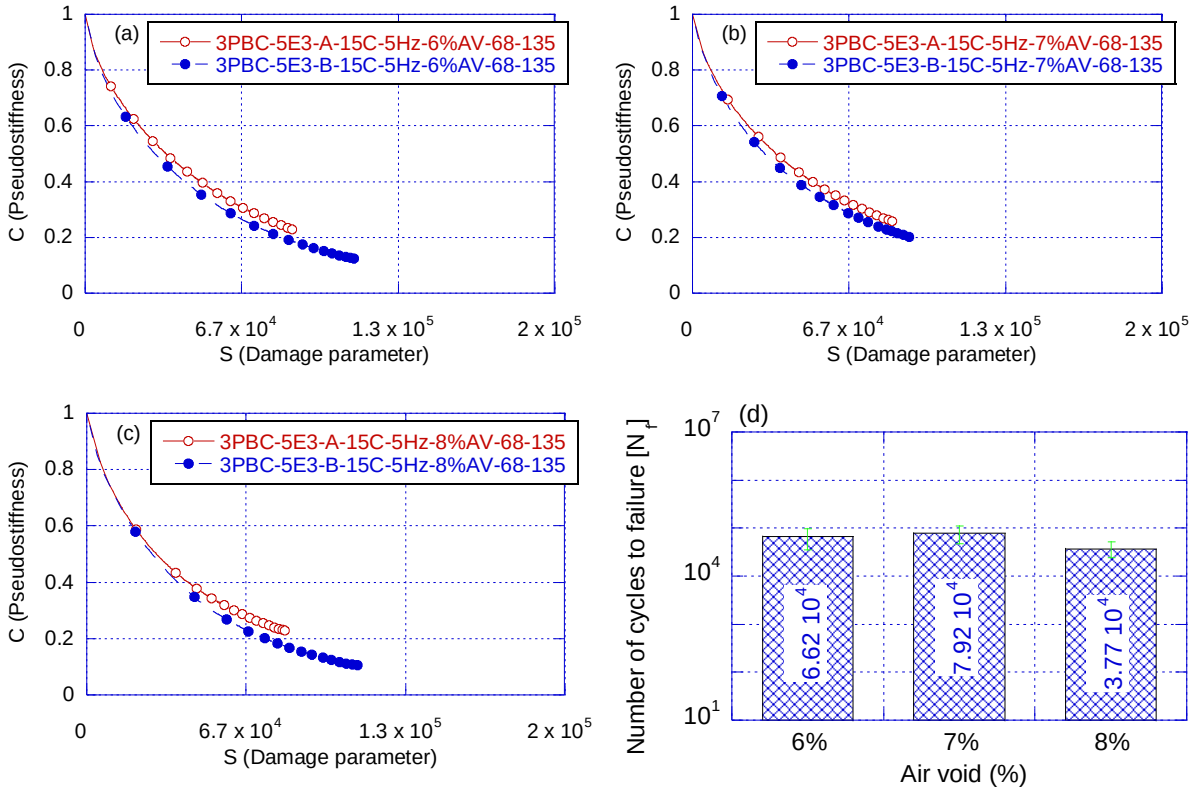

Figure 9.6. (a) – (c) Damage characteristic curves for 6 %, 7 % and 8 % air void contents, respectively and (d) number of cycles to failure (N_f) results at frequency of 5 Hz, temperature of 15 °C and strain level of 150 microstrain, for 68 mm - 135 mm geometry (5E3 mix).

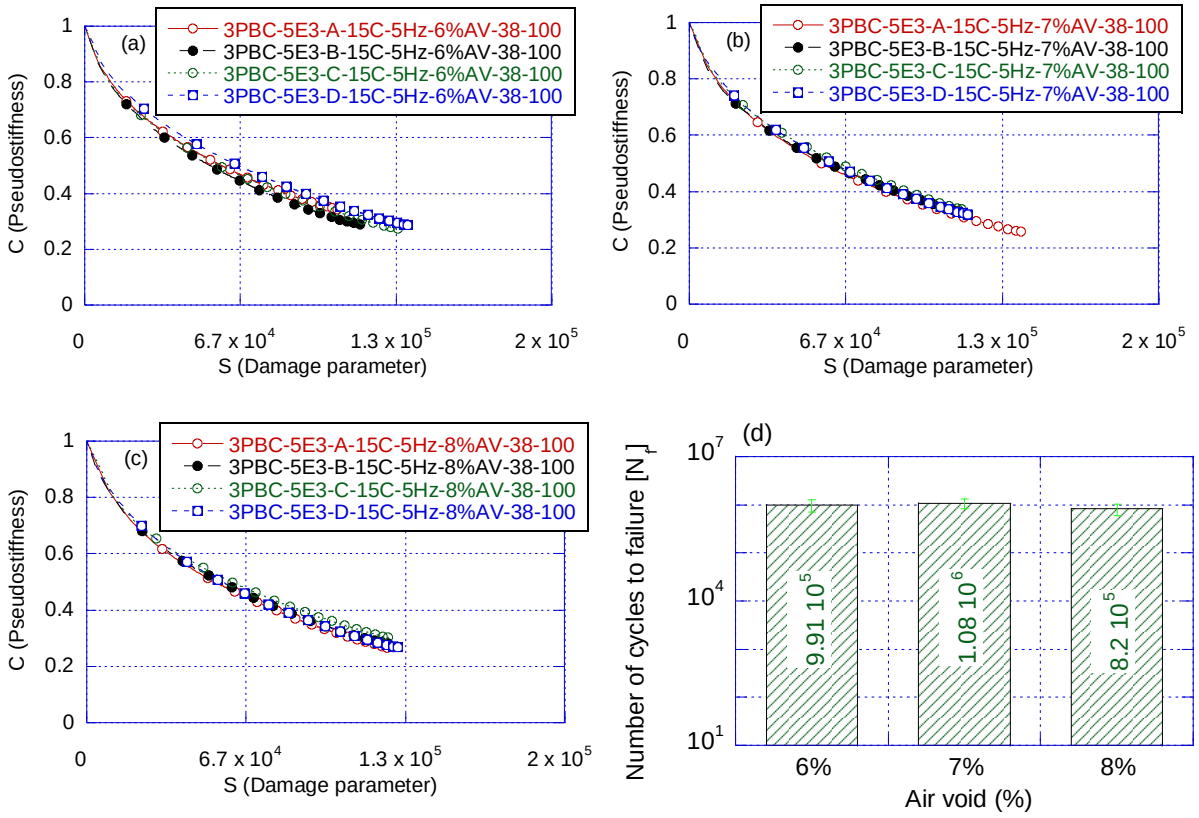

Figure 9.7. (a) – (c) Damage characteristic curves for 6 %, 7 % and 8 % air void contents, respectively and (d) number of cycles to failure (N_f) results at frequency of 5 Hz, temperature of 15 °C and strain level of 150 microstrain, for 38 mm - 100 mm geometry (5E3 mix).

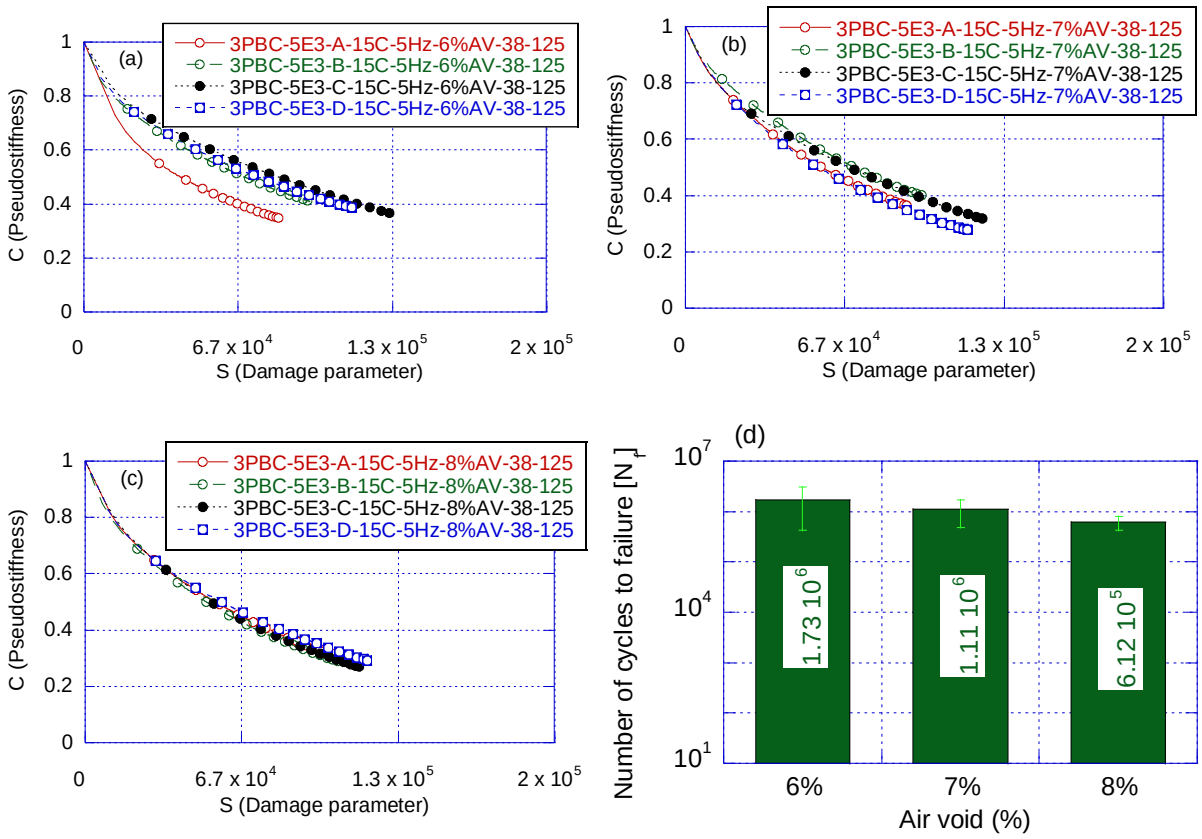

Figure 9.8. (a) – (c) Damage characteristic curves for 6 %, 7 % and 8 % air void contents, respectively and (d) number of cycles to failure (N_f) results at frequency of 5 Hz, temperature of 15 °C and strain level of 150 microstrain, for 38 mm - 125 mm geometry (5E3 mix).

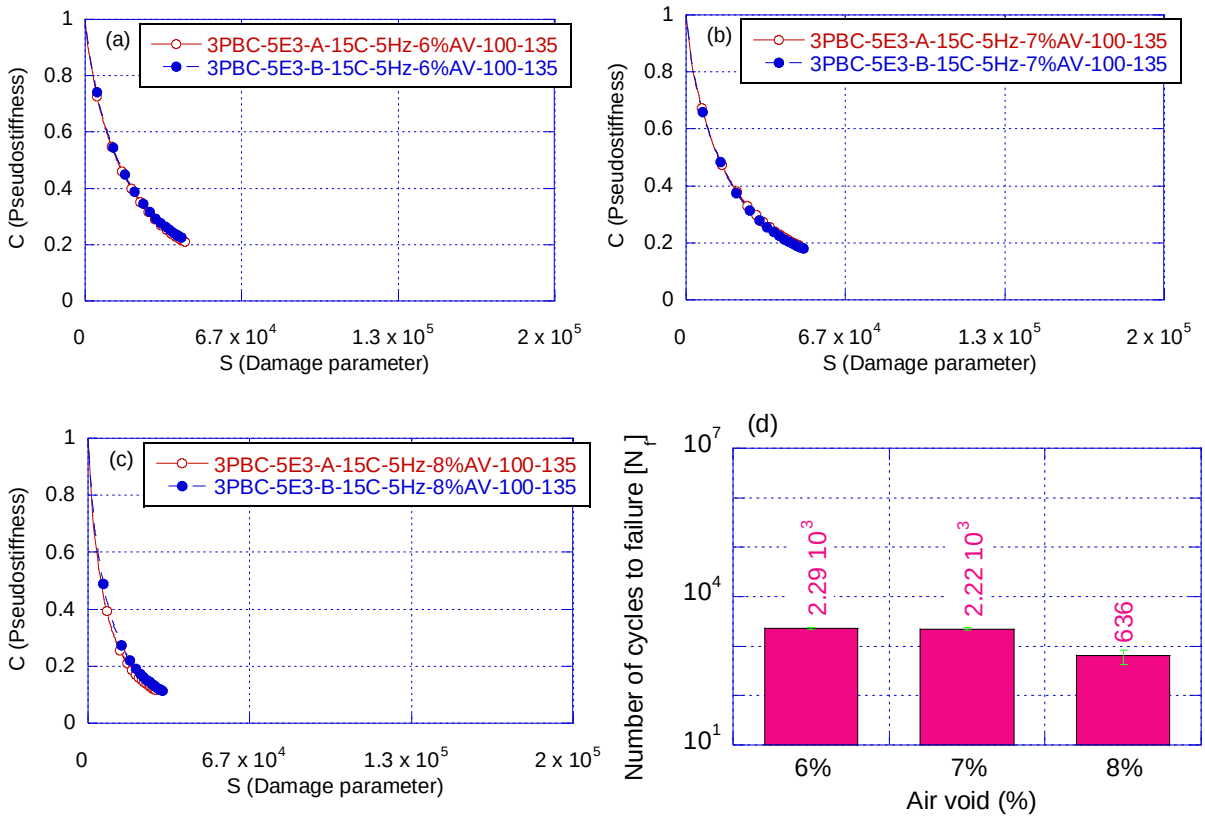

Figure 9.9. (a) – (c) Damage characteristic curves for 6 %, 7 % and 8 % air void contents, respectively and (d) number of cycles to failure (N_f) results at frequency of 5 Hz, temperature of 15 °C and strain level of 150 microstrain, for 100 mm - 135 mm (5E3 mix).

One-way analysis of variance (ANOVA) results are shown in Table 9.5. P-values were used to signify the magnitude of the differences with a 90 % confidence interval. The difference in N_f is defined as statistically significant when the p-value is lower than 0.1. Also, Tukey test results were examined to determine the likely ranges for the differences and to assess the practical significance of those differences. This test is usually used as a post hoc test especially when significance tests are engaged to compare group means. Tukey's test uses letters to group the results and highlights the differences. Factors that do not share a letter have a statistically significant difference in their mean value.

P-values for each combination are presented in Table 9.5. A comparison of the P-values indicates the effect of air void content on N_f values, generally, is not statistically significant. Likewise, Tukey's results confirm the same. It should be realized that the objective of this exercise is to identify controllable factors that potentially affect the test results and establish threshold limits for their control.

Overall, it can be said that the effect of air voids on the number of cycles to failure (N_f) results was minimal and there are no statistically significant differences in fatigue life within the air void range from 6 % to 8 %. Conforming to the results obtained from all the observed scenarios, the ± 1 % air void tolerance can be considered as a reasonable practice for the 3PBC test method.

Table 9.5 Statistical evaluation on the effect of air void content on fatigue life of asphalt mixture

One-way ANOVA															
Selected geometry		d = 68 mm l = 125 mm			d = 68 mm l = 135 mm			d = 38 mm l = 100 mm			d=38 mm l=125 mm			d=100 mm l=135 mm		
Air void (%)		6	7	Gr.+	6	7	Gr.	6	7	Gr.	6	7	Gr.	6	7	Gr.
6	P-Value*	-		A	-		A	-		A	-		A	-		A
7	P-Value	0.233	-	A	0.879	-	A	0.879	-	A	0.013	-	B	0.892	-	A
8	P-Value	0.089	0.529	A	0.588	0.381	A	0.373	0.188	A	0.004	0.575	B	0.001	0.001	B

*N_f is significantly different if P-Value < 0.1

+N_f that do not share a letter are significantly different; Gr. → Grouping

Table 9.6 Statistical evaluation on the effect of span length and diameter on fatigue life of asphalt mixture

One-way ANOVA							
Geometry combination			d = 68 mm l = 125 mm	d = 68 mm l = 135 mm	d = 38 mm l = 100 mm	d=38 mm l=125 mm	Grouping+
d = 68 mm	l = 125 mm		-				B\C
d = 68 mm	l = 135 mm	P-Value*	1.000	-			B\C
d = 38 mm	l = 100 mm	P-Value	0.064	0.066	-		A
d = 38 mm	l = 125 mm	P-Value	0.001	0.001	0.379	-	A
d = 100 mm	l = 135 mm	P-Value	1.000	1.000	0.043	0.001	C

*N_f is significantly different if P-Value < 0.1

+N_f that do not share a letter are significantly different

9.3.3 Span length

Span length is considered to be one of the parameters that might affect the stress-strain distribution on the specimen when subjected to loading. This effect becomes more pronounced when the so-called low aspect ratio or "thick-beams" are used, which is the case for the 3PBC test. Different span lengths were adopted and their effect on fatigue life (i.e. N_f) of asphalt mixtures was explored. It is worth noting that from the practical point of view, the span length should be compatible with horizontal-coring from field cores (i.e., 150mm diameter cores) or slabs.

The effects of span length on the fatigue performance of the asphalt mixture using the 3PBC test were explored. Figure 9.10 shows the damage characteristic curves (C-S) of all geometries (different span lengths and diameters) and all air void levels. As shown, in general, different span lengths of a given diameter collapsed in a single curve, with slight differences. The N_f values obtained at two different microstrain levels of 150 με and 300 με are presented in Figure 9.11a and Figure 9.11b, respectively. It can be seen that the change in span length affects the N_f value slightly. The differences are a bit more pronounced for the 38 mm diameter specimens when compared to the 68 mm diameter specimens. This could be because of the higher variability observed in the 38mm diameter, 125 mm long samples.

One-way ANOVA was performed to assess the effect of span length for a given diameter on the N_f. The measured N_f values at different air void contents (i.e., 6 %, 7 %, and 8 %) were, however, combined for each geometry, respectively. P-values and Tukey's analysis for each scenario are presented in Table 9.6. From the table, it is shown that the effect of span length on N_f is not statistically significant. Overall, the effects of span length on the 3PBC test results are minimal.

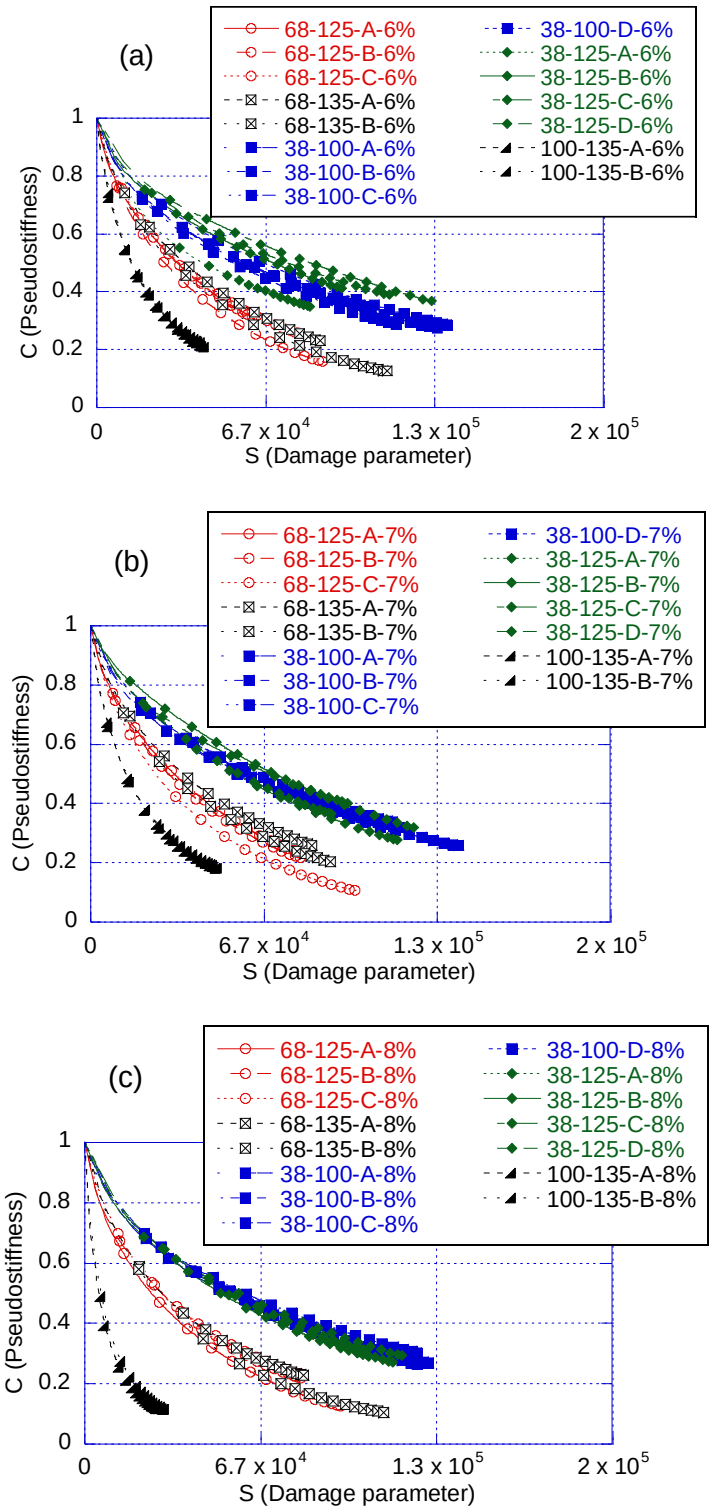

Figure 9.10. Damage characteristic curves (C-S) of all geometries plotted for (a) 6 %, (b) 7 % and (c) 8 % air void contents.

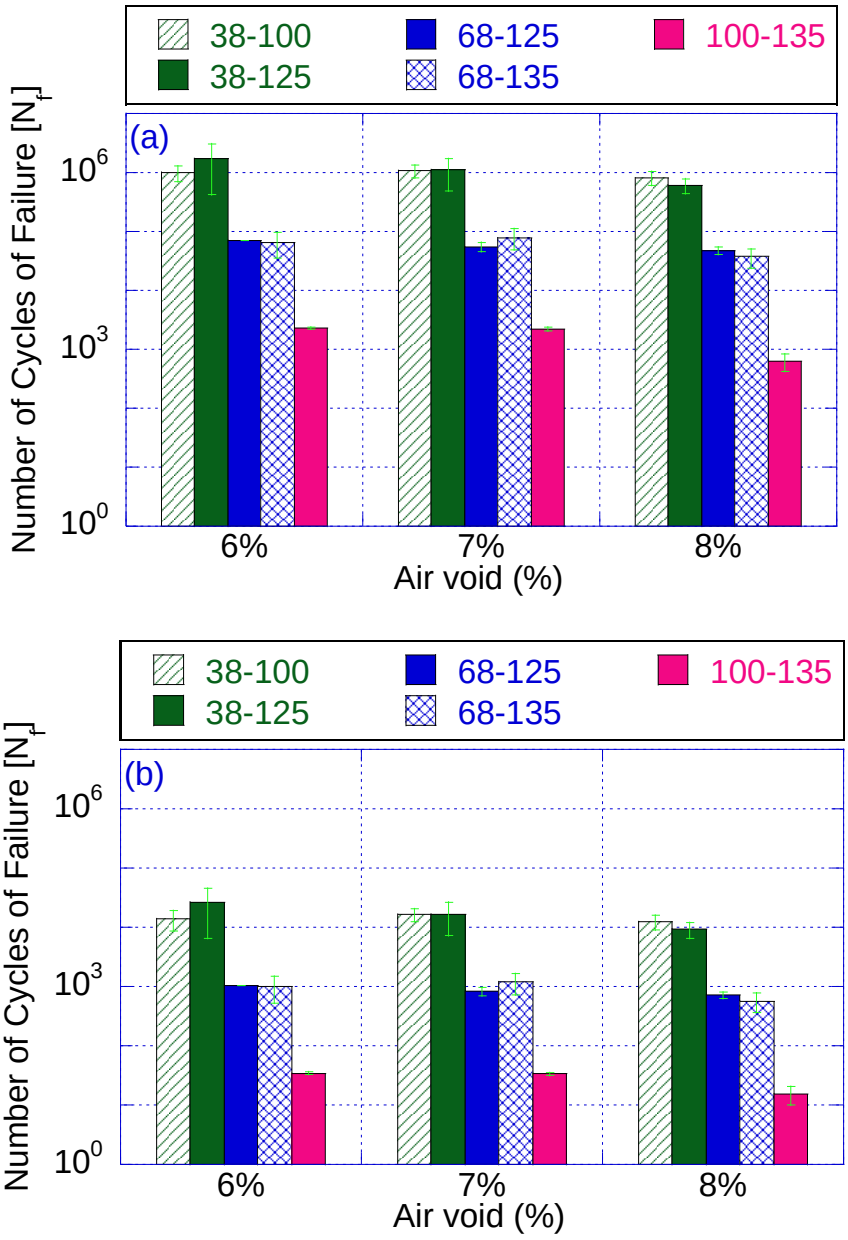

Figure 9.11. Number of cycles to failure (N_f) results for different length and diameter combinations at (a) 150 με and (b) 300 με.

9.3.4 Specimen diameter

The effects of specimen thickness are known to influence the fatigue resistance of asphalt mixtures when the so-called 'non-homogenous' test methods are adopted. Therefore, for this ruggedness study, various specimen diameter sizes mainly 38 mm (1.5"), 68 mm (2.7") and 100 mm (3.94"), were used to investigate diameter effects on the predicted fatigue life when the 3PBC

test is adopted. Looking into the applicability of 3PBC test to small sample diameters is important because the recommended sample thickness (i.e., 68 mm (2.7")) for the 3PBC test may prevent its use for thin lifts of asphalt mixture layers.

Figure 9.10 shows the effect of the diameter on the damage characteristic curves (C-S). As shown, C vs S curves of larger diameter samples are below those of the smaller-diameter samples. Figure 9.11 shows the number of cycles to failure based on the C versus S curves computed for each diameter. From the figure, differences in N_f values for the different scenarios are easily observed, where the N_f values tended to decrease with increasing diameter. The fatigue life for 38 mm diameter 3PBC test samples is higher compared to the reference geometry (68 mm) diameter and the 100 mm diameter has the shortest fatigue life. This trend is consistent in all air void contents and in strain levels (see Figure 9.11a and Figure 9.11b). P-values and Tukey's analysis for each scenario are presented in Table 9.6. From the table, it is confirmed that the effect of sample diameter on N_f is statistically significant. Non-homogenous distribution of stresses and strains are seen as one of the potential reasons affecting these changes in the N_f values. Also, the high presence of shear in larger diameter samples and incapability of the current VECD formulations to fully comprehend its effects might be influencing the results.

Numerous techniques were explored to relate the fatigue performance in terms of numbers of cycles to failure for the selected specimen diameters. In this context, the application of traditional analysis (i.e., multi-linear regression) and advanced novel computing techniques (i.e., multigene genetic programming and artificial neural network) were utilized to develop predictive models to relate fatigue performance among varying specimen diameters. A major advantage of such approaches is their potential to train complex patterns and develop statistically accurate and

sound models (Naser & Seitllari, 2019; A. Seitllari & Naser, 2019; Aksel Seitllari & Kutay, 2018)(Haider, Masud, & Chatti, 2020; Masud, 2018).

Before any actions to implement the modeling methods, expansion of the variable database (i.e., a set of inputs and outputs) is important to statistically reinforce the predictive models. On this basis, a new 3E3 mixture was tested, in addition to the existing 5E3 mixture. The 3E3 mixtures consist of 19.0 mm NMAS typically used for the construction of base layers in asphalt pavements. This is important because the bottom-up fatigue cracking performance of asphalt pavements heavily relies on the fatigue cracking characteristics of the base (lowermost) asphalt layer. On the other hand, the 5E3 is a surface mixture with NMAS of 9.5 mm and mainly used as the surface (top) layer, where the top-down fatigue cracking initiates. The 3E3 loose asphalt mixture was collected from a local asphalt plant in Lansing, MI. The mix design properties and volumetric details of the 3E3 loose mixture are summarized in Table 4.1 Mixture sampling, processing and sample preparation procedures were similar to the 5E3 mixture. Nonetheless, the 3E3 specimens were prepared only at 7 % ± 0.5 % target air void content (i.e., samples were not prepared at different air void contents).

The |E*| measurements were carried out in accordance with the AASHTO R84 protocol using the Asphalt Mixture Performance Testing (AMPT) device at three temperatures (4, 20, and 40 °C) and three frequencies (10, 1, and 0.1 Hz) at each temperature. Figure 9.1a and Figure 9.1b show the |E*| master curves in log scale and semi-log scale for each respective replicate. Also, the relationship between the shift factors and the temperature is shown in Figure 9.1c. The |E*| master curve and shift factor coefficients are summarized in Table 9.3.

One span length with one corresponding diameter (i.e, 38 mm – 100 mm, 68 mm – 125 mm and 100 mm – 135 mm) was used to investigate the relation of fatigue performance of the 3E3

asphalt mixture. The 3E3 samples for each respective specimen dimensions were cored from the SGC compacted material and processed similar to the 5E3 mixture described in section 9.1. A minimum of two replicates were tested at temperatures of 10 °C and 20 °C at 5 Hz, with on-specimen initial strain level ranging from 200-350 microstrains (με) (see APPENDIX A). While for 68 mm – 100 mm and 100 mm – 135 mm one test specimen was extracted for each SGC compacted material, for 38 mm – 100 mm combination, four replicates were extracted from one SGC sample having a total of eight replicates (see Figure 9.3a). In addition to high laboratory productivity, the 38 mm – 100 mm geometry combination is more advantageous as it is also able to facilitate the laboratory fatigue evaluation of thin asphalt pavements.

Viscoelastic Continuum Damage (VECD) theory was then adopted to analyze the data from the 3PBC test results. It is important to note that the higher the NMAS of an asphalt mixture, the more is the sample-to-sample variability. In this regard, the C-S curves for each testing conditions were constructed and individual fatigue life (N_f) at target strain level (i.e. 150 με), the temperature of 10 °C and 20 °C, and frequency of 5 Hz was determined as presented in Figure 9.12 to Figure 9.14. As shown in the figures, the C-S curves of different temperatures collapsed for all the tested dimensions regardless of the variable nature of the 3E3 mixture caused by its large NMAS (i.e., 19 mm), which is a crucial factor affecting the continuum medium. In the 38 mm diameter geometry, however, one of four replicates (i.e., 3PBC - 3E3 - 38-100 -4- 10C - 5Hz and 3PBC - 3E3 - 38-100 -1- 20C - 5Hz) extracted from each SGC compacted material, created variability and statistically affected the results. Likewise, for 68 mm – 125 mm geometry replicate 3PBC - 3E3 - 68-125 -1- 20C - 5Hz, the obtained C-S curve shifted upwards (see Figure 9.13a). In general, the observed abnormal shifts in C-S curves could be attributed to various factors but not limited to such as sample preparation related issues, machine compliances and\or other

technical related practices. Such cases were excluded from further considerations, but it is critical to be recorded as they, indeed, help improve the 3PBC test practice. The N_f values were shown to change with the variations in sample dimensions as illustrated in Figure 9.12b to Figure 9.14b. The revealed observations appear to agree with the conclusions derived from the 5E3 mixture.

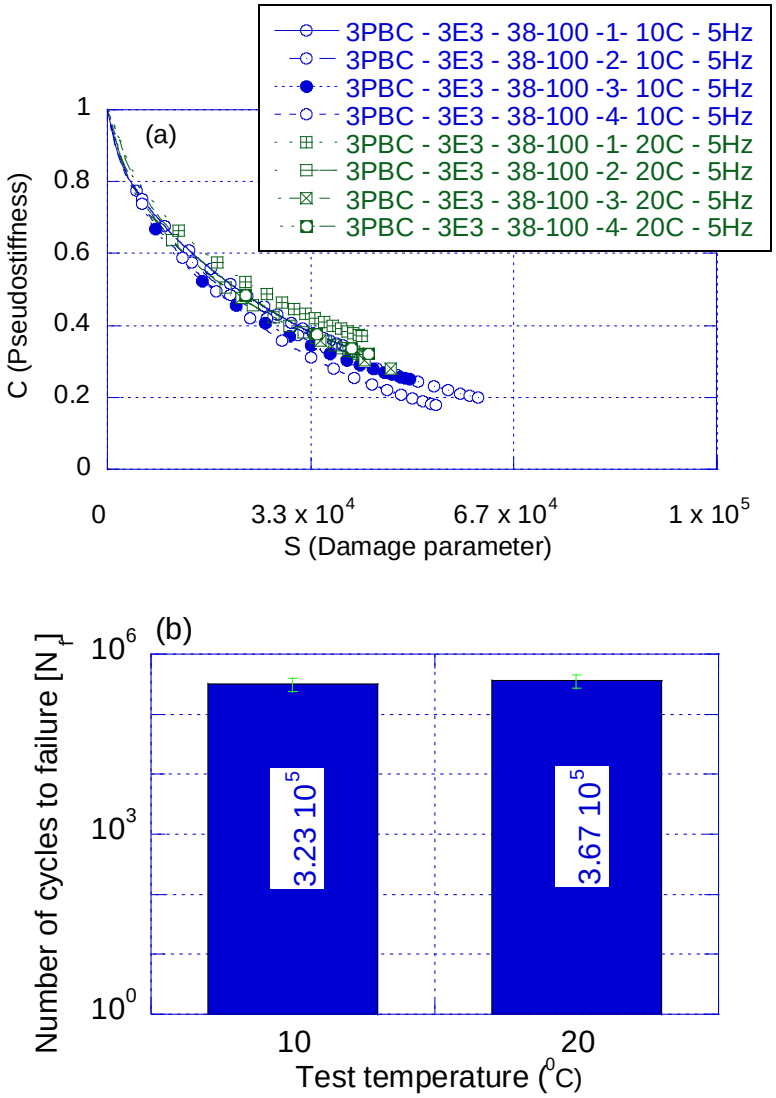

Figure 9.12. (a) Damage characteristic curves and (b) the number of cycles to failure N_f results at frequency of 5 Hz, temperature of 10 °C & 20 °C, and strain level of 150 με for 38 mm - 100 mm geometry.

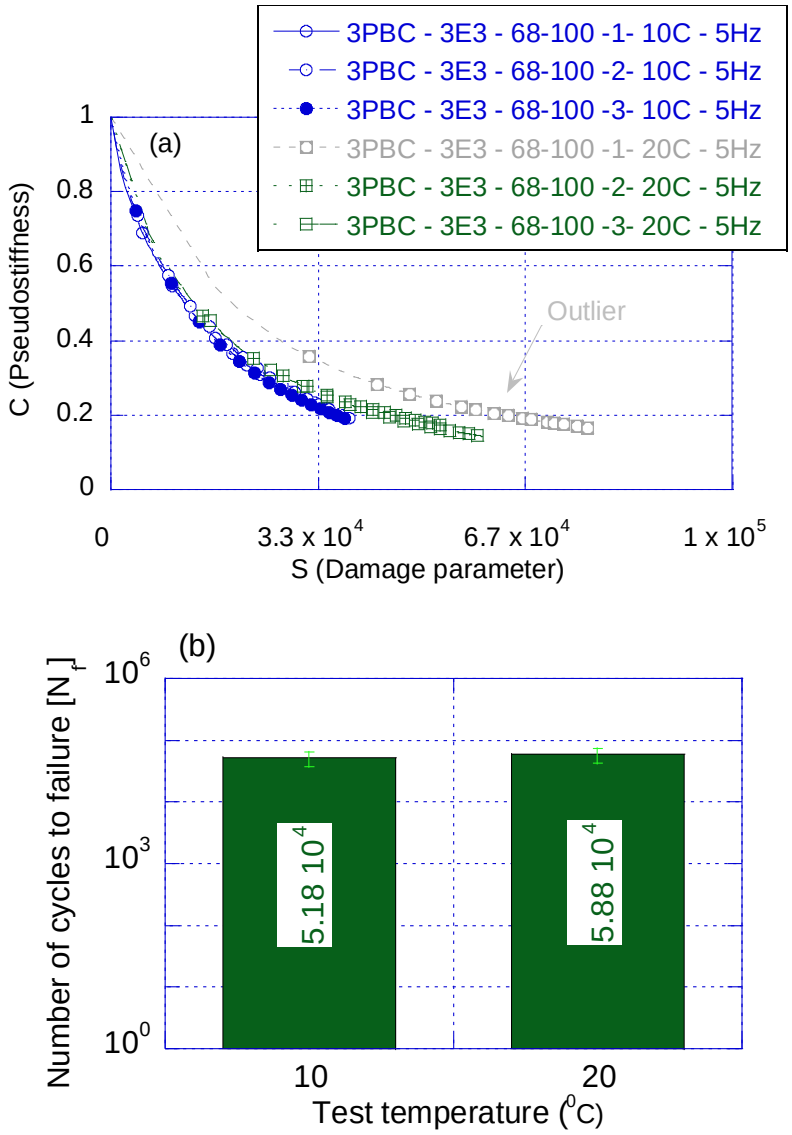

Figure 9.13. (a) Damage characteristic curves and (b) the number of cycles to failure results N_f results at frequency of 5 Hz, temperature of 10 °C & 20 °C, and strain level of 150 με for 68 mm - 125 mm (reference) geometry.

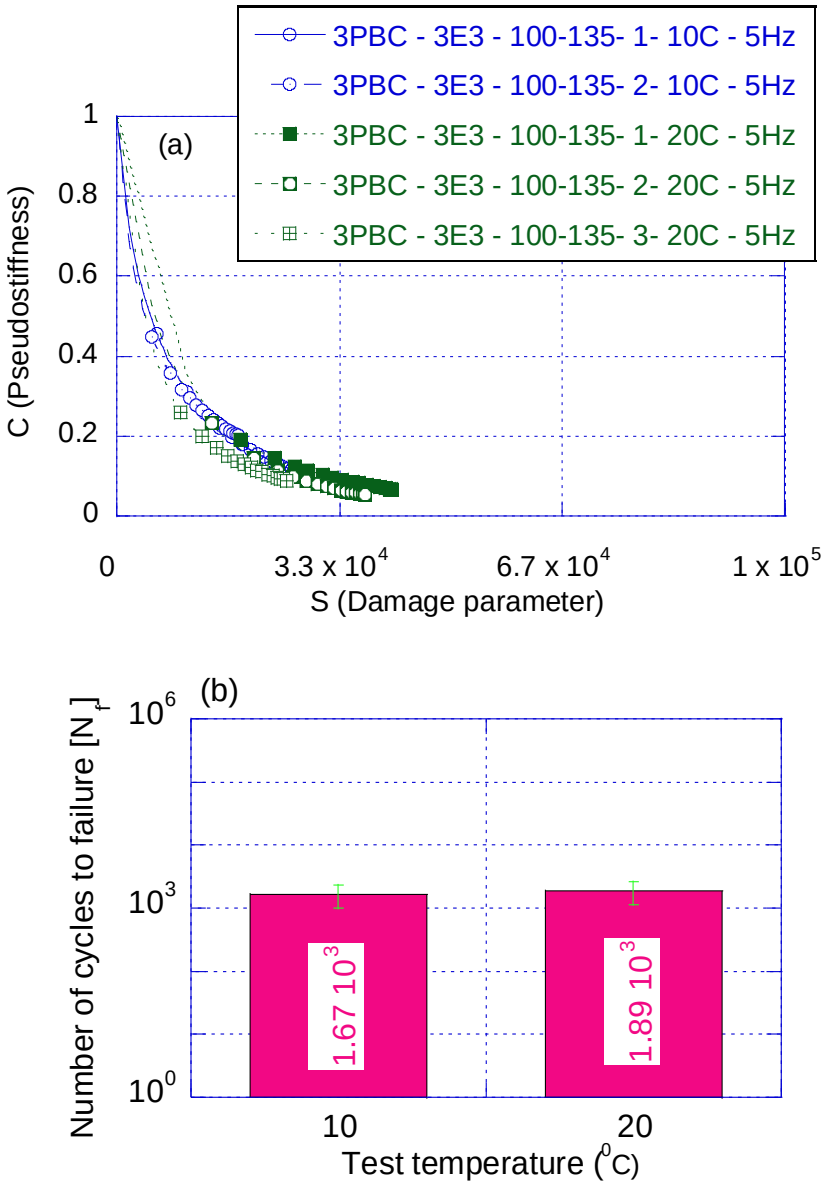

Figure 9.14. (a) Damage characteristic curves and (b) the number of cycles to failure N_f results at frequency of 5 Hz, temperature of 10 °C & 20 °C, and strain level of 150 με for 100 mm - 135 mm geometry.

To build the ground for the investigation of the fatigue life (N_f) relationship among different geometry combinations of 3PBC test, the C-S curves developed for 5E3 and 3E3 asphalt mixtures were used to calculate the N_f under the following conditions: frequency = 1, 5, 10 Hz, temperature = 5, 10, 15, 20, 25 and 30 ºC, and strain level = 100, 150, 200, 250, 300, 350, 400, 450, 500, 550 and 600 microstrain (mm/mm x 10^{-6}). The N_f values for each

temperature/frequency/strain level combination were computed using Equation [8.8] and summarized in APPENDIX B

Initially, the application of multi-linear regression (MLR) analysis was performed to inspect if any cogent relation could be achieved among the N_f values for different 3PBC sample diameters. In addition to the number of cycles to failure of the tested 3PBC sample diameter N_f (D_i), strain level (microstrain); 3PBC test sample diameter D_i (inch); and dynamic modulus |E*| (psi); were selected as input variables to correlate with the number of cycles to failure for the reference geometry $N_f(D_R)$ (i.e., D_R = 2.68 inches). A total of 792 data points obtained from the analysis of the C-S curve were used to develop and validate the MLR model. The data points were randomly divided into two data sets; training data set (80 %) and testing data set (20 %). Even though the division process was random, statistical parameters were used to ensure clarity regarding the range of the variables as presented in Table 9.7. It can be seen in the table that the strain level shows the highest skewed distribution. The data statistics for other input variables have a balanced distribution. It should be noted that the selected data were converted on a logarithmic scale with base 10. This practice was particularly implemented to minimize the large range that exists among the selected variables and avoid any potential overtraining of the developed models.

Table 9.7 Training data set and testing data set input statistics

	Training Phase				
Input	$\bar{x}$	s_x	c_{sx}	x_{min}	x_{max}
N_f for the tested sample diameter (N_f (D_i))	-3.510	0.234	-0.706	-4.000	-3.222
Strain level (με)	0.383	0.210	0.019	0.175	0.595
3PBC test sample diameter D_i (inch)	5.776	0.299	-0.533	5.048	6.218
Dynamic modulus |E*| (psi)	3.097	1.898	0.332	-0.329	8.791
Output					
N_f for the reference diameter (N_f (D_R=2.68))	3.231	1.415	0.648	1.017	7.471
	Testing Phase				
Input	$\bar{x}$	s_x	c_{sx}	x_{min}	x_{max}
N_f for the tested sample diameter (N_f (D_i))	-3.525	0.248	-0.555	-4.000	-3.222
Strain level (με)	0.390	0.211	-0.051	0.175	0.595
3PBC test sample diameter D_i (inch)	5.752	0.292	-0.364	5.048	6.218
Dynamic modulus |E*| (psi)	3.151	1.886	0.116	-0.060	8.134
Output					
N_f for the reference diameter (N_f (D_R=2.68))	3.350	1.468	0.465	1.016	7.471

Note: $\bar{x}$ =overall mean, s_x= standard deviation, c_{sx} =skewness coefficient, x_{min} =minimum and x_{max}= maximum.

The predictive strength and accuracy of the models were determined based on mean square error (MSE), mean absolute relative error (MARE) and coefficient of determination (R^2) as defined in Equations [9.1] to [9.3]. While R^2 represents how close the data are to the fitted line, the MSE and MARE parameters were used to determine if the relationship is significant (Aksel Seitllari, 2014; Aksel Seitllari, Kumbargeri, Biligiri, & Boz, 2018).

$$R^2 = \frac{\Sigma(o_i - p_i)^2}{\Sigma(p_i - p_{avg})^2} \quad [9.1]$$

$$MSE = \frac{1}{n}\sum_{i=0}^{n}(e_i)^2 = \frac{1}{n}\sum_{i=0}^{n}(o_i - p_i)^2 \quad [9.2]$$

$$\text{MARE} = \frac{1}{n}\sum_{i=1}^{n}\left|\frac{o_i - p_i}{o_i}\right| \times 100 \quad [9.3]$$

where, o_i is the observed output, p_i is the predicted output, p_{avg} is the averaged predicted output, n is the total number of data sets and e_i is the error for each input set.

As previously mentioned, the MLR model was developed using the training data set (i.e., 80 % = 634 data points). The final version of the MLR equation is in the following form:

$$N_{f\,(2.68)} = 10^{-3.851}\left(\frac{1}{strain}\right)^{1.671}\left(\frac{1}{|E^*|}\right)^{0.4469} D_i^{4.21}\, N_{f\,(Di)}^{0.7064} \qquad [9.4]$$

where, $strain = \frac{\text{mm}}{\text{mm}} \text{x } 10^{-6}, D_i = \text{inch}, |E^*| = \text{psi}$

Figure 9.15a illustrates the measured and the predicted N_f for the reference diameter (N_f (D_R=2.68)) in the training phase. As shown in the figure, the data points align to the line of equality for the MLR training set scatterplot. The calculated statistical measures used to evaluate the MLR model are presented in Table 9.8. According to the table, the training data set revealed the followings statistics: R^2 = 0.99, MSE = 0.02 and MARE = 4.50. Figure 9.15b shows the performance of the MLR model when applied to the testing data set. Note that the testing data set is independent and was not used to train the MLR model. The predicted versus measured values of N_f (D_R=2.68) for the testing data set exhibit a similar trend to the training data set. Likewise, the calculated MLR statistics of the testing data set exhibited the following measures R^2 = 0.99, MSE = 0.02 and MARE = 4.22.

Table 9.8 Model statistic results

	Training data set			Testing data set		
Statistics	R squared	Mean Absolute Relative Error	Mean Squared Error	R squared	Mean Absolute Relative Error	Mean Squared Error
MLR (Log scale)	0.99	4.50	0.02	0.99	4.22	0.02

In addition, multigene genetic programing (MGGP) and artificial neural network (ANN) analysis were performed to check if better fit can be achieved. Both these techniques, however,

revealed similar results to the MLR model. For clarity and ease of application, only the MLR model was pursued excluding the details of the other two techniques.

In essence, the obtained results clearly support the efficiency of the Equation [9.4] to correlate N_f of different sample diameters to $N_{f\,(D_R=2.68)}$ with high confidence. It is envisioned that this approach will leverage engineers' and\or road agencies' capacities to evaluate the fatigue performance of asphalt cores despite the layer thickness or aggregate size.

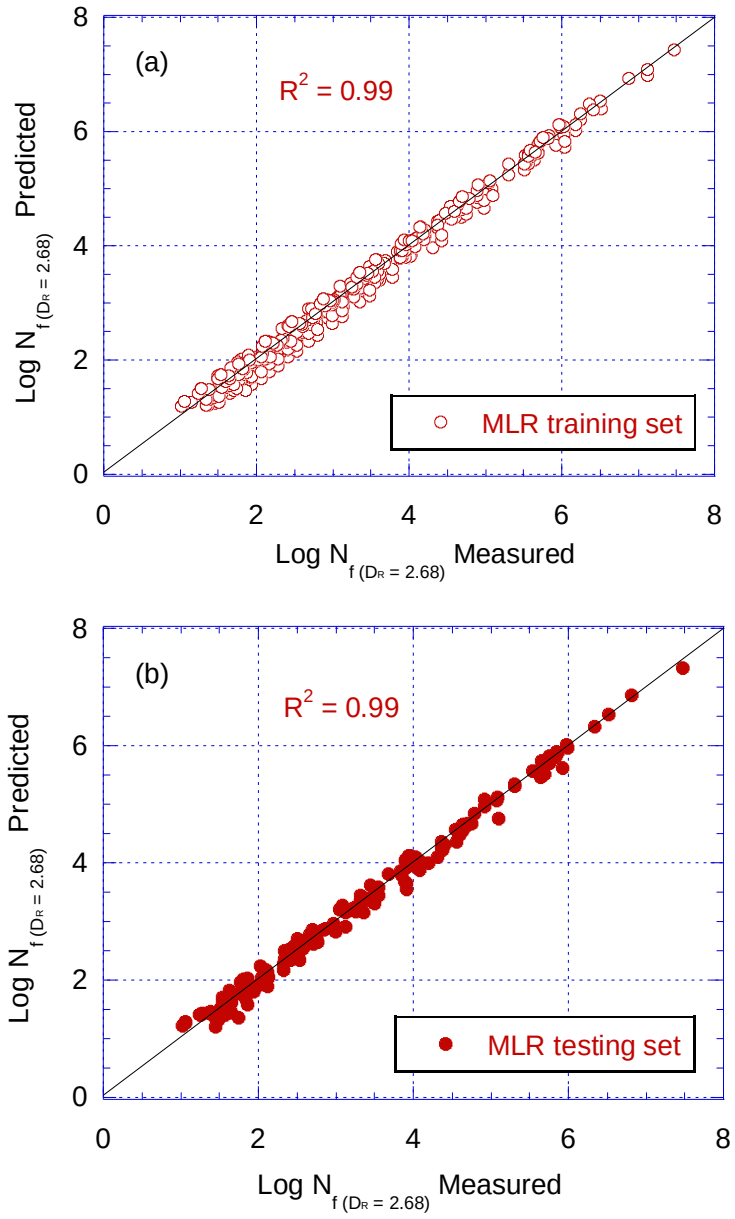

Figure 9.15. Performance of the developed MLR model for (a) training data set and (b) testing data set.

9.4 Summary of chapter findings

The objective of this part of the study was to perform a ruggedness evaluation of the 3PBC test. For this purpose, several factors that were believed to influence the 3PBC test results were identified. Cylindrical samples were prepared to materialize these factors and subjected to 3PBC tests. The research findings from this study have been summarized as follows:

- Three different fixtures were designed to address the influence of selected factors on the 3PBC test results. The general lateral displacement of these fixtures was measured using the lateral LVDT, and the maximum displacement limit of 10 % of the vertical displacement was recommended.
- The VECD theory was successfully applied to all selected geometries. The C-S curves were used to obtain the N_f value of each sample to get information about the sample-to-sample variability for each air void content.
- Based on the received results, the air void content tolerance range of ± 1 % was considered a reasonable practice for the 3PBC test method. This range is in alignment with the current state of practice for performance specimens.
- The variation in the span length on the 3PBC test did not have considerable effects on the fatigue life of the asphalt mixture.
- It was observed that the changes in specimen diameter affected the N_f values. Typically, specimens with smaller diameter exhibited longer fatigue life. This was consistent for all the air void contents and/or strain levels.
- Various techniques were explored to relate the fatigue performance in terms of numbers of cycles to failure for the selected specimen diameters. Results revealed that MLR developed equation can capture the relation between the $N_{f\,(D_R=2.68)}$ and other input variables with high

confidence. This allows the 3PBC test to run at various diameters to correlate with the reference geometry (i.e., $N_{f\,(D_R=2.68)}$).

Overall, this part of the research study led to ruggedness evaluation of the 3PBC testing approach through varying factors and their levels. The proposed research addresses an important long-standing issue for fatigue cracking characterization of asphalt pavements. Certainly, the proposed methodology possesses great potential to significantly reduce the testing cost and substantially increase the testing speed. A future objective of the study plan to improve by further modifying the VECD formulations to capture the diameter effects on fatigue life of the mixture. In that case, the 3PBC test will provide a mechanistic, yet practical protocol to evaluate cracking resistance of asphalt mixtures.

10. CONCLUSIONS

The objective of this study was to introduce a more practical fatigue testing approach to the uniaxial fatigue tests and corresponding analyses based on the Viscoelastic Continuum Damage (VECD) theory. This new approach referred to as the three-pint bending cylinder (3PBC) test, aimed at addressing the challenges present in the current state of practice, with a focus on test procedure simplicity, sensitive to asphalt mix design, repeatable and efficient. The new test setup was designed and data analysis methodology was developed, validated and verified using three-dimensional finite element (3D FE) analysis and laboratory results. Furthermore, the VECD theory was adopted and implemented to model the mechanical response of the specimens. Finally, ruggedness evaluation of the 3PBC test approach through varying factors and their levels were investigated and presented. The findings of this study can be summarized as follows:

- Based on 3D FE analyses, it was shown that the error in elastic $|E^*|_{3PBC}$ ranges from 0.2 % to 16 %, whereas for viscoelastic $|E^*|_{3PBC}$ is less than 12 %. The results also indicate that typically, the error increases with the decrease in loading frequency. The 3PBC tests are recommended to be performed at 5 Hz and above, where the maximum error is less than 5 %. Additionally, the back-calculated Poisson's ratio values match very well.
- The laboratory results indicated that the |E*| values obtained from the measured master curve (i.e., $|E^*|_{AMPT}$) and the corresponding |E*| (i.e., $|E^*|_{3PBC}$) calculated using Timoshenko beam theory match reasonably. The calculated error ranges from 0.4 % to 16 %. Generally, it was observed that the error increases with the decreasing frequency and increasing temperature.

- Also, the back-calculated Poisson's ratio for different |E*| values, where a and b coefficients retrieved from (Maher & Bennert, 2008) match well with the back-calculated values from 3PBC setup.
- It was shown that the viscoelastic continuum damage theory can be used to model the fatigue life of an asphalt mixture at many temperature/frequency/strain level combinations, by simply running the 3PBC tests at a few temperatures/strain levels.
- The 3PBC testing results were analyzed using the same VECD formulations developed for PP data analysis. The damage characteristic curves (C-S) were generated and compared. It was shown that the C-S curves obtained from the 3PBC test collapsed to form a unique curve, just like the C-S curves of PP tests. However, the C-S curves of 3PBC and PP tests were not the same. The C-S curves of 3PBC tests were generally shifted upwards compared to the PP-based C-S curve for a given mixture. This difference is understandable since the mode of loading is different.
- Asphalt mixture hierarchical ranking obtained from 3PBC and PP tests agreed very well with each other. Overall, the number of cycles to failure obtained from 3PBC tests were about 4.5 times those obtained from the PP tests.
- Three different fixtures were designed to address the influence of selected factors on the 3PBC test results. The general lateral displacement of these fixtures was measured using the lateral LVDT, and the maximum displacement limit of up to 10 % of the vertical displacement was set.
- The VECD theory was successfully applied to all selected geometries. The C-S curves were used to obtain the N_f value of each sample to get information about the sample-to-sample variability for each air void content.

- Based on the received results, the air void content tolerance range of ± 1 % was considered a reasonable practice for the 3PBC test method.
- The variation in the span length on the 3PBC test did not have considerable effects on the fatigue life of the asphalt mixture.
- It was observed that the changes in specimen diameter affected the N_f values. Typically, specimens with smaller diameter exhibited longer fatigue life. This was consistent for all the air void contents and/or strain levels.
- Various techniques were explored to relate the fatigue performance in terms of numbers of cycles to failure for the selected specimen diameters. Results revealed that MLR developed equation can capture the relation between the $N_{f\,(D_R=2.68)}$ and other input variables with high confidence. This allows the 3PBC test to run at various diameters to correlate with the reference geometry (i.e., $N_{f\,(D_R=2.68)}$).

11. RECOMMENDATIONS

The proposed research addresses an important long-standing issue for fatigue cracking characterization of asphalt pavements. Certainly, the proposed methodology possesses great potential to significantly reduce the testing cost and substantially increase the testing speed. Nevertheless, enhancements can be made to the practice presented in this study. A list of future works are listed below:

- Validate the Poisson's ratio obtained from the system via direct measurements: Selection of appropriate Poisson's ratio as part of mechanistic-empirical pavement design is important for the accuracy of the strains in a pavement system. Poisson's ratio may be measured during the AASHTO R83 test procedure, if additional radial LVDTs are available, which is not the case in the AMPT. Therefore, the Poisson's ratio of asphalt pavements is often not a measured property, rather a default value is used in pavement design when a design is done using the AASHTOWare Pavement ME Design software. The Timoshenko beam theory formulations allow indirect estimation of Poisson's ratio from the 3PBC test data. Since Poisson's ratio obtained from the 3PBC test is a calculated property, rather than a direct measurement, there is a need for its validation.
- Diameter effects on 3PBC fatigue life: The general purpose of this study is to provide a mechanistic, yet practical protocol to evaluate cracking resistance of asphalt mixtures. The obtained results show that the proposed approach possesses great potential to achieve this objective. However, in Chapter 9, this method couldn't apprehend the effects of varying diameters in the fatigue life of the tested asphalt samples. Hence, further investigations should be performed to improve the analytical formulations to capture the diameter effects on the fatigue life of the mixture.

- Inter-laboratory study: the results presented in this research study are quite promising, however, the 3PBC test method should still be considered to be under development. An inter-laboratory (round-robin) study should be performed to determine the accuracy and precision (i.e., ASTM C802, ASTM C670) of the developed test practice.

APPENDICES

APPENDIX A

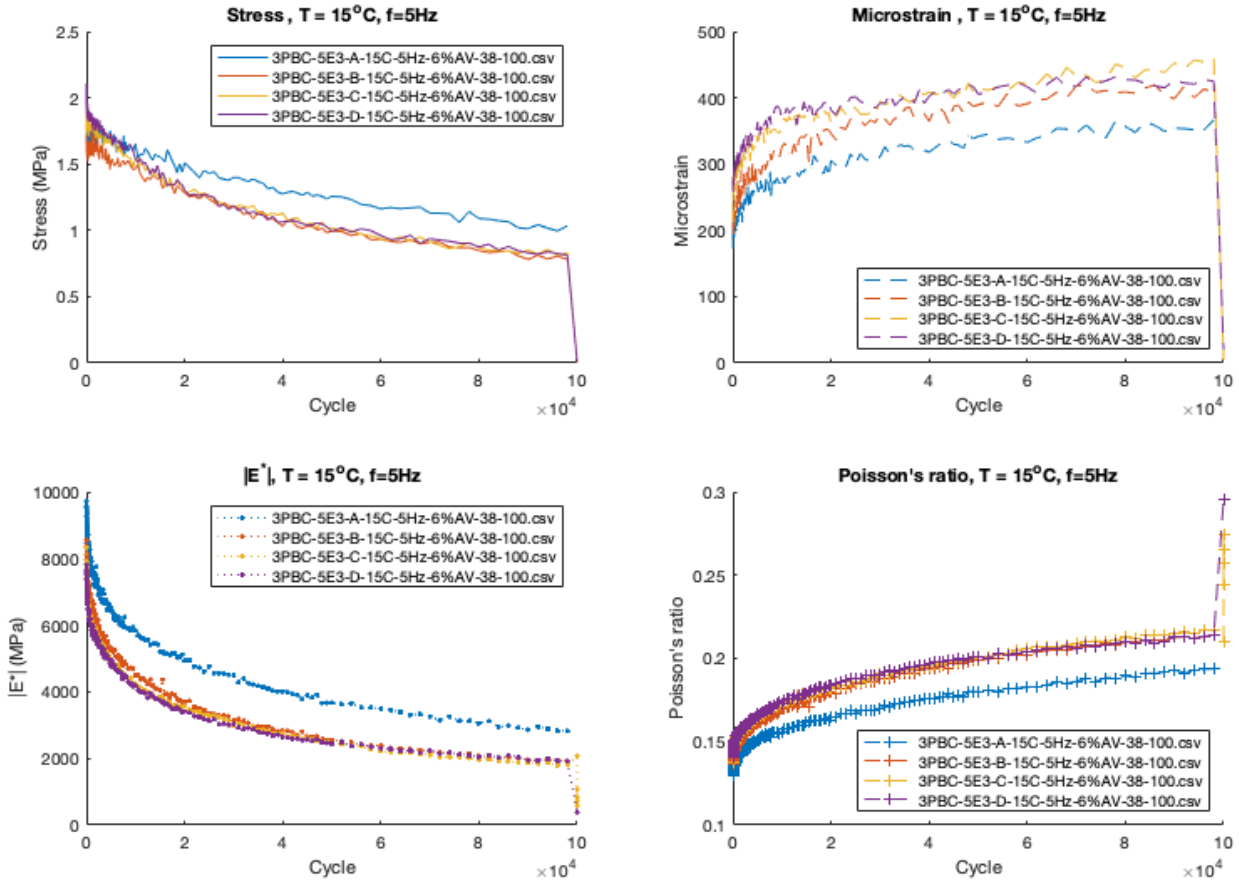

Figure A.1. Mix ID: 5E3, sample dimensions: diameter = 38 mm, length = 100 mm.

Figure A.1. (cont'd)

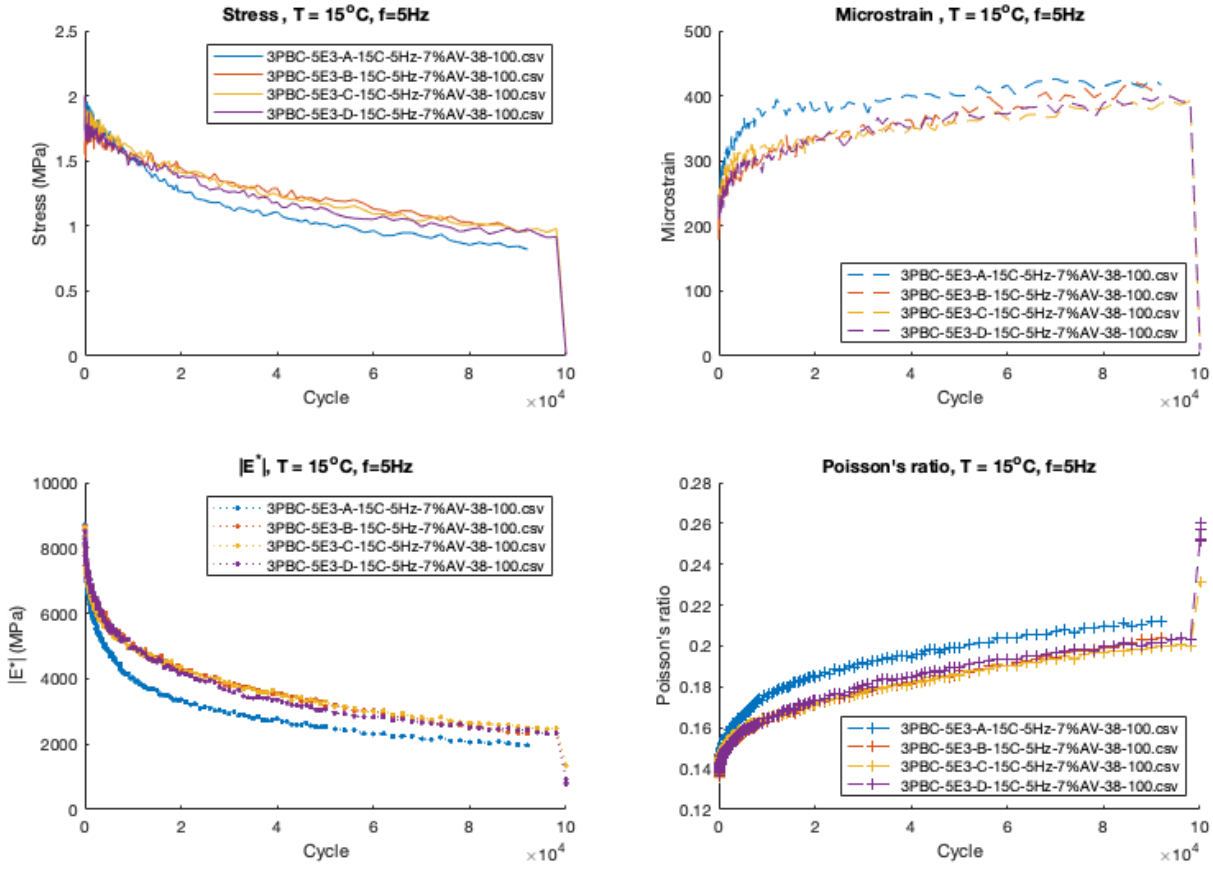

Figure A.1. (cont'd)

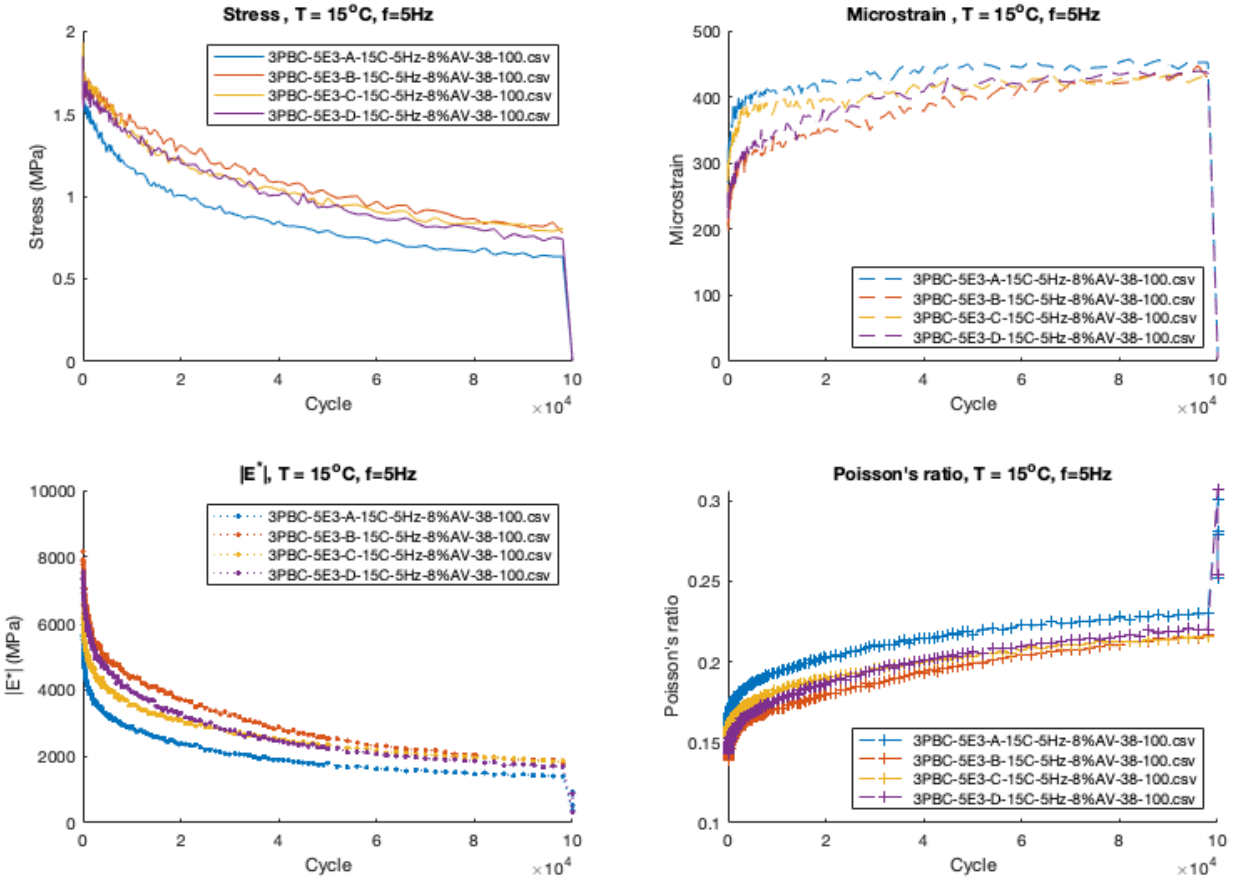

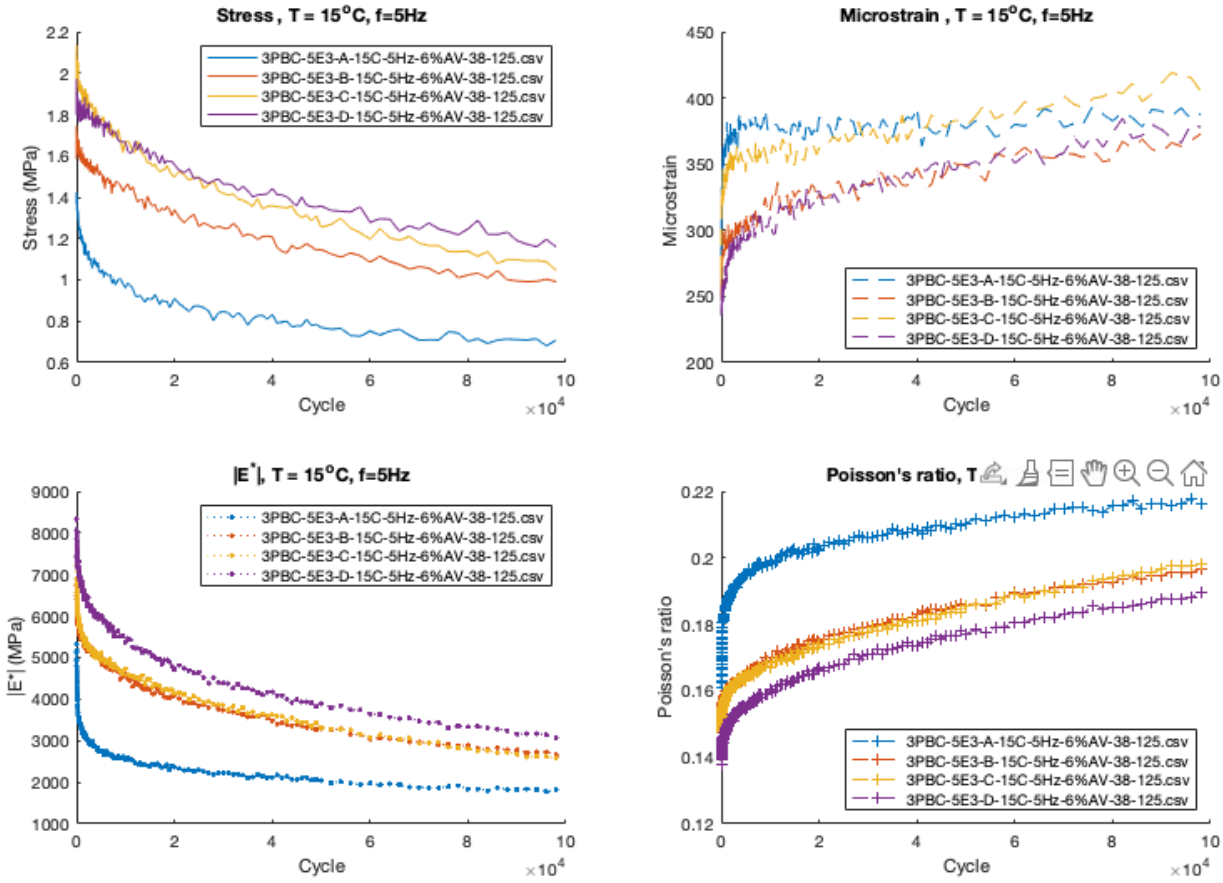

Figure A.2. Mix ID: 5E3, sample dimensions: diameter = 38 mm, length = 125 mm.

Figure A.2. (cont'd)

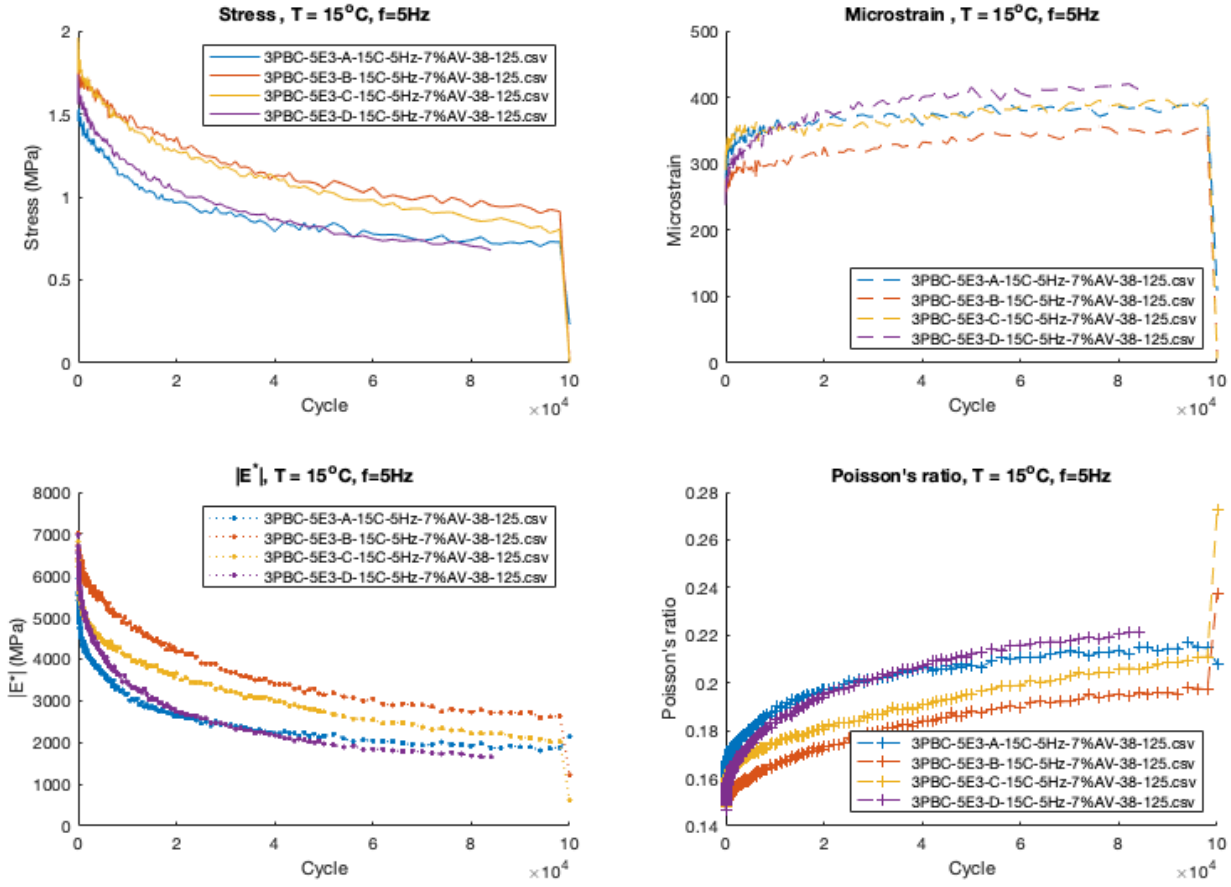

Figure A.2. (cont'd)

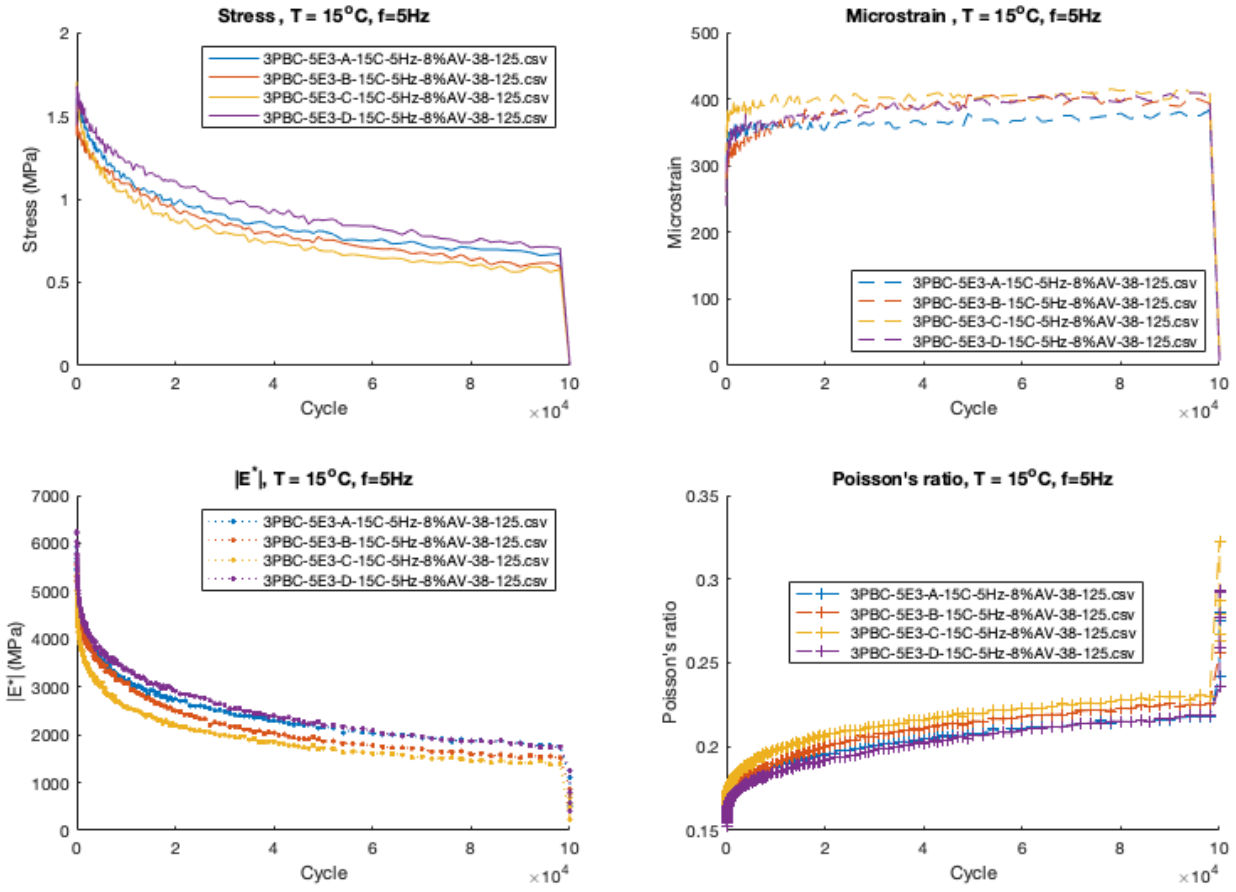

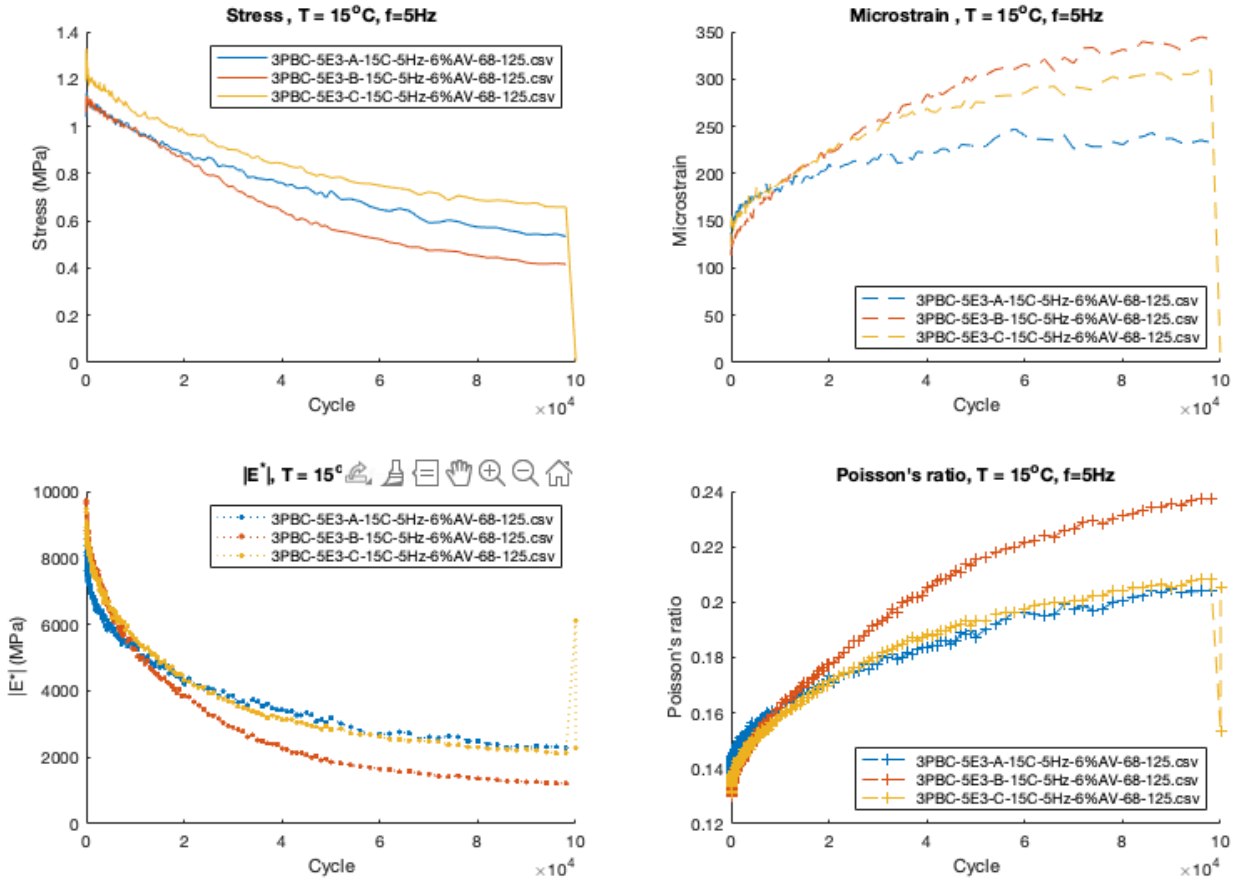

Figure A.3. Mix ID: 5E3, sample dimensions: diameter = 68 mm, length = 125 mm.

Figure A.3. (cont'd)

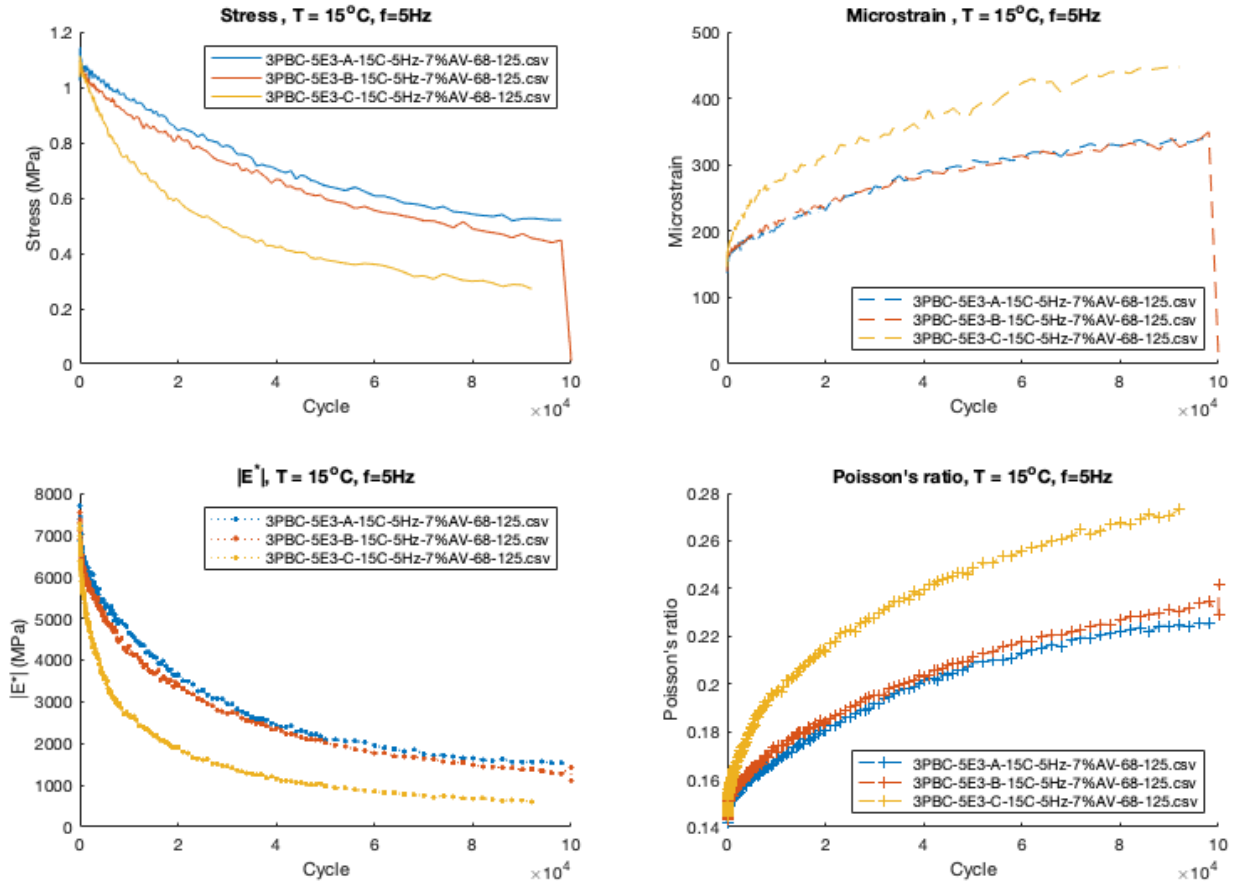

Figure A.3. (cont'd)

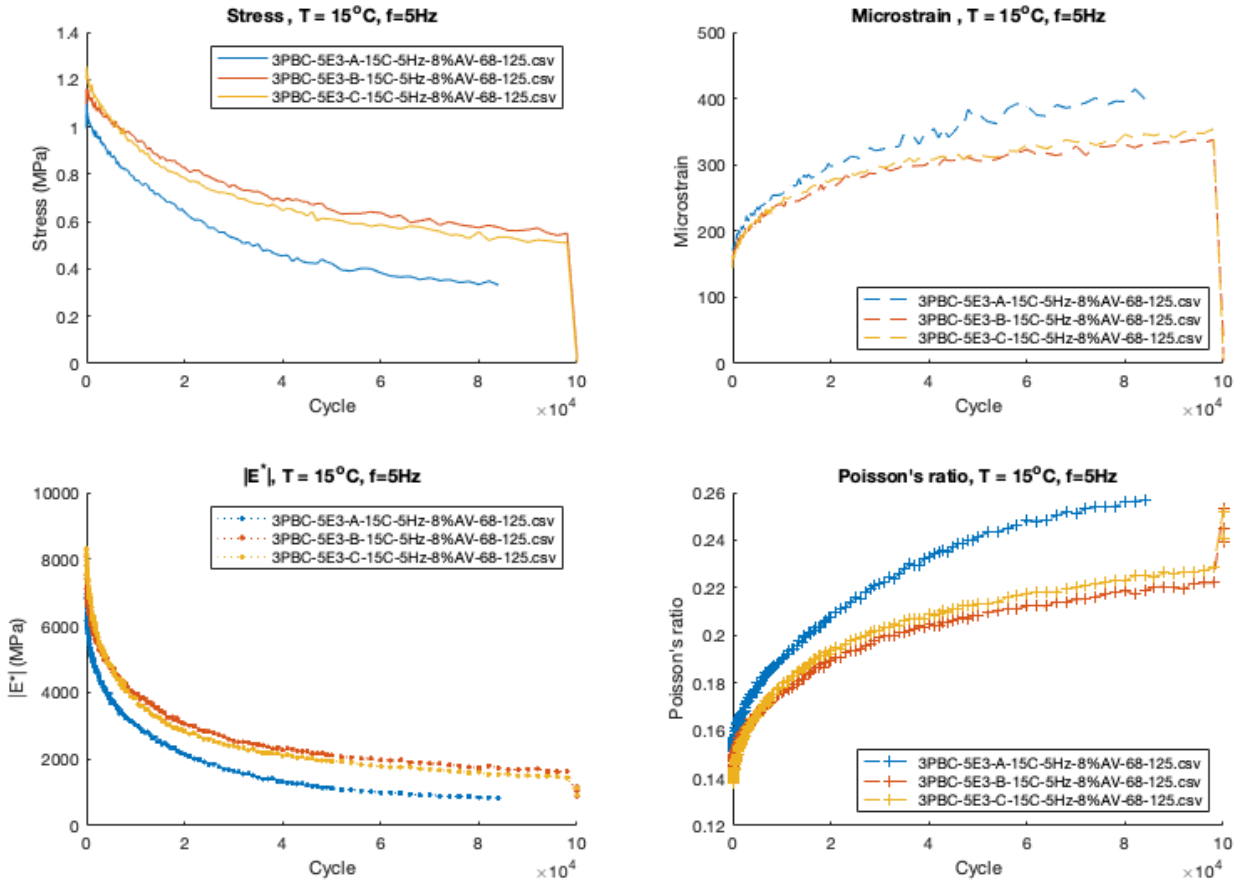

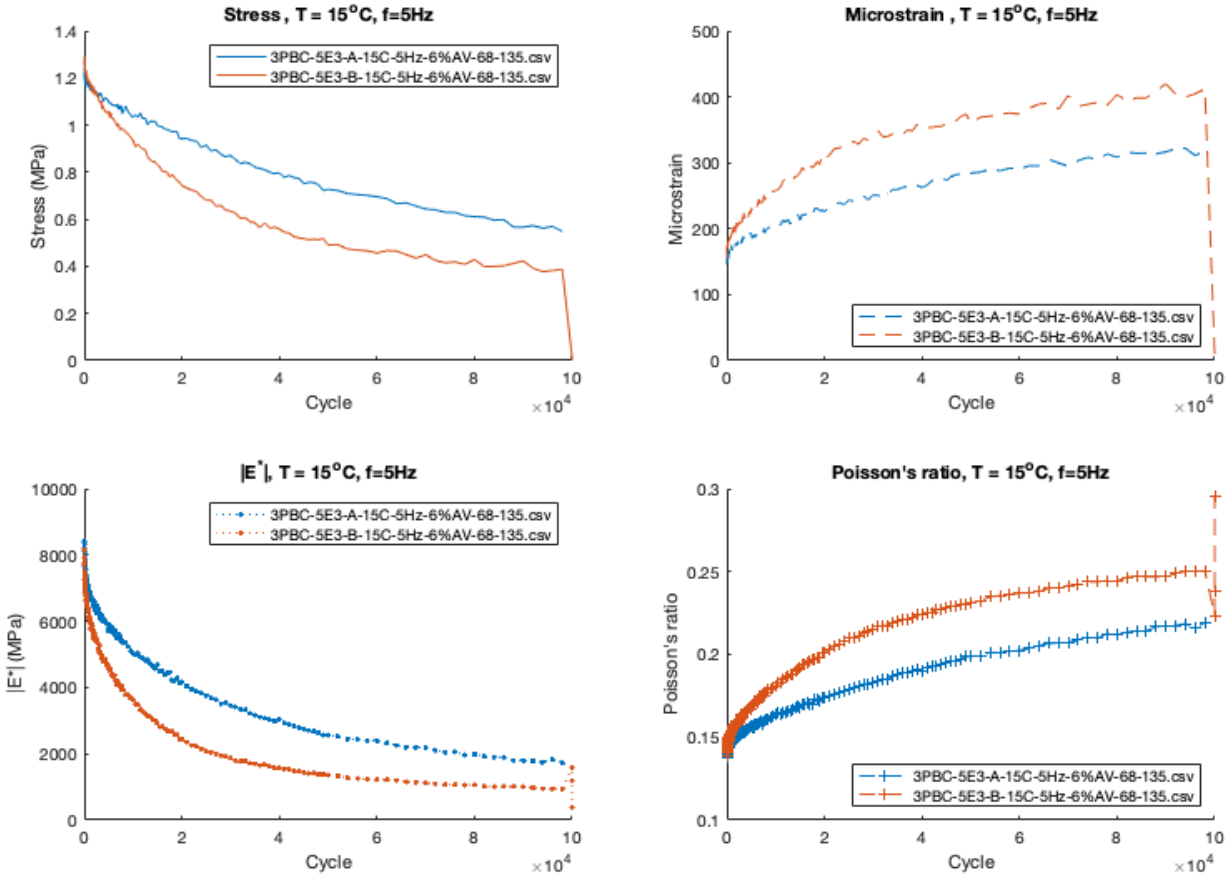

Figure A.4. Mix ID: 5E3, sample dimensions: diameter = 68 mm, length = 135 mm.

Figure A.4. (cont'd)

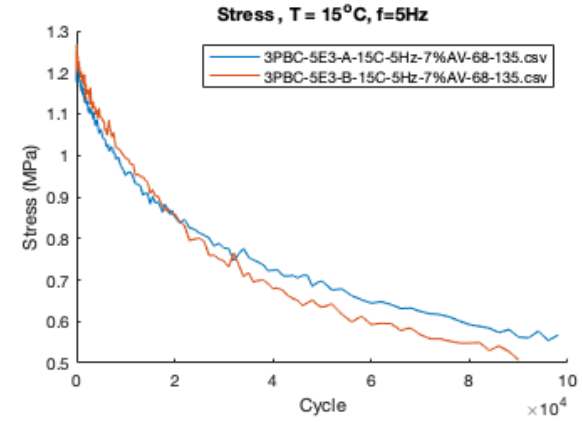

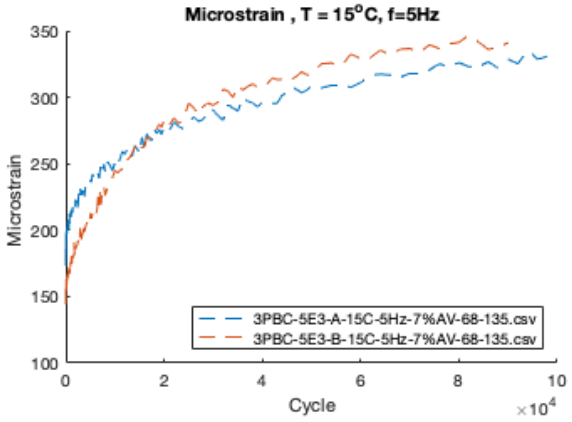

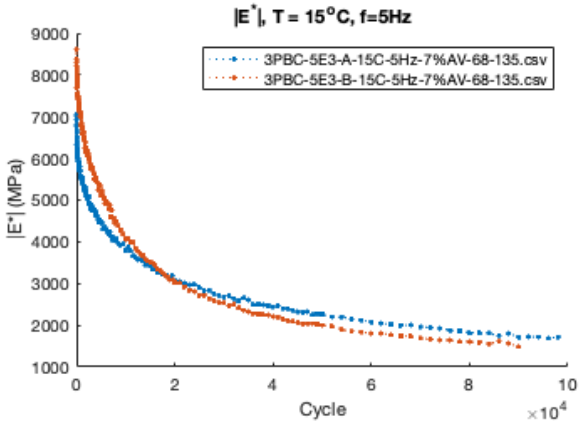

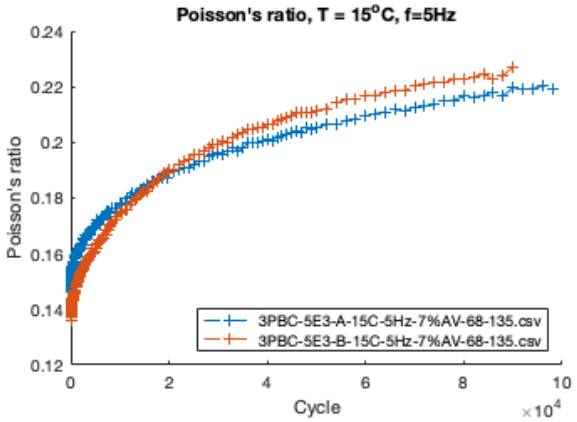

Figure A.4. (cont'd)

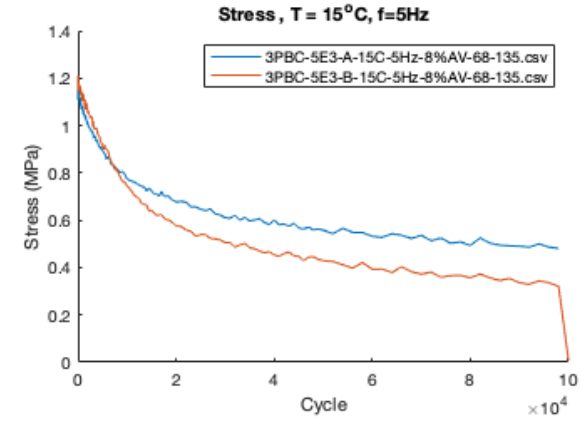

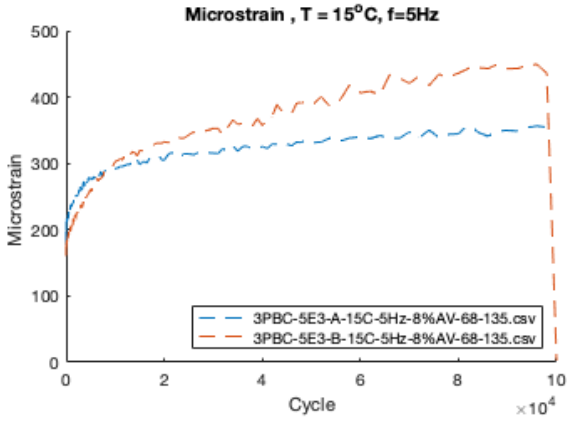

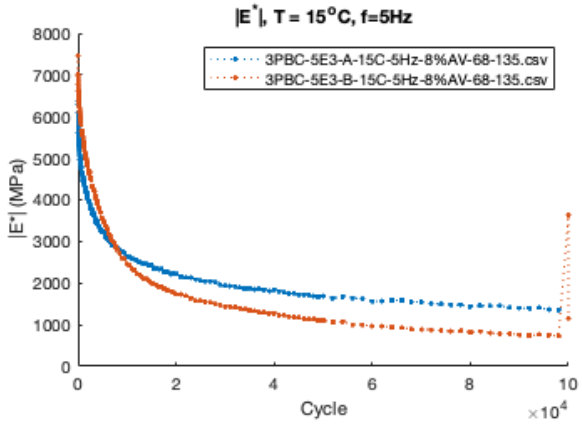

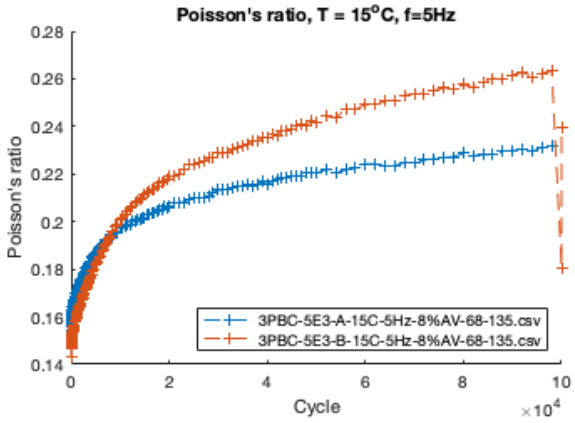

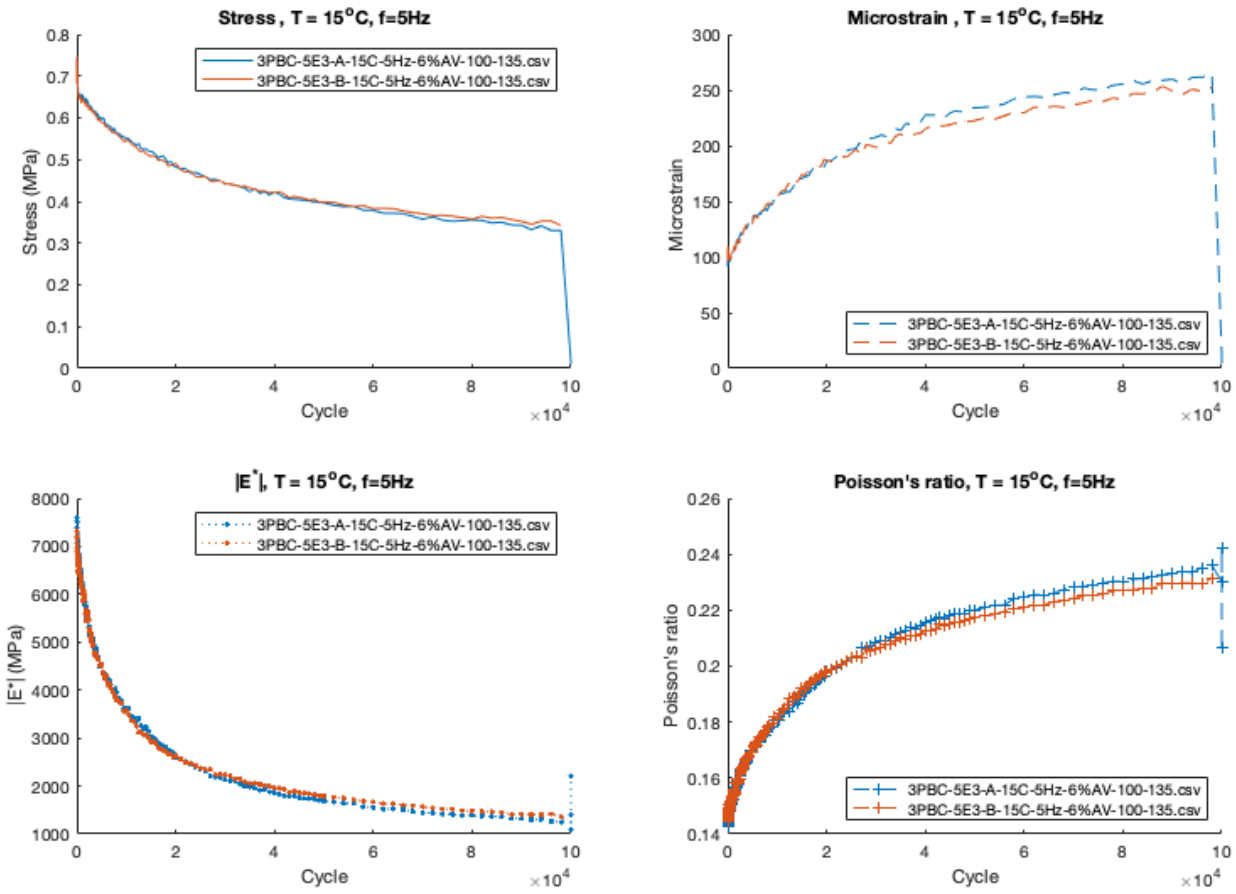

Figure A.5. Mix ID: 5E3, sample dimensions: diameter = 100 mm, length = 135 mm.

Figure A.5. (cont'd)

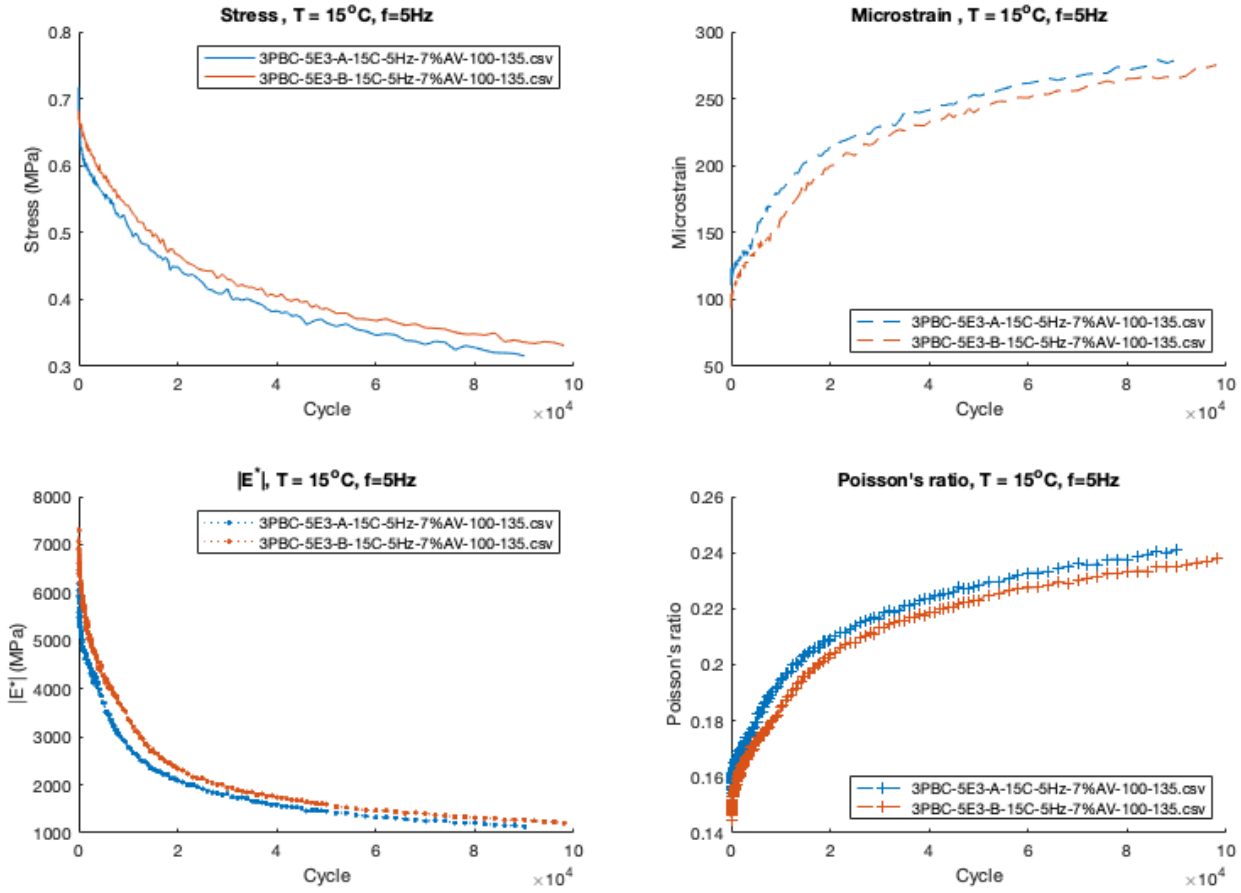

Figure A.5. (cont'd)

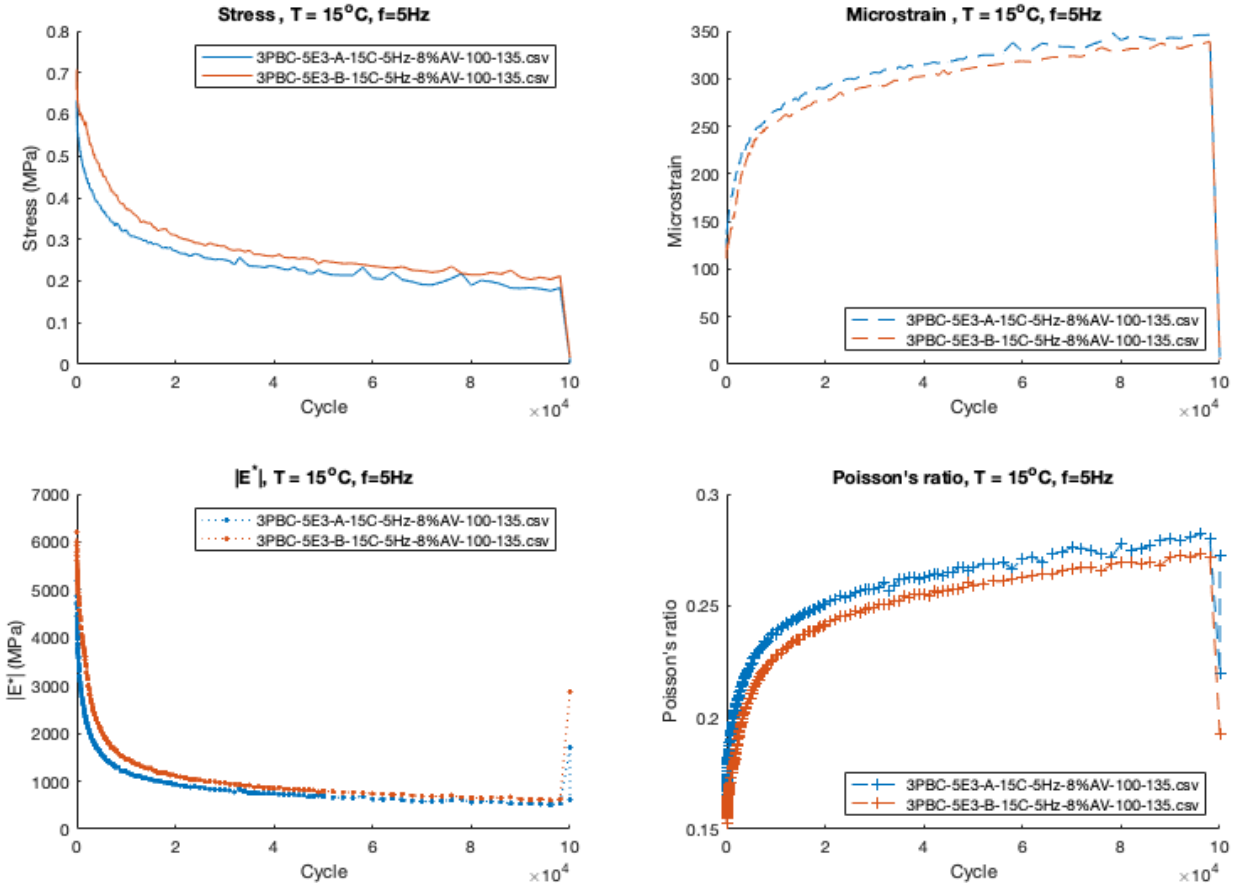

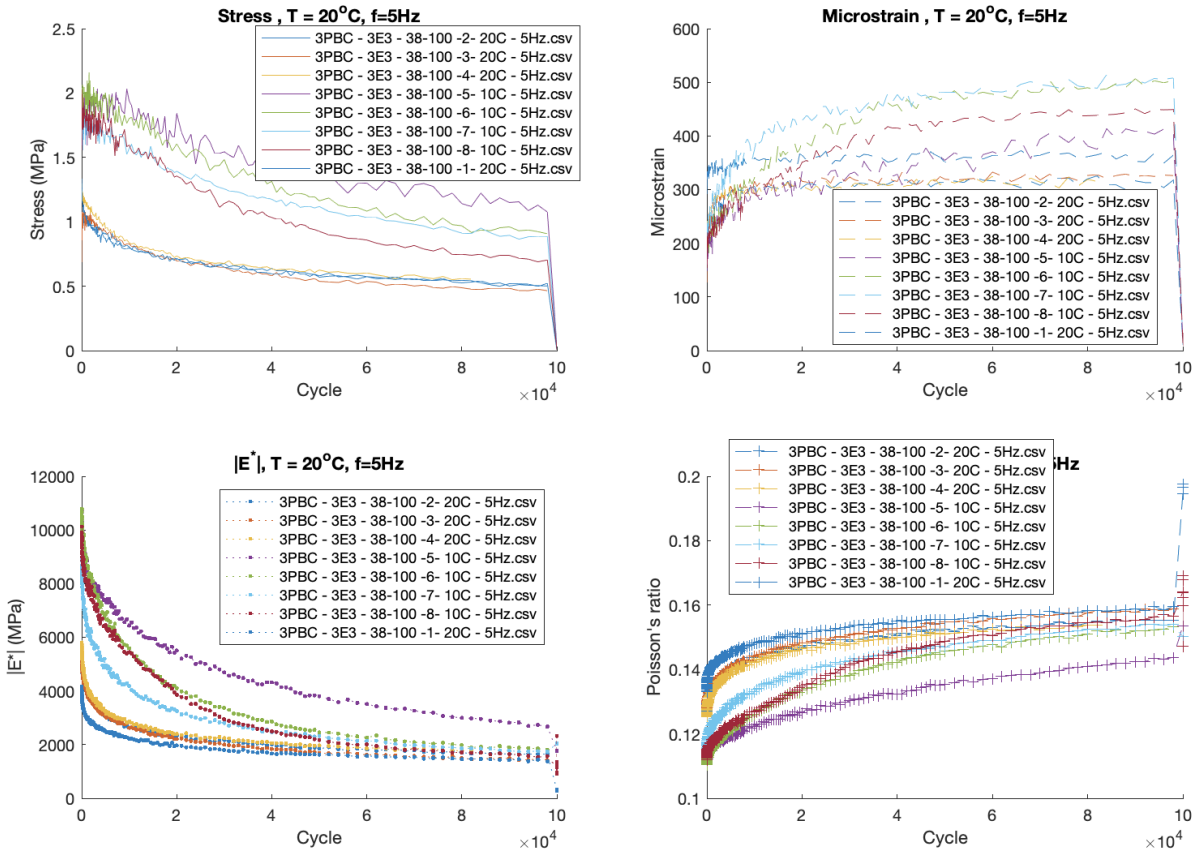

Figure A.6. Mix ID: 3E3, sample dimensions: diameter = 38 mm, length = 100 mm.

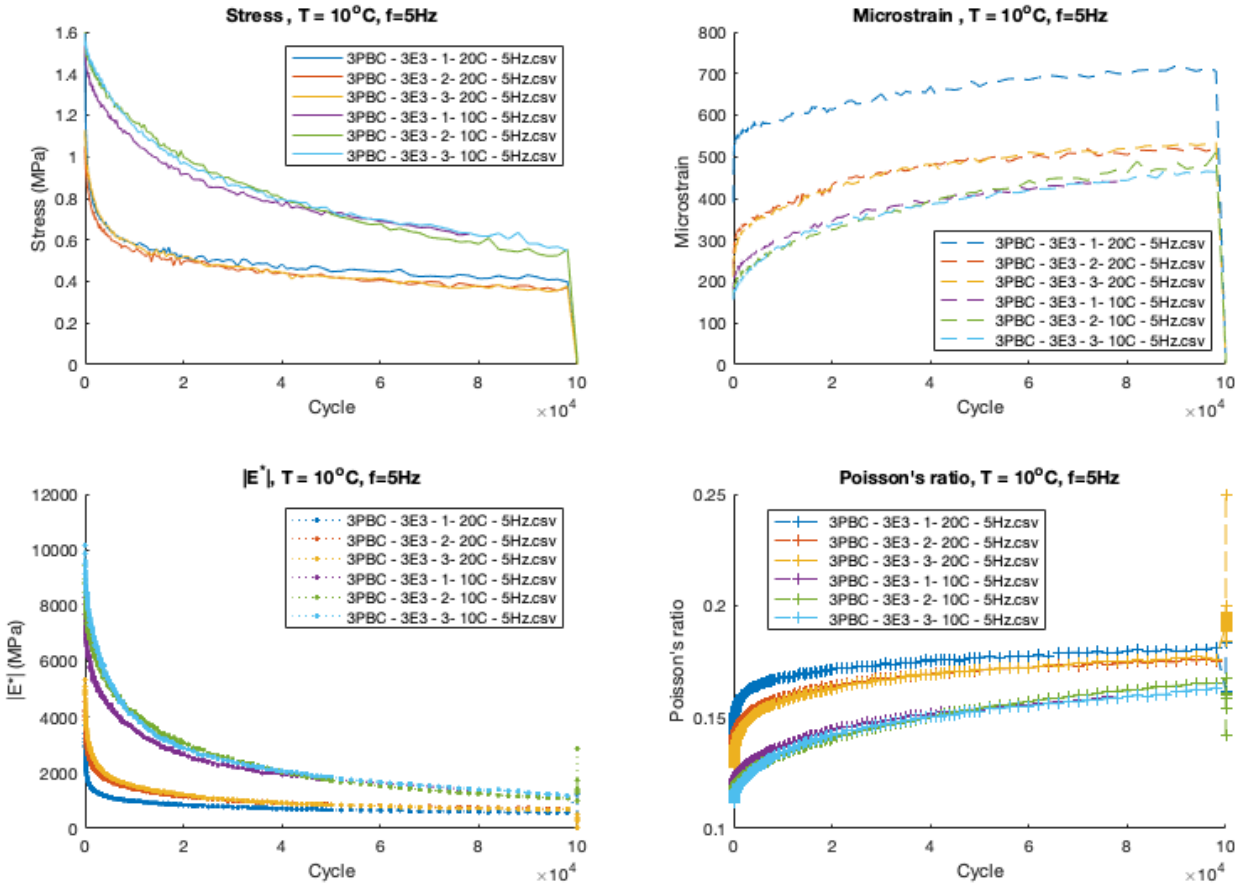

Figure A.7. Mix ID: 3E3, sample dimensions: diameter = 68 mm, length = 125 mm.

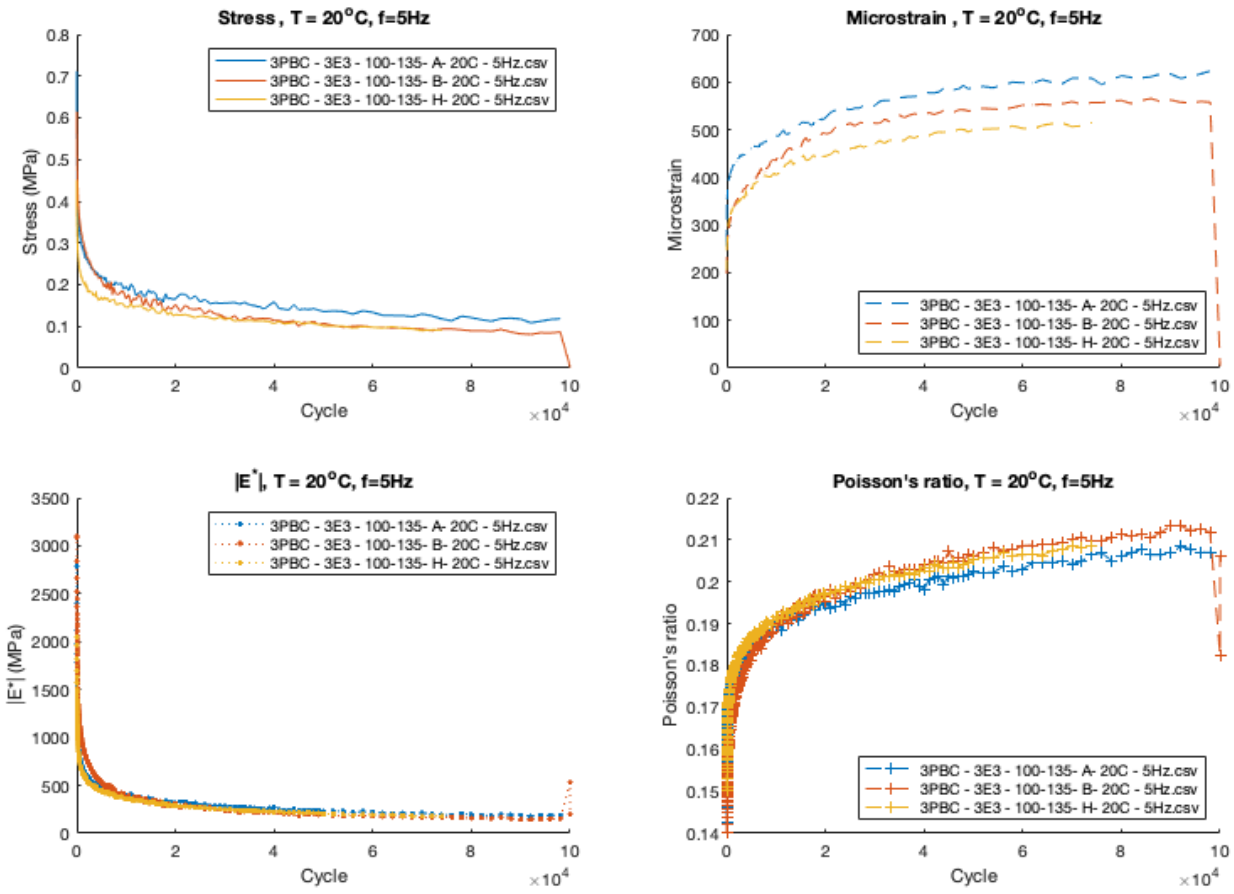

Figure A.8. Mix ID: 3E3, sample dimensions: diameter = 100 mm, length = 135 mm.

APPENDIX B

Table B. 1 MLR model database

f (Hz)	T (F)	Strain (ε)	D_i (inch)	|E*| psi	N_f (D_i) (inch)	N_f (D_R = 2.68 inch)
Mix ID: 3E3						
1	41	0.0001	1.50	1048381	3423720	436953
1	41	0.0002	1.50	1048381	386386	49313
1	41	0.0002	1.50	1048381	82182	10488
1	41	0.0003	1.50	1048381	24737	3157
1	41	0.0003	1.50	1048381	9275	1184
1	41	0.0004	1.50	1048381	4047	516
1	41	0.0004	1.50	1048381	1973	252
1	41	0.0005	1.50	1048381	1047	134
1	41	0.0005	1.50	1048381	594	76
1	41	0.0006	1.50	1048381	356	45
1	41	0.0006	1.50	1048381	223	28
1	50	0.0001	1.50	773444	2639539	336872
1	50	0.0002	1.50	773444	297887	38018
1	50	0.0002	1.50	773444	63359	8086
1	50	0.0003	1.50	773444	19071	2434
1	50	0.0003	1.50	773444	7150	913
1	50	0.0004	1.50	773444	3120	398
1	50	0.0004	1.50	773444	1521	194
1	50	0.0005	1.50	773444	807	103
1	50	0.0005	1.50	773444	458	58
1	50	0.0006	1.50	773444	274	35
1	50	0.0006	1.50	773444	172	22
1	59	0.0001	1.50	524549	3487425	445084
1	59	0.0002	1.50	524549	393576	50230
1	59	0.0002	1.50	524549	83711	10684
1	59	0.0003	1.50	524549	25197	3216
1	59	0.0003	1.50	524549	9447	1206
1	59	0.0004	1.50	524549	4122	526
1	59	0.0004	1.50	524549	2009	256
1	59	0.0005	1.50	524549	1066	136
1	59	0.0005	1.50	524549	605	77
1	59	0.0006	1.50	524549	362	46
1	59	0.0006	1.50	524549	227	29
1	68	0.0001	1.50	328959	7650815	976438
1	68	0.0002	1.50	328959	863438	110197
1	68	0.0002	1.50	328959	183648	23438
1	68	0.0003	1.50	328959	55278	7055
1	68	0.0003	1.50	328959	20726	2645

Table B. 1 (cont'd)

1	68	0.0004	1.50	328959	9043	1154
1	68	0.0004	1.50	328959	4408	563
1	68	0.0005	1.50	328959	2339	299
1	68	0.0005	1.50	328959	1327	169
1	68	0.0006	1.50	328959	795	101
1	68	0.0006	1.50	328959	497	63
1	77	0.0001	1.50	194511	25099981	3203393
1	77	0.0002	1.50	194511	2832675	361521
1	77	0.0002	1.50	194511	602492	76893
1	77	0.0003	1.50	194511	181350	23145
1	77	0.0003	1.50	194511	67995	8678
1	77	0.0004	1.50	194511	29666	3786
1	77	0.0004	1.50	194511	14462	1846
1	77	0.0005	1.50	194511	7674	979
1	77	0.0005	1.50	194511	4353	556
1	77	0.0006	1.50	194511	2607	333
1	77	0.0006	1.50	194511	1632	208
1	86	0.0001	1.50	111784	104580592	13347130
1	86	0.0002	1.50	111784	11802513	1506299
1	86	0.0002	1.50	111784	2510320	320380
1	86	0.0003	1.50	111784	755605	96434
1	86	0.0003	1.50	111784	283304	36157
1	86	0.0004	1.50	111784	123606	15775
1	86	0.0004	1.50	111784	60257	7690
1	86	0.0005	1.50	111784	31972	4080
1	86	0.0005	1.50	111784	18137	2315
1	86	0.0006	1.50	111784	10861	1386
1	86	0.0006	1.50	111784	6800	868
5	41	0.0001	1.50	1266889	5890037	841192
5	41	0.0002	1.50	1266889	664724	94933
5	41	0.0002	1.50	1266889	141383	20192
5	41	0.0003	1.50	1266889	42556	6078
5	41	0.0003	1.50	1266889	15956	2279
5	41	0.0004	1.50	1266889	6962	994
5	41	0.0004	1.50	1266889	3394	485
5	41	0.0005	1.50	1266889	1801	257
5	41	0.0005	1.50	1266889	1022	146
5	41	0.0006	1.50	1266889	612	87
5	41	0.0006	1.50	1266889	383	55
5	50	0.0001	1.50	1007293	3035533	433523
5	50	0.0002	1.50	1007293	342577	48926
5	50	0.0002	1.50	1007293	72864	10406
5	50	0.0003	1.50	1007293	21932	3132
5	50	0.0003	1.50	1007293	8223	1174
5	50	0.0004	1.50	1007293	3588	512

Table B. 1 (cont'd)

5	50	0.0004	1.50	1007293	1749	250
5	50	0.0005	1.50	1007293	928	133
5	50	0.0005	1.50	1007293	526	75
5	50	0.0006	1.50	1007293	315	45
5	50	0.0006	1.50	1007293	197	28
5	59	0.0001	1.50	744457	2525658	360705
5	59	0.0002	1.50	744457	285035	40708
5	59	0.0002	1.50	744457	60625	8658
5	59	0.0003	1.50	744457	18248	2606
5	59	0.0003	1.50	744457	6842	977
5	59	0.0004	1.50	744457	2985	426
5	59	0.0004	1.50	744457	1455	208
5	59	0.0005	1.50	744457	772	110
5	59	0.0005	1.50	744457	438	63
5	59	0.0006	1.50	744457	262	37
5	59	0.0006	1.50	744457	164	23
5	68	0.0001	1.50	509918	3447217	492318
5	68	0.0002	1.50	509918	389038	55561
5	68	0.0002	1.50	509918	82746	11817
5	68	0.0003	1.50	509918	24906	3557
5	68	0.0003	1.50	509918	9338	1334
5	68	0.0004	1.50	509918	4074	582
5	68	0.0004	1.50	509918	1986	284
5	68	0.0005	1.50	509918	1054	151
5	68	0.0005	1.50	509918	598	85
5	68	0.0006	1.50	509918	358	51
5	68	0.0006	1.50	509918	224	32
5	77	0.0001	1.50	326060	7422059	1059990
5	77	0.0002	1.50	326060	837621	119626
5	77	0.0002	1.50	326060	178157	25444
5	77	0.0003	1.50	326060	53625	7659
5	77	0.0003	1.50	326060	20106	2871
5	77	0.0004	1.50	326060	8772	1253
5	77	0.0004	1.50	326060	4276	611
5	77	0.0005	1.50	326060	2269	324
5	77	0.0005	1.50	326060	1287	184
5	77	0.0006	1.50	326060	771	110
5	77	0.0006	1.50	326060	483	69
5	86	0.0001	1.50	198270	22822529	3259426
5	86	0.0002	1.50	198270	2575652	367845
5	86	0.0002	1.50	198270	547825	78238
5	86	0.0003	1.50	198270	164895	23550
5	86	0.0003	1.50	198270	61825	8830
5	86	0.0004	1.50	198270	26974	3852
5	86	0.0004	1.50	198270	13150	1878

Table B. 1 (cont'd)

5	86	0.0005	1.50	198270	6977	996
5	86	0.0005	1.50	198270	3958	565
5	86	0.0006	1.50	198270	2370	338
5	86	0.0006	1.50	198270	1484	212
10	41	0.0001	1.50	1352618	8691675	1109278
10	41	0.0002	1.50	1352618	980905	125188
10	41	0.0002	1.50	1352618	208632	26627
10	41	0.0003	1.50	1352618	62798	8015
10	41	0.0003	1.50	1352618	23545	3005
10	41	0.0004	1.50	1352618	10273	1311
10	41	0.0004	1.50	1352618	5008	639
10	41	0.0005	1.50	1352618	2657	339
10	41	0.0005	1.50	1352618	1507	192
10	41	0.0006	1.50	1352618	903	115
10	41	0.0006	1.50	1352618	565	72
10	50	0.0001	1.50	1105596	3860400	492685
10	50	0.0002	1.50	1105596	435668	55602
10	50	0.0002	1.50	1105596	92664	11826
10	50	0.0003	1.50	1105596	27892	3560
10	50	0.0003	1.50	1105596	10458	1335
10	50	0.0004	1.50	1105596	4563	582
10	50	0.0004	1.50	1105596	2224	284
10	50	0.0005	1.50	1105596	1180	151
10	50	0.0005	1.50	1105596	670	85
10	50	0.0006	1.50	1105596	401	51
10	50	0.0006	1.50	1105596	251	32
10	59	0.0001	1.50	844854	2683764	342516
10	59	0.0002	1.50	844854	302878	38655
10	59	0.0002	1.50	844854	64420	8222
10	59	0.0003	1.50	844854	19390	2475
10	59	0.0003	1.50	844854	7270	928
10	59	0.0004	1.50	844854	3172	405
10	59	0.0004	1.50	844854	1546	197
10	59	0.0005	1.50	844854	820	105
10	59	0.0005	1.50	844854	465	59
10	59	0.0006	1.50	844854	279	36
10	59	0.0006	1.50	844854	175	22
10	68	0.0001	1.50	600374	3005124	383530
10	68	0.0002	1.50	600374	339145	43284
10	68	0.0002	1.50	600374	72134	9206
10	68	0.0003	1.50	600374	21712	2771
10	68	0.0003	1.50	600374	8141	1039
10	68	0.0004	1.50	600374	3552	453
10	68	0.0004	1.50	600374	1731	221
10	68	0.0005	1.50	600374	919	117

Table B. 1 (cont'd)

10	68	0.0005	1.50	600374	521	67
10	68	0.0006	1.50	600374	312	40
10	68	0.0006	1.50	600374	195	25
10	77	0.0001	1.50	398030	5326749	679828
10	77	0.0002	1.50	398030	601154	76722
10	77	0.0002	1.50	398030	127862	16318
10	77	0.0003	1.50	398030	38486	4912
10	77	0.0003	1.50	398030	14430	1842
10	77	0.0004	1.50	398030	6296	804
10	77	0.0004	1.50	398030	3069	392
10	77	0.0005	1.50	398030	1628	208
10	77	0.0005	1.50	398030	924	118
10	77	0.0006	1.50	398030	553	71
10	77	0.0006	1.50	398030	346	44
10	86	0.0001	1.50	249551	13893534	1773166
10	86	0.0002	1.50	249551	1567964	200112
10	86	0.0002	1.50	249551	333496	42563
10	86	0.0003	1.50	249551	100382	12811
10	86	0.0003	1.50	249551	37637	4803
10	86	0.0004	1.50	249551	16421	2096
10	86	0.0004	1.50	249551	8005	1022
10	86	0.0005	1.50	249551	4248	542
10	86	0.0005	1.50	249551	2410	308
10	86	0.0006	1.50	249551	1443	184
10	86	0.0006	1.50	249551	903	115
1	41	0.0001	3.94	1048381	15246	436953
1	41	0.0002	3.94	1048381	1721	49313
1	41	0.0002	3.94	1048381	366	10488
1	41	0.0003	3.94	1048381	110	3157
1	41	0.0003	3.94	1048381	41	1184
1	41	0.0004	3.94	1048381	18	516
1	41	0.0004	3.94	1048381	9	252
1	41	0.0005	3.94	1048381	5	134
1	41	0.0005	3.94	1048381	3	76
1	41	0.0006	3.94	1048381	2	45
1	41	0.0006	3.94	1048381	1	28
1	50	0.0001	3.94	773444	11754	336872
1	50	0.0002	3.94	773444	1327	38018
1	50	0.0002	3.94	773444	282	8086
1	50	0.0003	3.94	773444	85	2434
1	50	0.0003	3.94	773444	32	913
1	50	0.0004	3.94	773444	14	398
1	50	0.0004	3.94	773444	7	194
1	50	0.0005	3.94	773444	4	103
1	50	0.0005	3.94	773444	2	58

Table B. 1 (cont'd)

1	50	0.0006	3.94	773444	1	35
1	50	0.0006	3.94	773444	1	22
1	59	0.0001	3.94	524549	15530	445084
1	59	0.0002	3.94	524549	1753	50230
1	59	0.0002	3.94	524549	373	10684
1	59	0.0003	3.94	524549	112	3216
1	59	0.0003	3.94	524549	42	1206
1	59	0.0004	3.94	524549	18	526
1	59	0.0004	3.94	524549	9	256
1	59	0.0005	3.94	524549	5	136
1	59	0.0005	3.94	524549	3	77
1	59	0.0006	3.94	524549	2	46
1	59	0.0006	3.94	524549	1	29
1	68	0.0001	3.94	328959	34070	976438
1	68	0.0002	3.94	328959	3845	110197
1	68	0.0002	3.94	328959	818	23438
1	68	0.0003	3.94	328959	246	7055
1	68	0.0003	3.94	328959	92	2645
1	68	0.0004	3.94	328959	40	1154
1	68	0.0004	3.94	328959	20	563
1	68	0.0005	3.94	328959	10	299
1	68	0.0005	3.94	328959	6	169
1	68	0.0006	3.94	328959	4	101
1	68	0.0006	3.94	328959	2	63
1	77	0.0001	3.94	194511	111772	3203393
1	77	0.0002	3.94	194511	12614	361521
1	77	0.0002	3.94	194511	2683	76893
1	77	0.0003	3.94	194511	808	23145
1	77	0.0003	3.94	194511	303	8678
1	77	0.0004	3.94	194511	132	3786
1	77	0.0004	3.94	194511	64	1846
1	77	0.0005	3.94	194511	34	979
1	77	0.0005	3.94	194511	19	556
1	77	0.0006	3.94	194511	12	333
1	77	0.0006	3.94	194511	7	208
1	86	0.0001	3.94	111784	465703	13347130
1	86	0.0002	3.94	111784	52557	1506299
1	86	0.0002	3.94	111784	11179	320380
1	86	0.0003	3.94	111784	3365	96434
1	86	0.0003	3.94	111784	1262	36157
1	86	0.0004	3.94	111784	550	15775
1	86	0.0004	3.94	111784	268	7690
1	86	0.0005	3.94	111784	142	4080
1	86	0.0005	3.94	111784	81	2315
1	86	0.0006	3.94	111784	48	1386

Table B. 1 (cont'd)

1	86	0.0006	3.94	111784	30	868
5	41	0.0001	3.94	1266889	28708	841192
5	41	0.0002	3.94	1266889	3240	94933
5	41	0.0002	3.94	1266889	689	20192
5	41	0.0003	3.94	1266889	207	6078
5	41	0.0003	3.94	1266889	78	2279
5	41	0.0004	3.94	1266889	34	994
5	41	0.0004	3.94	1266889	17	485
5	41	0.0005	3.94	1266889	9	257
5	41	0.0005	3.94	1266889	5	146
5	41	0.0006	3.94	1266889	3	87
5	41	0.0006	3.94	1266889	2	55
5	50	0.0001	3.94	1007293	14795	433523
5	50	0.0002	3.94	1007293	1670	48926
5	50	0.0002	3.94	1007293	355	10406
5	50	0.0003	3.94	1007293	107	3132
5	50	0.0003	3.94	1007293	40	1174
5	50	0.0004	3.94	1007293	17	512
5	50	0.0004	3.94	1007293	9	250
5	50	0.0005	3.94	1007293	5	133
5	50	0.0005	3.94	1007293	3	75
5	50	0.0006	3.94	1007293	2	45
5	50	0.0006	3.94	1007293	1	28
5	59	0.0001	3.94	744457	12310	360705
5	59	0.0002	3.94	744457	1389	40708
5	59	0.0002	3.94	744457	295	8658
5	59	0.0003	3.94	744457	89	2606
5	59	0.0003	3.94	744457	33	977
5	59	0.0004	3.94	744457	15	426
5	59	0.0004	3.94	744457	7	208
5	59	0.0005	3.94	744457	4	110
5	59	0.0005	3.94	744457	2	63
5	59	0.0006	3.94	744457	1	37
5	59	0.0006	3.94	744457	1	23
5	68	0.0001	3.94	509918	16802	492318
5	68	0.0002	3.94	509918	1896	55561
5	68	0.0002	3.94	509918	403	11817
5	68	0.0003	3.94	509918	121	3557
5	68	0.0003	3.94	509918	46	1334
5	68	0.0004	3.94	509918	20	582
5	68	0.0004	3.94	509918	10	284
5	68	0.0005	3.94	509918	5	151
5	68	0.0005	3.94	509918	3	85
5	68	0.0006	3.94	509918	2	51
5	68	0.0006	3.94	509918	1	32

Table B. 1 (cont'd)

5	77	0.0001	3.94	326060	36175	1059990
5	77	0.0002	3.94	326060	4083	119626
5	77	0.0002	3.94	326060	868	25444
5	77	0.0003	3.94	326060	261	7659
5	77	0.0003	3.94	326060	98	2871
5	77	0.0004	3.94	326060	43	1253
5	77	0.0004	3.94	326060	21	611
5	77	0.0005	3.94	326060	11	324
5	77	0.0005	3.94	326060	6	184
5	77	0.0006	3.94	326060	4	110
5	77	0.0006	3.94	326060	2	69
5	86	0.0001	3.94	198270	111236	3259426
5	86	0.0002	3.94	198270	12554	367845
5	86	0.0002	3.94	198270	2670	78238
5	86	0.0003	3.94	198270	804	23550
5	86	0.0003	3.94	198270	301	8830
5	86	0.0004	3.94	198270	131	3852
5	86	0.0004	3.94	198270	64	1878
5	86	0.0005	3.94	198270	34	996
5	86	0.0005	3.94	198270	19	565
5	86	0.0006	3.94	198270	12	338
5	86	0.0006	3.94	198270	7	212
10	41	0.0001	3.94	1352618	38705	1109278
10	41	0.0002	3.94	1352618	4368	125188
10	41	0.0002	3.94	1352618	929	26627
10	41	0.0003	3.94	1352618	280	8015
10	41	0.0003	3.94	1352618	105	3005
10	41	0.0004	3.94	1352618	46	1311
10	41	0.0004	3.94	1352618	22	639
10	41	0.0005	3.94	1352618	12	339
10	41	0.0005	3.94	1352618	7	192
10	41	0.0006	3.94	1352618	4	115
10	41	0.0006	3.94	1352618	3	72
10	50	0.0001	3.94	1105596	17191	492685
10	50	0.0002	3.94	1105596	1940	55602
10	50	0.0002	3.94	1105596	413	11826
10	50	0.0003	3.94	1105596	124	3560
10	50	0.0003	3.94	1105596	47	1335
10	50	0.0004	3.94	1105596	20	582
10	50	0.0004	3.94	1105596	10	284
10	50	0.0005	3.94	1105596	5	151
10	50	0.0005	3.94	1105596	3	85
10	50	0.0006	3.94	1105596	2	51
10	50	0.0006	3.94	1105596	1	32
10	59	0.0001	3.94	844854	11951	342516

Table B. 1 (cont'd)

10	59	0.0002	3.94	844854	1349	38655
10	59	0.0002	3.94	844854	287	8222
10	59	0.0003	3.94	844854	86	2475
10	59	0.0003	3.94	844854	32	928
10	59	0.0004	3.94	844854	14	405
10	59	0.0004	3.94	844854	7	197
10	59	0.0005	3.94	844854	4	105
10	59	0.0005	3.94	844854	2	59
10	59	0.0006	3.94	844854	1	36
10	59	0.0006	3.94	844854	1	22
10	68	0.0001	3.94	600374	13382	383530
10	68	0.0002	3.94	600374	1510	43284
10	68	0.0002	3.94	600374	321	9206
10	68	0.0003	3.94	600374	97	2771
10	68	0.0003	3.94	600374	36	1039
10	68	0.0004	3.94	600374	16	453
10	68	0.0004	3.94	600374	8	221
10	68	0.0005	3.94	600374	4	117
10	68	0.0005	3.94	600374	2	67
10	68	0.0006	3.94	600374	1	40
10	68	0.0006	3.94	600374	1	25
10	77	0.0001	3.94	398030	23720	679828
10	77	0.0002	3.94	398030	2677	76722
10	77	0.0002	3.94	398030	569	16318
10	77	0.0003	3.94	398030	171	4912
10	77	0.0003	3.94	398030	64	1842
10	77	0.0004	3.94	398030	28	804
10	77	0.0004	3.94	398030	14	392
10	77	0.0005	3.94	398030	7	208
10	77	0.0005	3.94	398030	4	118
10	77	0.0006	3.94	398030	2	71
10	77	0.0006	3.94	398030	2	44
10	86	0.0001	3.94	249551	61869	1773166
10	86	0.0002	3.94	249551	6982	200112
10	86	0.0002	3.94	249551	1485	42563
10	86	0.0003	3.94	249551	447	12811
10	86	0.0003	3.94	249551	168	4803
10	86	0.0004	3.94	249551	73	2096
10	86	0.0004	3.94	249551	36	1022
10	86	0.0005	3.94	249551	19	542
10	86	0.0005	3.94	249551	11	308
10	86	0.0006	3.94	249551	6	184
10	86	0.0006	3.94	249551	4	115
Mix ID: 5E3						
1	41	0.0001	1.50	1235891	11029925	527307

Table B. 1 (cont'd)

1	41	0.0002	1.50	1235891	951211	45474
1	41	0.0002	1.50	1235891	167166	7992
1	41	0.0003	1.50	1235891	43393	2075
1	41	0.0003	1.50	1235891	14416	689
1	41	0.0004	1.50	1235891	5678	271
1	41	0.0004	1.50	1235891	2534	121
1	41	0.0005	1.50	1235891	1243	59
1	41	0.0005	1.50	1235891	658	31
1	41	0.0006	1.50	1235891	370	18
1	41	0.0006	1.50	1235891	218	10
1	50	0.0001	1.50	923935	11929009	570289
1	50	0.0002	1.50	923935	1028747	49181
1	50	0.0002	1.50	923935	180792	8643
1	50	0.0003	1.50	923935	46930	2244
1	50	0.0003	1.50	923935	15591	745
1	50	0.0004	1.50	923935	6141	294
1	50	0.0004	1.50	923935	2740	131
1	50	0.0005	1.50	923935	1345	64
1	50	0.0005	1.50	923935	711	34
1	50	0.0006	1.50	923935	400	19
1	50	0.0006	1.50	923935	236	11
1	59	0.0001	1.50	649823	19873936	950112
1	59	0.0002	1.50	649823	1713911	81937
1	59	0.0002	1.50	649823	301203	14400
1	59	0.0003	1.50	649823	78187	3738
1	59	0.0003	1.50	649823	25975	1242
1	59	0.0004	1.50	649823	10231	489
1	59	0.0004	1.50	649823	4565	218
1	59	0.0005	1.50	649823	2240	107
1	59	0.0005	1.50	649823	1185	57
1	59	0.0006	1.50	649823	666	32
1	59	0.0006	1.50	649823	394	19
1	68	0.0001	1.50	433274	48700894	2328240
1	68	0.0002	1.50	433274	4199923	200785
1	68	0.0002	1.50	433274	738094	35286
1	68	0.0003	1.50	433274	191596	9160
1	68	0.0003	1.50	433274	63653	3043
1	68	0.0004	1.50	433274	25072	1199
1	68	0.0004	1.50	433274	11186	535
1	68	0.0005	1.50	433274	5489	262
1	68	0.0005	1.50	433274	2904	139
1	68	0.0006	1.50	433274	1632	78
1	68	0.0006	1.50	433274	965	46
1	77	0.0001	1.50	278141	159857337	7642288
1	77	0.0002	1.50	278141	13785960	659064

Table B. 1 (cont'd)

1	77	0.0002	1.50	278141	2422743	115824
1	77	0.0003	1.50	278141	628902	30066
1	77	0.0003	1.50	278141	208935	9989
1	77	0.0004	1.50	278141	82297	3934
1	77	0.0004	1.50	278141	36718	1755
1	77	0.0005	1.50	278141	18018	861
1	77	0.0005	1.50	278141	9531	456
1	77	0.0006	1.50	278141	5358	256
1	77	0.0006	1.50	278141	3167	151
1	86	0.0001	1.50	175580	618663867	29576417
1	86	0.0002	1.50	175580	53353041	2550645
1	86	0.0002	1.50	175580	9376256	448250
1	86	0.0003	1.50	175580	2433915	116358
1	86	0.0003	1.50	175580	808600	38657
1	86	0.0004	1.50	175580	318499	15226
1	86	0.0004	1.50	175580	142103	6794
1	86	0.0005	1.50	175580	69733	3334
1	86	0.0005	1.50	175580	36888	1763
1	86	0.0006	1.50	175580	20735	991
1	86	0.0006	1.50	175580	12255	586
5	41	0.0001	1.50	1531662	15078089	720837
5	41	0.0002	1.50	1531662	1300321	62164
5	41	0.0002	1.50	1531662	228518	10925
5	41	0.0003	1.50	1531662	59319	2836
5	41	0.0003	1.50	1531662	19707	942
5	41	0.0004	1.50	1531662	7762	371
5	41	0.0004	1.50	1531662	3463	166
5	41	0.0005	1.50	1531662	1700	81
5	41	0.0005	1.50	1531662	899	43
5	41	0.0006	1.50	1531662	505	24
5	41	0.0006	1.50	1531662	299	14
5	50	0.0001	1.50	1222672	10970079	524446
5	50	0.0002	1.50	1222672	946050	45228
5	50	0.0002	1.50	1222672	166259	7948
5	50	0.0003	1.50	1222672	43158	2063
5	50	0.0003	1.50	1222672	14338	685
5	50	0.0004	1.50	1222672	5648	270
5	50	0.0004	1.50	1222672	2520	120
5	50	0.0005	1.50	1222672	1236	59
5	50	0.0005	1.50	1222672	654	31
5	50	0.0006	1.50	1222672	368	18
5	50	0.0006	1.50	1222672	217	10
5	59	0.0001	1.50	922624	11944736	571041
5	59	0.0002	1.50	922624	1030104	49246
5	59	0.0002	1.50	922624	181030	8655

Table B. 1 (cont'd)

5	59	0.0003	1.50	922624	46992	2247
5	59	0.0003	1.50	922624	15612	746
5	59	0.0004	1.50	922624	6149	294
5	59	0.0004	1.50	922624	2744	131
5	59	0.0005	1.50	922624	1346	64
5	59	0.0005	1.50	922624	712	34
5	59	0.0006	1.50	922624	400	19
5	59	0.0006	1.50	922624	237	11
5	68	0.0001	1.50	658577	19383902	926685
5	68	0.0002	1.50	658577	1671651	79916
5	68	0.0002	1.50	658577	293776	14045
5	68	0.0003	1.50	658577	76259	3646
5	68	0.0003	1.50	658577	25335	1211
5	68	0.0004	1.50	658577	9979	477
5	68	0.0004	1.50	658577	4452	213
5	68	0.0005	1.50	658577	2185	104
5	68	0.0005	1.50	658577	1156	55
5	68	0.0006	1.50	658577	650	31
5	68	0.0006	1.50	658577	384	18
5	77	0.0001	1.50	447932	44866064	2144909
5	77	0.0002	1.50	447932	3869211	184975
5	77	0.0002	1.50	447932	679975	32507
5	77	0.0003	1.50	447932	176510	8438
5	77	0.0003	1.50	447932	58640	2803
5	77	0.0004	1.50	447932	23098	1104
5	77	0.0004	1.50	447932	10305	493
5	77	0.0005	1.50	447932	5057	242
5	77	0.0005	1.50	447932	2675	128
5	77	0.0006	1.50	447932	1504	72
5	77	0.0006	1.50	447932	889	42
5	86	0.0001	1.50	294341	136235454	6512998
5	86	0.0002	1.50	294341	11748829	561675
5	86	0.0002	1.50	294341	2064738	98709
5	86	0.0003	1.50	294341	535970	25623
5	86	0.0003	1.50	294341	178061	8513
5	86	0.0004	1.50	294341	70136	3353
5	86	0.0004	1.50	294341	31292	1496
5	86	0.0005	1.50	294341	15356	734
5	86	0.0005	1.50	294341	8123	388
5	86	0.0006	1.50	294341	4566	218
5	86	0.0006	1.50	294341	2699	129
10	41	0.0001	1.50	1651947	19095547	912899
10	41	0.0002	1.50	1651947	1646784	78728
10	41	0.0002	1.50	1651947	289406	13836
10	41	0.0003	1.50	1651947	75125	3591

Table B. 1 (cont'd)

10	41	0.0003	1.50	1651947	24958	1193
10	41	0.0004	1.50	1651947	9831	470
10	41	0.0004	1.50	1651947	4386	210
10	41	0.0005	1.50	1651947	2152	103
10	41	0.0005	1.50	1651947	1139	54
10	41	0.0006	1.50	1651947	640	31
10	41	0.0006	1.50	1651947	378	18
10	50	0.0001	1.50	1352178	11939111	570772
10	50	0.0002	1.50	1352178	1029619	49223
10	50	0.0002	1.50	1352178	180945	8650
10	50	0.0003	1.50	1352178	46970	2246
10	50	0.0003	1.50	1352178	15605	746
10	50	0.0004	1.50	1352178	6146	294
10	50	0.0004	1.50	1352178	2742	131
10	50	0.0005	1.50	1352178	1346	64
10	50	0.0005	1.50	1352178	712	34
10	50	0.0006	1.50	1352178	400	19
10	50	0.0006	1.50	1352178	236	11
10	59	0.0001	1.50	1049741	10949560	523465
10	59	0.0002	1.50	1049741	944281	45143
10	59	0.0002	1.50	1049741	165948	7933
10	59	0.0003	1.50	1049741	43077	2059
10	59	0.0003	1.50	1049741	14311	684
10	59	0.0004	1.50	1049741	5637	269
10	59	0.0004	1.50	1049741	2515	120
10	59	0.0005	1.50	1049741	1234	59
10	59	0.0005	1.50	1049741	653	31
10	59	0.0006	1.50	1049741	367	18
10	59	0.0006	1.50	1049741	217	10
10	68	0.0001	1.50	771841	14856204	710229
10	68	0.0002	1.50	771841	1281186	61250
10	68	0.0002	1.50	771841	225156	10764
10	68	0.0003	1.50	771841	58446	2794
10	68	0.0003	1.50	771841	19417	928
10	68	0.0004	1.50	771841	7648	366
10	68	0.0004	1.50	771841	3412	163
10	68	0.0005	1.50	771841	1675	80
10	68	0.0005	1.50	771841	886	42
10	68	0.0006	1.50	771841	498	24
10	68	0.0006	1.50	771841	294	14
10	77	0.0001	1.50	539810	29054283	1388996
10	77	0.0002	1.50	539810	2505616	119786
10	77	0.0002	1.50	539810	440337	21051
10	77	0.0003	1.50	539810	114304	5465
10	77	0.0003	1.50	539810	37974	1815

Table B. 1 (cont'd)

10	77	0.0004	1.50	539810	14958	715
10	77	0.0004	1.50	539810	6674	319
10	77	0.0005	1.50	539810	3275	157
10	77	0.0005	1.50	539810	1732	83
10	77	0.0006	1.50	539810	974	47
10	77	0.0006	1.50	539810	576	28
10	86	0.0001	1.50	362933	76818988	3672480
10	86	0.0002	1.50	362933	6624804	316711
10	86	0.0002	1.50	362933	1164242	55659
10	86	0.0003	1.50	362933	302217	14448
10	86	0.0003	1.50	362933	100403	4800
10	86	0.0004	1.50	362933	39548	1891
10	86	0.0004	1.50	362933	17645	844
10	86	0.0005	1.50	362933	8659	414
10	86	0.0005	1.50	362933	4580	219
10	86	0.0006	1.50	362933	2575	123
10	86	0.0006	1.50	362933	1522	73
1	41	0.0001	3.94	1235891	23816	527307
1	41	0.0002	3.94	1235891	2054	45474
1	41	0.0002	3.94	1235891	361	7992
1	41	0.0003	3.94	1235891	94	2075
1	41	0.0003	3.94	1235891	31	689
1	41	0.0004	3.94	1235891	12	271
1	41	0.0004	3.94	1235891	5	121
1	41	0.0005	3.94	1235891	3	59
1	41	0.0005	3.94	1235891	1	31
1	41	0.0006	3.94	1235891	1	18
1	41	0.0006	3.94	1235891	0	10
1	50	0.0001	3.94	923935	25758	570289
1	50	0.0002	3.94	923935	2221	49181
1	50	0.0002	3.94	923935	390	8643
1	50	0.0003	3.94	923935	101	2244
1	50	0.0003	3.94	923935	34	745
1	50	0.0004	3.94	923935	13	294
1	50	0.0004	3.94	923935	6	131
1	50	0.0005	3.94	923935	3	64
1	50	0.0005	3.94	923935	2	34
1	50	0.0006	3.94	923935	1	19
1	50	0.0006	3.94	923935	1	11
1	59	0.0001	3.94	649823	42913	950112
1	59	0.0002	3.94	649823	3701	81937
1	59	0.0002	3.94	649823	650	14400
1	59	0.0003	3.94	649823	169	3738
1	59	0.0003	3.94	649823	56	1242
1	59	0.0004	3.94	649823	22	489

Table B. 1 (cont'd)

1	59	0.0004	3.94	649823	10	218
1	59	0.0005	3.94	649823	5	107
1	59	0.0005	3.94	649823	3	57
1	59	0.0006	3.94	649823	1	32
1	59	0.0006	3.94	649823	1	19
1	68	0.0001	3.94	433274	105158	2328240
1	68	0.0002	3.94	433274	9069	200785
1	68	0.0002	3.94	433274	1594	35286
1	68	0.0003	3.94	433274	414	9160
1	68	0.0003	3.94	433274	137	3043
1	68	0.0004	3.94	433274	54	1199
1	68	0.0004	3.94	433274	24	535
1	68	0.0005	3.94	433274	12	262
1	68	0.0005	3.94	433274	6	139
1	68	0.0006	3.94	433274	4	78
1	68	0.0006	3.94	433274	2	46
1	77	0.0001	3.94	278141	345174	7642288
1	77	0.0002	3.94	278141	29767	659064
1	77	0.0002	3.94	278141	5231	115824
1	77	0.0003	3.94	278141	1358	30066
1	77	0.0003	3.94	278141	451	9989
1	77	0.0004	3.94	278141	178	3934
1	77	0.0004	3.94	278141	79	1755
1	77	0.0005	3.94	278141	39	861
1	77	0.0005	3.94	278141	21	456
1	77	0.0006	3.94	278141	12	256
1	77	0.0006	3.94	278141	7	151
1	86	0.0001	3.94	175580	1335857	29576417
1	86	0.0002	3.94	175580	115203	2550645
1	86	0.0002	3.94	175580	20246	448250
1	86	0.0003	3.94	175580	5255	116358
1	86	0.0003	3.94	175580	1746	38657
1	86	0.0004	3.94	175580	688	15226
1	86	0.0004	3.94	175580	307	6794
1	86	0.0005	3.94	175580	151	3334
1	86	0.0005	3.94	175580	80	1763
1	86	0.0006	3.94	175580	45	991
1	86	0.0006	3.94	175580	26	586
5	41	0.0001	3.94	1531662	32558	720837
5	41	0.0002	3.94	1531662	2808	62164
5	41	0.0002	3.94	1531662	493	10925
5	41	0.0003	3.94	1531662	128	2836
5	41	0.0003	3.94	1531662	43	942
5	41	0.0004	3.94	1531662	17	371
5	41	0.0004	3.94	1531662	7	166

Table B. 1 (cont'd)

5	41	0.0005	3.94	1531662	4	81
5	41	0.0005	3.94	1531662	2	43
5	41	0.0006	3.94	1531662	1	24
5	41	0.0006	3.94	1531662	1	14
5	50	0.0001	3.94	1222672	23687	524446
5	50	0.0002	3.94	1222672	2043	45228
5	50	0.0002	3.94	1222672	359	7948
5	50	0.0003	3.94	1222672	93	2063
5	50	0.0003	3.94	1222672	31	685
5	50	0.0004	3.94	1222672	12	270
5	50	0.0004	3.94	1222672	5	120
5	50	0.0005	3.94	1222672	3	59
5	50	0.0005	3.94	1222672	1	31
5	50	0.0006	3.94	1222672	1	18
5	50	0.0006	3.94	1222672	0	10
5	59	0.0001	3.94	922624	25792	571041
5	59	0.0002	3.94	922624	2224	49246
5	59	0.0002	3.94	922624	391	8655
5	59	0.0003	3.94	922624	101	2247
5	59	0.0003	3.94	922624	34	746
5	59	0.0004	3.94	922624	13	294
5	59	0.0004	3.94	922624	6	131
5	59	0.0005	3.94	922624	3	64
5	59	0.0005	3.94	922624	2	34
5	59	0.0006	3.94	922624	1	19
5	59	0.0006	3.94	922624	1	11
5	68	0.0001	3.94	658577	41855	926685
5	68	0.0002	3.94	658577	3610	79916
5	68	0.0002	3.94	658577	634	14045
5	68	0.0003	3.94	658577	165	3646
5	68	0.0003	3.94	658577	55	1211
5	68	0.0004	3.94	658577	22	477
5	68	0.0004	3.94	658577	10	213
5	68	0.0005	3.94	658577	5	104
5	68	0.0005	3.94	658577	2	55
5	68	0.0006	3.94	658577	1	31
5	68	0.0006	3.94	658577	1	18
5	77	0.0001	3.94	447932	96878	2144909
5	77	0.0002	3.94	447932	8355	184975
5	77	0.0002	3.94	447932	1468	32507
5	77	0.0003	3.94	447932	381	8438
5	77	0.0003	3.94	447932	127	2803
5	77	0.0004	3.94	447932	50	1104
5	77	0.0004	3.94	447932	22	493
5	77	0.0005	3.94	447932	11	242

Table B. 1 (cont'd)

5	77	0.0005	3.94	447932	6	128
5	77	0.0006	3.94	447932	3	72
5	77	0.0006	3.94	447932	2	42
5	86	0.0001	3.94	294341	294168	6512998
5	86	0.0002	3.94	294341	25369	561675
5	86	0.0002	3.94	294341	4458	98709
5	86	0.0003	3.94	294341	1157	25623
5	86	0.0003	3.94	294341	384	8513
5	86	0.0004	3.94	294341	151	3353
5	86	0.0004	3.94	294341	68	1496
5	86	0.0005	3.94	294341	33	734
5	86	0.0005	3.94	294341	18	388
5	86	0.0006	3.94	294341	10	218
5	86	0.0006	3.94	294341	6	129
10	41	0.0001	3.94	1651947	41232	912899
10	41	0.0002	3.94	1651947	3556	78728
10	41	0.0002	3.94	1651947	625	13836
10	41	0.0003	3.94	1651947	162	3591
10	41	0.0003	3.94	1651947	54	1193
10	41	0.0004	3.94	1651947	21	470
10	41	0.0004	3.94	1651947	9	210
10	41	0.0005	3.94	1651947	5	103
10	41	0.0005	3.94	1651947	2	54
10	41	0.0006	3.94	1651947	1	31
10	41	0.0006	3.94	1651947	1	18
10	50	0.0001	3.94	1352178	25780	570772
10	50	0.0002	3.94	1352178	2223	49223
10	50	0.0002	3.94	1352178	391	8650
10	50	0.0003	3.94	1352178	101	2246
10	50	0.0003	3.94	1352178	34	746
10	50	0.0004	3.94	1352178	13	294
10	50	0.0004	3.94	1352178	6	131
10	50	0.0005	3.94	1352178	3	64
10	50	0.0005	3.94	1352178	2	34
10	50	0.0006	3.94	1352178	1	19
10	50	0.0006	3.94	1352178	1	11
10	59	0.0001	3.94	1049741	23643	523465
10	59	0.0002	3.94	1049741	2039	45143
10	59	0.0002	3.94	1049741	358	7933
10	59	0.0003	3.94	1049741	93	2059
10	59	0.0003	3.94	1049741	31	684
10	59	0.0004	3.94	1049741	12	269
10	59	0.0004	3.94	1049741	5	120
10	59	0.0005	3.94	1049741	3	59
10	59	0.0005	3.94	1049741	1	31

Table B. 1 (cont'd)

10	59	0.0006	3.94	1049741	1	18
10	59	0.0006	3.94	1049741	0	10
10	68	0.0001	3.94	771841	32078	710229
10	68	0.0002	3.94	771841	2766	61250
10	68	0.0002	3.94	771841	486	10764
10	68	0.0003	3.94	771841	126	2794
10	68	0.0003	3.94	771841	42	928
10	68	0.0004	3.94	771841	17	366
10	68	0.0004	3.94	771841	7	163
10	68	0.0005	3.94	771841	4	80
10	68	0.0005	3.94	771841	2	42
10	68	0.0006	3.94	771841	1	24
10	68	0.0006	3.94	771841	1	14
10	77	0.0001	3.94	539810	62736	1388996
10	77	0.0002	3.94	539810	5410	119786
10	77	0.0002	3.94	539810	951	21051
10	77	0.0003	3.94	539810	247	5465
10	77	0.0003	3.94	539810	82	1815
10	77	0.0004	3.94	539810	32	715
10	77	0.0004	3.94	539810	14	319
10	77	0.0005	3.94	539810	7	157
10	77	0.0005	3.94	539810	4	83
10	77	0.0006	3.94	539810	2	47
10	77	0.0006	3.94	539810	1	28
10	86	0.0001	3.94	362933	165872	3672480
10	86	0.0002	3.94	362933	14305	316711
10	86	0.0002	3.94	362933	2514	55659
10	86	0.0003	3.94	362933	653	14448
10	86	0.0003	3.94	362933	217	4800
10	86	0.0004	3.94	362933	85	1891
10	86	0.0004	3.94	362933	38	844
10	86	0.0005	3.94	362933	19	414
10	86	0.0005	3.94	362933	10	219
10	86	0.0006	3.94	362933	6	123
10	86	0.0006	3.94	362933	3	73

REFERENCES

REFERENCES

AASHTO. (1962). *The AASHO Road Test, Report 7, Summary Report*. Washington D.C: Highway Research Board, Special Report 61G, National Academy of Sciences-National Research Council.

AASHTO T321. (2017). *Standard Method of Test for Determining the Fatigue Life of Compacted Asphalt Mixtures Subjected to Repeated Flexural Bending*. Washington D.C. Retrieved from https://global.ihs.com/doc_detail.cfm?document_name=AASHTO T 321

Al-Qadi, I., Ozer, H., Lambros, J., Khatib, A. El, & Singhvi, P. (2015). *Testing protocols to ensure performance of high asphalt binder replacement mixes using RAP and RAS, Report No. FHWA-ICT-15-017*. Rantoul, IL. Retrieved from https://www.ideals.illinois.edu/handle/2142/88680

American Wood Council. (2005). Beam Design Formulas with Shear and Moment Diagrams. Retrieved from www.afandpa.org.

ARA Inc. ERES Consultants Division. (2004). NCHRP 1-37A Design Guide, Mechanistic-Empirical Design of New and Rehabilitated Pavement Structures. Washington D.C. Retrieved from http://onlinepubs.trb.org/onlinepubs/archive/mepdg/home.htm

Arambula, E., & Kutay, M. E. (2009). Tension-compression fatigue test evaluation using fracture mechanics and field data. *Road Materials and Pavement Design*, *10*(1), 83–108. https://doi.org/10.1080/14680629.2009.9690183

Aschenbrenter, T. (1995). Evaluation of Hamburg Wheel-Tracking Device to Predict Moisture Damage in Hot-Mix Asphalt. *Transportation Research Record*, *1492*, 193–201. Retrieved from http://onlinepubs.trb.org/Onlinepubs/trr/1995/1492/1492-021.pdf

ASTM D7460 − 10. (2013). *Standard Test Method for Determining Fatigue Failure of Compacted Asphalt Concrete Subjected to Repeated Flexural Bending*. Pennsylvania. Retrieved from https://compass.astm.org/download/D7460.3922.pdf

Barksdale, R. ., & Miller, J. H. (1977). Development of Equipment and Techniques for Evaluating Fatigue and Rutting Characteristics of Asphalt Concrete Mixes. Atlanta: School of Civil Engineering, Georgia Institute of Technology.

Bennert, T., Haas, E., & Wass, E. (2018). Indirect Tensile Test (IDT) to Determine Asphalt Mixture Performance Indicators during Quality Control Testing in New Jersey. *Transportation Research Record: Journal of the Transportation Research Board*, *2672*(28), 394–403. https://doi.org/10.1177/0361198118793276

Bhattacharjee, S., Gould, J. S., Mallick, R. B., & Hugo, F. (2004). An Evaluation of use of Accelerated Loading Equipment for Determination of Fatigue Performance of Asphalt

Pavement in Laboratory. *International Journal of Pavement Engineering*, *5*(2), 61–79. https://doi.org/10.1080/10298430412331312472

Bonaquist, R. (2008). *Refining the Simple Performance Tester for Use in Routine Practice*. *Refining the Simple Performance Tester for Use in Routine Practice (vol. 614)*. Transportation Research Board. National Cooperative Highway Research Program (Project NCHRP 9-29), Washington, DC. https://doi.org/10.17226/14158

Braham, A., & Underwood, B. S. (2016). *State of the Art and Practice in Fatigue Cracking Evaluation of Asphalt Concrete Pavements*. Lino Lakes, MN.: Association of Asphalt Paving Technologists, Version 1.0. Retrieved from http://asphalttechnology.org/downloads/Fatigue_Cracking_of_Asphalt_Pavements_2017_06.pdf

Chehab, G. R., Kim, R. Y., Schapery, R. A., Witczak, M. W., & Bonaquist, R. F. (2002). Time-Temperature Superposition Principle for Asphalt Concrete with Growing Damage in Tension State. *Journal of the Association of Asphalt Paving Technologists*, *71*(September 2015), 559–593.

Chiangmai, C. N. (2010). *Fatigue-fracture relation on asphalt concrete mixtures*. MS thesis, University of Illinois at Urbana–Champaign, Urbana,. Retrieved from http://citeseerx.ist.psu.edu/viewdoc/download?doi=10.1.1.224.9685&rep=rep1&type=pdf

Christensen, D. W., & Bonaquist, R. (2009). Analysis of HMA fatigue data using the concepts of reduced loading cycles and endurance limit. *Journal of the Association of Asphalt Paving Technologists*, *78*, 377–416.

Christensen Jr, D., & Bonaquist, R. (2005). Practical application of continuum damage theory to fatigue phenomena in asphalt concrete mixtures (With Discussion and Closure). *Journal of the Association of Asphalt Paving Technologists*, *74*, 963–1002. Retrieved from https://trid.trb.org/view/777870

Cowher, C. E., & Kennedy, T. W. (1975). *Cumulative damage of asphalt materials under repeated-load indirect tension*. Washington, DC. Retrieved from https://trid.trb.org/view/30688

Cowper, G. R. (1966). The Shear Coefficient in Timoshenko's Beam Theory. *Journal of Applied Mechanics*, *33*(2), 335. https://doi.org/10.1115/1.3625046

Diefenderfer, B. K., Bowers, B. F., & Diefenderfer, S. D. (2015). *Asphalt Mixture Performance Characterization Using Small-Scale Cylindrical Specimens*. Charlottesville, VA. Retrieved from http://www.virginiadot.org/vtrc/main/online_reports/pdf/15-r26.pdf

Diefenderfer, S. D., & Bowers, B. F. (2019). Initial Approach to Performance (Balanced) Mix Design: The Virginia Experience. *Transportation Research Record: Journal of the Transportation Research Board*, *2673*(2), 335–345. https://doi.org/10.1177/0361198118823732

Du, P., Lin, I.-K., Lu, H., & Zhang, X. (2010). Extension of the beam theory for polymer bio-transducers with low aspect ratios and viscoelastic characteristics. *Journal of Micromechanics and Microengineering*, *20*(9), 095016. https://doi.org/10.1088/0960-1317/20/9/095016

Germann, F., & Lytton, R. (1979). *Methodology for predicting the reflection cracking life of asphalt concrete overlays*. *The Texas State Department of Highways and Pucblic Transportation*. College Station. Retrieved from http://adsabs.harvard.edu/abs/1979tamu.reptQ....G

Haider, S. W., Masud, M. M., & Chatti, K. (2020). Influence of moisture infiltration on flexible pavement cracking and optimum timing for surface seals. *Canadian Journal of Civil Engineering*, *47*(5), 487–497. https://doi.org/10.1139/cjce-2019-0008

Harvey, J., & Tsai, B.-W. (1996). Effects of Asphalt Content and Air Void Content on Mix Fatigue and Stiffness. *Transportation Research Record: Journal of the Transportation Research Board*, *1543*(05), 38–45. https://doi.org/10.3141/1543-05

Hu, S., Zhou, F., Scullion, T., & Leidy, J. (2012). Calibrating and Validating Overlay Tester–Based Fatigue Cracking Model with Data from National Center for Asphalt Technology. *Transportation Research Record: Journal of the Transportation Research Board*, *2296*(1), 57–68. https://doi.org/10.3141/2296-06

Hutchinson, J. R. (2001). Shear Coefficients for Timoshenko Beam Theory. *Journal of Applied Mechanics*, *68*(1), 87. https://doi.org/10.1115/1.1349417

Huurman, M., & Pronk, A. C. (2012). A detailed FEM simulation of a 4-point bending test device. In J. Harvey & J. Pais (Eds.), *Four-Point Bending* (pp. 3–12). DAVIS: CRC Press.

Hveem, F. N. (1955). Pavement deflections and fatigue failures. *Highway Research Board Bulletin*, (114).

Kaseer, F., Yin, F., Arámbula-Mercado, E., Epps Martin, A., Daniel, J. S., & Salari, S. (2018). Development of an index to evaluate the cracking potential of asphalt mixtures using the semi-circular bending test. *Construction and Building Materials*, *167*, 286–298. https://doi.org/10.1016/J.CONBUILDMAT.2018.02.014

Kennedy, T. W. (1977). Characterization of Asphalt Pavement Materials Using the Indirect Tensile Test. *Asphalt Paving Technology: Association of Asphalt Paving Technologists-Proceedings of the Technical Sessions*, *46*, 132–150. Retrieved from https://trid.trb.org/view/87356

Kim, Y. R., Castorena, C., Elwardany, M., Rad, F. Y., Underwood, S., Gundha, A., … Glaser, R. R. (2018). *Long-Term Aging of Asphalt Mixtures for Performance Testing and Prediction*. *NCHRP report 871*. Transportation Research Board. https://doi.org/10.17226/24959

Kim, Y. R., Hyon-Jong, L., & Little, D. N. (1997). Fatigue characterization of asphalt concrete using viscoelasticity and continuum damage theory (with discussion). *Journal of the*

Association of Asphalt Paving Technologists, *66*. Retrieved from https://trid.trb.org/view/488044

Kim, Y. R., Lee, H.-J., & Little, D. N. (1997). Fatigue characterization of asphalt concrete using viscoelasticity and continuum damage theory (with discussion). *Journal of the Association of Asphalt Paving Technologists*, *66*, 520–569. Retrieved from https://trid.trb.org/view/488044

Kim, Y. R., & Wen, H. (2002). Fracture energy from indirect tension testing. *Asphalt Paving Technology 2002, March 18, 2002 - March 20, 2002*, *71*(August), 779–793.

Kutay, M. E., Gibson, N., & Youtcheff, J. (2008). Conventional and Viscoelastic Continuum Damage (VECD) - Based Fatigue Analysis of Polymer Modified Asphalt Pavements. *Journal of the Association of Asphalt Paving Technologists*, *77*, 1–32.

Kutay, M. E., Gibson, N., Youtcheff, J., & Dongré, R. (2009). Use of Small Samples to Predict Fatigue Lives of Field Cores Newly Developed Formulation Based on Viscoelastic Continuum Damage Theory. *Transportation Research Record: Journal of the Transportation Research Board*, *2127*, 90–97. https://doi.org/10.3141/2127-11

Kutay, M. E., & Lanotte, M. (2017). Viscoelastic continuum damage (VECD) models for cracking problems in asphalt mixtures. *InternatIonal Journal of Pavement EngIneerIng*, *19*(3), 231–242. https://doi.org/10.1080/10298436.2017.1279492

Lee, H.-J., & Kim, Y. R. (1998). Viscoelastic Constitutive Model for Asphalt Concrete under Cyclic Loading. *Journal of Engineering Mechanics*, *124*(1), 32–40. https://doi.org/10.1061/(ASCE)0733-9399(1998)124:1(32)

Li, N, Molenaar, A. A. A., Van De Ven, M. F. C., & Wu, S. (2013). Comparison of Uniaxial and Four-Point Bending Fatigue Tests for Asphalt Mixtures. *Transportation Research Record Journal of the Transportation Research Board Transportation Research Board of the National Academies*, (2373), 44–53. https://doi.org/10.3141/2373-05

Li, Ning, Molenaar, A. A. A., Van De Ven, M. F. C., & Wu, S. (2013). Characterization of fatigue performance of asphalt mixture using a new fatigue analysis approach. *Construction and Building Materials*, *45*, 45–52. https://doi.org/10.1016/j.conbuildmat.2013.04.007

Luo, X., Luo, R., & Lytton, R. L. (2013). Energy-Based Mechanistic Approach to Characterize Crack Growth of Asphalt Mixtures. *Journal of Materials in Civil Engineering*, *25*(9), 1198–1208. https://doi.org/10.1061/(ASCE)MT.1943-5533.0000666

Lytton, R. L., Zhang, Y., Gu, F., & Luo, X. (2018). Characteristics of damaged asphalt mixtures in tension and compression. *International Journal of Pavement Engineering*, *19*(3), 292–306. https://doi.org/10.1080/10298436.2017.1347439

Maher, A., & Bennert, T. (2008). *Evaluation of Poisson ' s Ratio for Use in the Mechanistic Empirical Pavement Design Guide*. No. FHWA-NJ-2008-004.

Majidzadeh, K., & Kauffmann, E. M Ramsamooj, D. V. (1971). Application of fracture mechanics

in the analysis of pavement fatigue. *Association of Asphalt Paving Technologists Proc*, *40*, 227–246.

Masud, M. M. (2018). *Quantification of Moisture Related Damage in Flexible and Rigid Pavements and Incorporation of Pavement Preservation Treatments in AASHTOWare Pavement-ME Design and Analysis*. Michigan State University.

Mateos, A., Wu, R., Denneman, E., & Harvey, J. (2018). Sine versus Haversine Displacement Waveform Comparison for Hot Mix Asphalt Four-Point Bending Fatigue Testing. *Transportation Research Record: Journal of the Transportation Research Board*, 1–11. https://doi.org/10.1177/0361198118782795

Mello, L. G. R. de, Farias, M. M. de, & Kaloush, K. E. (2018). Using damage theory to analyze fatigue of asphalt mixtures on flexural tests. *International Journal of Pavement Research and Technology*, *11*(6), 617–626. https://doi.org/10.1016/J.IJPRT.2018.02.003

Miller, J. S., & Bellinger, W. Y. (2014). Distress Identification Manual for the Long-Term Pavement Performance Program (Fifth Revised Edition). McLean, VA 22101-2296: FHWA-HRT-13-092. Retrieved from https://www.fhwa.dot.gov/publications/research/infrastructure/pavements/ltpp/13092/13092.pdf

Mohammad, L., Kim, M., & Challa, H. (2016). *Development of Performance-Based Specifications for Louisiana Asphalt Mixtures*. Report No. FHWA/LA.14/558, Louisiana Transportation Research Center, Baton Rouge, Louisiana.

Monismith, C.L. (1966). Fatigue of Asphalt Paving Mixtures. *Paper Prepared for Presentation at the First Annual Street and Highway Conference, University of Nevada*. Reno.

Monismith, C L, Secor, K. E., & Blackmer, E. W. (1961). Asphalt Mixture Behaviour in Repeated Flexure (with Discussion and Closure). *Asphalt Paving Technology: Association of Asphalt Paving Technologists-Proceedings of the Technical Sessions*, *30*, 188–222. Retrieved from https://trid.trb.org/view/728292

Monismith, Carl L. (1994). *Fatigue Response of Asphalt-Aggregate Mixes*. Washington D.C. Retrieved from http://onlinepubs.trb.org/onlinepubs/shrp/shrp-a-404.pdf

Moore, R. K., & Kennedy, T. W. (1971). *Tensile behavior of subbase materials under repetitive loading*. University of Texas, Austin. Retrieved from https://trid.trb.org/view/124634

Naser, M. Z., & Seitllari, A. (2019). Concrete under fire: an assessment through intelligent pattern recognition. *Engineering with Computers*, 1–14. https://doi.org/10.1007/s00366-019-00805-1

Nemati, R., Haslett, K., Dave, E. V., & Sias, J. E. (2019). Development of a rate-dependent cumulative work and instantaneous power-based asphalt cracking performance index. *Road Materials and Pavement Design*, *20*(sup1), S315–S331. https://doi.org/10.1080/14680629.2019.1586753

Nguyen, H. M., Pouget, S., Di Benedetto, H., & Sauzéat, C. (2009). Time-temperature superposition principle for bituminous mixtures. *European Journal of Environmental and Civil Engineering*, *13*(9), 1095–1107. https://doi.org/10.1080/19648189.2009.9693176

Nsengiyumva, G., Kim, Y. ., & You, T. (2015). *Development of a Semicircular Bend (SCB) Test Method for Performance Testing of Nebraska Asphalt Mixtures*. Final Report 26-1121-4023-001. Nebraska Transportation Center, Lincoln.

Ozer, H., Al-Qadi, I. L., Singhvi, P., Bausano, J., Carvalho, R., Li, X., & Gibson, N. (2018). Prediction of pavement fatigue cracking at an accelerated testing section using asphalt mixture performance tests. *International Journal of Pavement Engineering*, *19*(3), 264–278. https://doi.org/10.1080/10298436.2017.1347435

Park, S. W., Kim, Y. R., & Schapery, R. A. (1996). A viscoelastic continuum damage model and its application to uniaxial behavior of asphalt concrete. *Mechanics of Materials*, *24*(4), 241–255. https://doi.org/10.1016/S0167-6636(96)00042-7

Pell, P. S., & Cooper, K. E. (1975). The Effect of Testing and Mix Variables on the Fatigue Performance of Bituminous Materials. *Asphalt Paving Technology: Association of Asphalt Paving Technologists-Proceedings of the Technical Sessions*, *44*, 1–37.

Prowell, B. D., Brown, E. R., Anderson, R. M., Daniel, J. S., Swamy, A. K., Von Quintus, H., … Maghsoodloo, S. (2010). *Validating the fatigue endurance limit for hot mix asphalt*. *NCHRP 9-44 Report,*. Washington, DC: Transportation Research Board. Retrieved from https://trid.trb.org/view/914979

Raithby, K. D., & Sterling, A. B. (1972). Some Effects of Loading History on the Performance of Rolled Asphalt. TRRL-LR 496.

Roque, R., Birgisson, B., Drakos, C., & Dietrich, B. (2004). DEVELOPMENT AND FIELD EVALUATION OF ENERGY-BASED CRITERIA FOR TOP-DOWN CRACKING PERFORMANCE OF HOT MIX ASPHALT (WITH DISCUSSION). *Journal of the Association of Asphalt Paving Technologists*, *73*, 229–260. Retrieved from https://trid.trb.org/view/749993

Roque, R., & Buttlar, W. . (1992). THE DEVELOPMENT OF A MEASUREMENT AND ANALYSIS SYSTEM TO ACCURATELY DETERMINE ASPHALT CONCRETE PROPERTIES USING THE INDIRECT TENSILE MODE (WITH DISCUSSION). *Journal of the Association of Asphalt Paving Technologists*, *61*, 304–332. Retrieved from https://trid.trb.org/view/486940

Rowe, G. (1993). Performance of asphalt mixtures in the trapezoidal fatigue test. *Journal of the Association of Asphalt Paving Technologists*, *62*, 344–384. Retrieved from http://www.abatech.com/documents/1993_Rowe_Perf_of_Asphal_Mixtures_in_the_Trapezoidal_Fatigue_Test_v62p343.pdf

Rowe, G. M., & Brown, S. F. (1997). Validation of the fatigue performance of asphalt mixtures with small scale wheel tracking experiments. *Asphalt Paving Technology: Association of*

Asphalt Paving Technologists-Proceedings of the Technical Sessions, *66*, 31–73. Retrieved from https://trid.trb.org/view/1163610

Sabouri, M., & Kim, Y. R. (2014). Development of a Failure Criterion for Asphalt Mixtures under Different Modes of Fatigue Loading. *Transportation Research Record: Journal of the Transportation Research Board*, *2447*(1), 117–125. https://doi.org/10.3141/2447-13

Schapery, R. A. (1984). Correspondence principles and a generalized J integral for large deformation and fracture analysis of viscoelastic media. *International Journal of Fracture*, *25*, 195–223. Retrieved from https://link.springer.com/content/pdf/10.1007%2FBF01140837.pdf

Schapery, R. A. (1990). A theory of mechanical behavior of elastic media with growing damage and other changes in structure. *Journal of the Mechanics and Physics of Solids*, *38*(2), 215–253. https://doi.org/10.1016/0022-5096(90)90035-3

Seitllari, A., & Naser, M. Z. (2019). Leveraging artificial intelligence to assess explosive spalling in fire-exposed RC columns. *Computers and Concrete*, *24*(3), 271–282. https://doi.org/10.12989/CAC.2019.24.3.271

Seitllari, Aksel. (2014). Traffic Flow Simulation by Neuro-Fuzzy Approach. In *Proceedings of Second International Conference on Traffic and Transport Engineering (ICTTE)* (pp. 97–102). Belgrade. Retrieved from https://trid.trb.org/view/1408239

Seitllari, Aksel, Boz, I., Habbouche, J., & Diefenderfer, S. D. (2020). Assessment of cracking performance indices of asphalt mixtures at intermediate temperatures. *International Journal of Pavement Engineering*, 1–10. https://doi.org/10.1080/10298436.2020.1730838

Seitllari, Aksel, Kumbargeri, Y., Biligiri, P. K., & Boz, I. (2018). A Soft Computing Approach to Predict and Evaluate Asphalt Mixture Aging Characteristics using Asphaltene as a Performance Indicator. *Materials and Structures/Materiaux et Constructions*.

Seitllari, Aksel, & Kutay, M. E. (2018). Soft Computing Tools to Predict Progression of Percent Embedment of Aggregates in Chip Seals. *Transportation Research Record: Journal of the Transportation Research Board*, *2672*(12), 32–39. https://doi.org/10.1177/0361198118756868

Seitllari, Aksel, & Kutay, M. E. (2019). Development of 3-Point Bending Beam Fatigue Test System and Implementation of Viscoelastic Continuum Damage (VECD) Theory. *Journal of the Association of Asphalt Paving Technologists*, *88*, 783–810.

Seitllari, Aksel, Lanotte, M. A., & Kutay, M. E. (2019a). Calibration of the MEPDG Rutting Model: Issues and Consequences on Rutting Prediction. In *Transportation Research Board 98th Annual Meeting* (p. 6p). Washington DC: No. 19-02795. Retrieved from https://trid.trb.org/view/1572341

Seitllari, Aksel, Lanotte, M. A., & Kutay, M. E. (2019b). Comparison of uniaxial tension-compression fatigue test results with SCB test performance indicators developed for

performance-based mix design procedure. (A. F. Nikolaides & E. Manthos, Eds.), *Bituminous Mixtures and Pavements VII: Proceedings of the 7th International Conference 'Bituminous Mixtures and Pavements'(7ICONFBMP)*. Thessaloniki, Greece: CRC Press.

Soltani, A., & Anderson, D. (2005). New Test Protocol to Measure Fatigue Damage in Asphalt Mixtures. *Road Materials and Pavement Design*, *6*(4), 485–514. https://doi.org/10.1080/14680629.2005.9690017

Tapsoba, N., Sauzéat, C., Di Benedetto, H., Baaj, H., & Ech, M. (2015). Three-dimensional analysis of fatigue tests on bituminous mixtures. *Fatigue & Fracture of Engineering Materials & Structures*, *38*(6), 730–741. https://doi.org/10.1111/ffe.12278

Tapsoba, Nouffou, Sauzéat, C., Di Benedetto, H., Baaj, H., Ech, M., & Sauzéat Hervé Di Benedetto, C. (2014). Behaviour of asphalt mixtures containing reclaimed asphalt pavement and asphalt shingle. *Road Materials and Pavement Design*, *15*(2), 330–347. https://doi.org/10.1080/14680629.2013.871091

Tarefder, R. A., Bateman, D., & Swamy, A. K. (2013). Comparison of fatigue failure criterion in flexural fatigue test. *International Journal of Fatigue*, *55*, 213–219. https://doi.org/10.1016/J.IJFATIGUE.2013.07.004

Tayebali, A. A., Deacon, J. C. A., Coplantz, J., Harvey, J. T., & Monismith, C. L. (1994). Mix and mode-of-loading effects on fatigue response of asphalt-aggregate mixes. Retrieved from https://www.semanticscholar.org/paper/Mix-and-mode-of-loading-effects-on-fatigue-response-Tayebali-Deacon/174246cf831ba4eeadefb6a140e6e3f2a704e92e

Timoshenko, S. (1940). *Strength of materials Part 1*. D. Van Nostrand Co., Inc,.

Timoshenko, S., & Gere, J. M. (1972). *Mechanics of materials*. New York: Van Nostrand Reinhold Co. Retrieved from http://www.worldcat.org/title/mechanics-of-materials/oclc/251209

Ullidtz, P., Harvey, J., Tsai, B.-W., & Monismith, C. (2006). *Calibration of Incremental-Recursive Flexible Damage Models in CalME Using HVS Experiments. Report prepared for the California Department of Transportation (Caltrans) Division of Research and Innovation*. Davis and Berkeley. https://doi.org/UCPRC-RR-2005-06

Underwood, B. Shane, et al. (2006). Characterization and performance prediction of ALF mixtures using a viscoelastoplastic continuum damage model. *Association of Asphalt Paving Technologists-Proceedings of the Technical Sessions 2006 Annual Meeting*.

Van Dijk, W. (1975). Practical Fatigue Characterization of Bituminous Mixes. *Journal of the Association of Asphalt Paving Technologists*, *44*, 38.

Verstraeten, J. (1972). Moduli and Critical Strains in Repeated Bending of Bituminous Mixes-Application to Pavement Design. *Asphalt Paving Technology: Association of Asphalt Paving Technologists-Proceedings of the Technical Sessions*, *1*, 729–738. Retrieved from https://trid.trb.org/view/138847

Walubita, L. F., Martin, A. E., Cleveland, G. S., & Lytton, R. L. (2006). Computation of pseudo strain energy and Paris law fracture coefficients from surface energy and uniaxial strain-controlled tension test data Computation of pseudo strain energy and Paris law fracture coefficients from surface energy and uniaxial strain-co. *International Journal of Pavement Engineering*, *7*(3), 167–178. https://doi.org/10.1080/10298430500501944org/10.1080/10298430500501944

Wang, C., Castorena, C., Zhang, J., & Richard Kim, Y. (2015). Unified failure criterion for asphalt binder under cyclic fatigue loading. *Road Materials and Pavement Design*, *16*(sup2), 125–148. https://doi.org/10.1080/14680629.2015.1077010

Wang, Y. D., Keshavarzi, B., & Kim, Y. R. (2018). Fatigue Performance Prediction of Asphalt Pavements with FlexPAVETM, the S-VECD Model, and DR Failure Criterion. *Transportation Research Record*, *2672*(40), 217–227. https://doi.org/10.1177/0361198118756873

WASHO. (1955). *The WASHO Road Test Part 2: Test Data, Analyses, Findings*.

West, R., Rodezno, C., Leiva, F., & Taylor, A. (2018). *Regressing Air Voids for Balanced HMA Mix Design*. WisDOT ID no. 0092-16-06, Wisconsin Highway Research Program, Madison, WI. Retrieved from https://wisconsindot.gov/documents2/research/0092-16-06-final-report.pdf

West, R., Rodezno, C., Leiva, F., & Yin, F. (2018). *Project NCHRP 20-07/Task 406, Development of a Framework for Balanced Mix Design*. Auburn. Retrieved from http://onlinepubs.trb.org/onlinepubs/nchrp/docs/NCHRP20-07(406)_Revised_final_report.pdf

Witzcak, M. W., Kaloush, K., Pellinen, T., El-Basyouny, M., & Von Quintus, H. (2002). *NCHRP Report 465: Simple performance test for Superpave mix design*. Retrieved from http://onlinepubs.trb.org/onlinepubs/nchrp/nchrp_rpt_465.pdf

Wu, H., Huang, B., & Shu, X. (2014). Characterizing Fatigue Behavior of Asphalt Mixtures Utilizing Loaded Wheel Testers. *JOURNAL OF MATERIALS IN CIVIL ENGINEERING*, *26*(1), 152–159. Retrieved from https://ascelibrary.org/doi/pdf/10.1061/%28ASCE%29MT.1943-5533.0000791

Zeiada, W. A., Kaloush, K. E., Underwood, B. S., & Mamlouk, M. (2016). Development of a Test Protocol to Measure Uniaxial Fatigue Damage and Healing. *Transportation Research Record: Journal of the Transportation Research Board*, *2576*, 10–18. https://doi.org/10.3141/2576-02

Zhang, J., Sabouri, M., Guddati, M. N., & Kim, Y. R. (2013). Development of a failure criterion for asphalt mixtures under fatigue loading Development of a failure criterion for asphalt mixtures under fatigue loading. *Road Materials and Pavement Design*, *14*(S2), 1–15. https://doi.org/10.1080/14680629.2013.812843

Zhou, F., Hu, S., Chen, D.-H., & Scullion, T. (2007). Overlay Tester: Simple Performance Test

for Fatigue Cracking. *Transportation Research Record: Journal of the Transportation Research Board*, *2001*(1), 1–8. https://doi.org/10.3141/2001-01

Zhou, F., Hu, S., Hu, X., & Scullion, T. (2009). *Mechanistic Empirical Asphalt Overlay Thickness Design and Analysis System. FHWA / TX-09 / 0-5123-3* (Vol. 7). College Station.

Zhou, F., Im, S., Sun, L., & Scullion, T. (2017). Development of an IDEAL cracking test for asphalt mix design and QC/QA. *Road Materials and Pavement Design*, *18*(4), 405–427. https://doi.org/10.1080/14680629.2017.1389082org/10.1080/14680629.2017.1389082

Zhou, F., Newcomb, D., Gurganus, C., Banihashemrad, S., Sakhaeifar, M., Park, E. S., & Lytton, R. L. (2016). *Field Validation of Laboratory Tests to Assess Cracking Resistance of Asphalt Mixtures: An Experimental Design.* Washington, DC. Retrieved from https://doi.org/10.17226/23608

Zhu, Y., Dave, E. V, Rahbar-Rastegar, R., Sias Daniel, J., & Zofka, A. (2017). Comprehensive evaluation of low-temperature fracture indices for asphalt mixtures. *Road Materials and Pavement Design*, *18*(S4), 467–490. https://doi.org/10.1080/14680629.2017.1389085